ISTANBUL TECHNICAL UNIVERSITY ★ GRADUATE SCHOOL OF SCIENCE ENGINEERING AND TECHNOLOGY

MODEL PREDICTIVE CONTROL OF A FIXED WING UNMANNED AERIAL VEHICLE

Ph.D. THESIS

Hakan ÜLKER

Mechanical Engineering Department

Mechanical Engineering Doctorate Program

SEPTEMBER 2016

ISTANBUL TECHNICAL UNIVERSITY ★ GRADUATE SCHOOL OF SCIENCE ENGINEERING AND TECHNOLOGY

MODEL PREDICTIVE CONTROL OF A FIXED WING UNMANNED AERIAL VEHICLE

Ph.D. THESIS

Hakan ÜLKER
(503102020)

Mechanical Engineering Department

Mechanical Engineering Doctorate Program

Thesis Advisor: Assoc. Prof. Dr. Cemal BAYKARA

SEPTEMBER 2016

İSTANBUL TEKNİK ÜNİVERSİTESİ ★ FEN BİLİMLERİ ENSTİTÜSÜ

SABİT KANATLI BİR İNSANSIZ HAVA ARACININ MODEL ÖNGÖRÜLÜ KONTROLÜ

DOKTORA TEZİ

Hakan ÜLKER
(503102020)

Makina Mühendisliği Anabilim Dalı

Makina Mühendisliği Doktora Programı

Tez Danışmanı: Doç. Dr. Cemal BAYKARA

EYLÜL 2016

Hakan ÜLKER, a Ph.D. student of ITU Graduate School of Science Engineering and Technology 503102020 successfully defended the thesis entitled "MODEL PREDICTIVE CONTROL OF A FIXED WING UNMANNED AERIAL VEHICLE", which he prepared after fulfilling the requirements specified in the associated legislations, before the jury whose signatures are below.

Thesis Advisor :	**Assoc. Prof. Dr. Cemal BAYKARA** Istanbul Technical University	.....
Jury Members :	**Prof. Dr. Can ÖZSOY** Beykent University	.....
	Prof. Dr. Hikmet KOCABAŞ İstanbul Technical University	.....
	Assoc. Prof. Dr. Mahmut Cüneyt FETVACI İstanbul University	.....
	Assist. Prof. Dr. İbrahim Mehmet PALABIYIK İstanbul Technical University	.....

Date of Submission : **19 July 2016**
Date of Defense : **02 September 2016**

To all of my family,
especially my wife and little baby son,

FOREWORD

This PhD thesis was investigated and written at department of Mechanical Engineering in Istanbul Technical University. It is about Model Predictive Control of a fixed wing Unmanned Aerial Vehicle under the flight and test conditions considered. Control of an Unmanned Aerial Vehicle is significant in the way of the usage in various civil and military applications.

I feel very lucky that there are lots of valuable people around me whom I will always thank for their valuable help and support during my thesis and PhD. Firstly, I would like to thank my supervisor Assoc. Prof. Dr. Cemal BAYKARA for giving me his valuable advice and support during the thesis. I really do not know how to thank Prof. Dr. Can ÖZSOY for sharing his great time, knowledge, advice and experience all time. I would like to give my special thanks to steering committee members, Prof. Dr. Hikmet KOCABAŞ and Assoc. Prof. Dr. Cüneyt FETVACI for their support and understanding. I appreciate Prof. Dr. Metin GÜRGÖZE for his memorable motivation, support and knowledge since I started PhD. I am grateful for the great support and guidance of Assoc. Prof. Dr. İlker Murat KOÇ and Assoc. Prof. Dr. Ayhan KURAL. Many thanks for the valuable help and knowledge of Prof. Dr. Brian TAYLOR and Raghu VENKATARAMAN from University of Minnesota. Lastly, I would like to thank my friends Ömer Faruk ARGIN, Turgay ERAY and Cihat Bora YİĞİT for their support all time.

I have a great family who are always near me and support me during all my life. I would like to thank all of my family especially my wife and our little baby son. I am the happiest man in the world that I have them.

September 2016

Hakan ÜLKER
(Mechanical Engineer, MSc.)

TABLE OF CONTENTS

Page

FOREWORD ... **ix**
TABLE OF CONTENTS ... **xi**
ABBREVIATIONS ... **xiii**
SYMBOLS ... **xv**
LIST OF TABLES ... **xix**
LIST OF FIGURES ... **xxi**
SUMMARY ... **xxiii**
ÖZET ... **xxv**
1. INTRODUCTION ... **1**
2. UAV DYNAMICS ... **7**
2.1 UAV platform ... 7
2.2 Coordinate Frames ... 7
2.2.1 Inertial frame ... 7
2.2.2 Vehicle frame ... 8
2.2.3 Vehicle 1 frame ... 8
2.2.4 Vehicle 2 frame ... 9
2.2.5 Body frame ... 9
2.2.6 Stability frame ... 10
2.2.7 Wind frame ... 11
2.3 UAV Speeds ... 12
2.4 Kinematics ... 16
2.5 Dynamics ... 17
2.5.1 Translational motion ... 17
2.5.2 Rotational motion ... 18
2.5.3 Forces and moments ... 20
2.5.4 Gravitational force ... 20
2.5.5 Aerodynamic forces and moments ... 20
2.5.5.1 Longitudinal aerodynamic forces and moment ... 21
2.5.5.2 Lateral aerodynamic force and moments ... 23
2.5.5.3 Propulsion force and moment ... 24
2.5.6 Wind models ... 26
2.5.7 Trim ... 28
2.5.8 Linear models ... 30
3. MODEL PREDICTIVE CONTROL ... **33**
3.1 MPC Concept ... 33
3.2 Prediction Model ... 35
3.3 State Estimation ... 36

3.3.1 Unmeasured disturbance model 36
3.3.2 Measurement noise model 37
3.3.3 State observer 38
3.4 Optimization Problem 38
4. NONLINEAR AND PROCESSOR IN THE LOOP SIMULATIONS..... 45
4.1 Nonlinear Simulations 45
4.2 Processor In The Loop Simulations 56
5. CONCLUSIONS AND RECOMMENDATIONS 67
REFERENCES 69
APPENDICES 75
APPENDIX A 77
CURRICULUM VITAE 126

ABBREVIATIONS

FWUAV : Fixed Wing Unmanned Aerial Vehicle
HIL : Hardware In the Loop
LTI : Linear Time Invariant
MD : Measured Disturbance
MIMO : Multi Input Multi Output
MN : Measurement Noise
MO : Measured Output
MPC : Model Predictive Control
MPO : Maximum Percentage Overshoot
MV : Manipulated Variable
NED : North-East-Down
NL : Nonlinear
NMPC : Nonlinear Model Predictive Control
PI : Proportional–Integral
PID : Proportional–Integral-Derivative
PIL : Processor In the Loop
QP : Quadratic Programming
SIL : Software In the Loop
SISO : Single Input Single Output
SSE : Steady State Error
SW : Steady Wind
UAV : Unmanned Aerial Vehicle
UMN : University of Minnesota
UO : Unmeasured Output
UOD : Unmeasured Output Disturbance
WG : Wind Gust

SYMBOLS

$()_j$	: $j-th$ component of an input-output vector
$(k+i \mid k)$	: Value predicted for time $k+i$ based on the information available as time k
A	: System matrix
$\overline{A}$	: System matrix of unmeasured input disturbance model
$\tilde{A}$	: System matrix of measurement noise model
A_c	: Linear constraint coefficients matrix
A_f	: System matrix of full linearised state space model
A_{lat}	: System matrix of lateral state space model
A_{lon}	: System matrix of longitudinal state space model
A_w	: Wing reference area
AR	: Wing aspect ratio
a_x, a_y, a_z	: Translational accelerations
$\overline{B}$	: Unmeasured disturbance matrix of unmeasured input disturbance model
$\tilde{B}$	: Unmeasured disturbance matrix of measurement noise model
b	: Wing span
B_d	: Unmeasured disturbance matrix
B_f	: Input matrix of full linearised state space model
B_{lat}	: Input matrix of lateral state space model
B_{lon}	: Input matrix of longitudinal state space model
B_u	: Input control matrix
B_v	: Measured disturbance matrix
C	: Overall output matrix
$\overline{C}$	: Output matrix of unmeasured input disturbance model
$\tilde{C}$	: Output matrix of measurement noise model
c	: Wing chord
C_D	: Drag force aerodynamic coefficient
C_f	: Output matrix of full linearised state space model
C_L	: Lift force aerodynamic coefficient
C_l	: Roll moment aerodynamic coefficient
C_{lat}	: Output matrix of lateral state space model
C_{lon}	: Output matrix of longitudinal state space model
C_m	: Pitch moment aerodynamic coefficient
C_{mo}	: Measured output matrix
C_n	: Yaw moment aerodynamic coefficient
C_P	: Coefficient of power
C_T	: Coefficient of thrust
C_u	: Unmeasured output matrix
C_Y	: Side force aerodynamic coefficient
$\overline{D}$	: Feedthrough unmeasured disturbance matrix of unmeasured input disturbance model
$\tilde{D}$	: Feedthrough unmeasured disturbance matrix of measurement noise model

$d(k)$: Unmeasured disturbances (UD) vector
D_d : Overall feedthrough unmeasured disturbance matrix
D_{dm} : Feedthrough unmeasured disturbance matrix of measured output
D_{du} : Feedthrough unmeasured disturbance matrix of unmeasured output
D_f : Feedforward matrix of full linearised state space model
D_{lat} : Feedforward matrix of lateral state space model
D_{lon} : Feedforward matrix of longitudinal state space model
d_m : Length of wind gust
D_p : Propeller diameter
D_u : Feedthrough input control matrix
D_v : Overall feedthrough measured disturbance
D_{vm} : Feedthrough measured disturbance matrix of measured output
D_{vu} : Feedthrough measured disturbance matrix of unmeasured output
e : Oswald efficiency factor
e_{δ_r} : Error of the control input rudder generated by the model and the object code
e_{δ_a} : Error of the control input aileron generated by the model and the object code
e_{δ_t} : Error of the control input throttle generated by the model and the object code
e_{δ_e} : Error of the control input elevator generated by the model and the object code
$\mathbf{f}$: Total external forces acting on UAV in inertial frame F^i
$\mathbf{f}_a$: Aerodynamic force acting on UAV in body frame F^b
$\mathbf{f}_g$: Gravitational force acting on UAV in body frame F^b
$\mathbf{f}_p$: Propulsion force acting on UAV in body frame F^b
F_{drag} : Drag force
F_{lift} : Lift force
F_p : Propeller thrust
F^b : Body frame
F^i : Inertial frame
F^s : Stability frame
F^v : Vehicle frame
F^{v1} : Vehicle 1 frame
F^{v2} : Vehicle 2 frame
F^w : Wind frame
g : Gravitational acceleration
H : Hessian matrix
$\mathbf{h}$: Angular momentum vector
$\mathbf{h}_p$: Angular momentum of rotating mass propeller
h : Altitude above ground level or negative of inertial down position p_d
$\mathbf{i}, \mathbf{j}, \mathbf{k}$: Unit vectors
$\mathbf{J}$: Inertia matrix
J_{ar} : Advance ratio
J_m : Moment of inertia of rotating motor body
J_p : Moment of inertia of propeller
J_x, J_y, J_z : Products of inertia
J_{xy}, J_{xz}, J_{yz} : Moments of inertia
K_{ob} : Observer gain
L, M, N : Components of the total moments about center of UAV in body frame F^b
$\mathbf{m}$: Total external moments about center of UAV in inertial frame F^i

m : Gross take off weight
m_h : Control horizon
$n_d(k)$: Random Gaussian noise with zero mean and unit covariance matrix
$n_m(k)$: Random Gaussian noise with zero mean and unit covariance matrix
n_u : Number of manipulated variables
n_v : Number of measured disturbances
n_x : Number of plant state variables
n_y : Number of plant output variables
P_0 : Output power
$\mathbf{p}$: Position vector
p, q, r : Roll, pitch and yaw rates measured in body frame F^b, respectively
p_h : Prediction horizon
p_n, p_e, p_d : Inertial north, east and down positions of UAV, respectively
$\overline{q}$: Aerodynamic pressure
R : Rotation matrix
S : Planform area
T : Thrust force
T_m : Output torque at motor shaft
T_p : Propeller torque
u, v, w : Components of the ground speed in body frame F^b
$\triangle u$: Increments of u
$u(k)$: Manipulated variables (MV) vector
u_f : Input vector of full linearised state space model
$u_{j,min}$: Lower bound on u
$u_{j,max}$: Upper bound on u
$\triangle u_{j,min}$: Lower bound on $\triangle u$
$\triangle u_{j,max}$: Upper bound on $\triangle u$
u_{lat} : Input vector of lateral state space model
u_{lon} : Input vector of longitudinal state space model
u_r, v_r, w_r : Components of the airspeed in body frame F^b
u_w, v_w, w_w : Components of the wind speed in body frame F^b
u_{w_g},v_{w_g},w_{w_g} : Components of the wind gust in body frame F^b
U_{w_s} : Absolute magnitude of steady wind
u_{w_s}, v_{w_s} : Axial and lateral components of steady wind, respectively
$v(k)$: Measured disturbances (MD) vector
V_a : Airspeed
V_g : Ground speed
$w_{i,j}^{\triangle u}$: Weight of $\triangle u$
$w_{i,j}^{u}$: Weight of u
$w_{i,j}^{y}$: Weight of y
V_m : Amplitude of wind gust
V_w : Wind speed
V_{w_s} : Steady wind velocity
V_{w_g} : Wind gust velocity
w_n, w_e, w_d : Components of the wind speed in north, east and down directions, respectively

w_{n_s},w_{e_s},w_{d_s} : Components of the steady wind in north, east and down directions in inertial frame F^i, respectively

X, Y, Z : Components of the total external forces acting on UAV in body frame F^b

$x(k)$: Plant state vector

$\hat{x}(k)$: Estimated state vector

$x_d(k)$: state vector of unmeasured input disturbance model

x_f : State vector of full linearised state space model

x_{lat} : State vector of lateral state space model

x_{lon} : State vector of longitudinal state space model

x_m : Distance travelled during wind gust

$x_m(k)$: State vector of measurement noise model

$y(k)$: Overall output vector

$\hat{y}(k)$: Estimated output vector

y_f : Output vector of full linearised state space model

$y_{j,min}$: Lower bound on y

$y_{j,max}$: Upper bound on y

y_{lat} : Output vector of lateral state space model

y_{lon} : Output vector of longitudinal state space model

$y_m(k)$: Measured outputs (MO) vector

$y_u(k)$: Unmeasured outputs (UO) vector

zo : Free optimization variables

ϕ : Roll (bank) angle

θ : Pitch angle

θ_{w_s} : Angle of steady wind

ψ : Yaw (heading) angle

α : Angle of attack

β : Sideslip angle

γ : Inertial-referenced flight path angle

γ_a : Air-mass-referenced flight path angle

χ : Course angle

χ_b : Crab angle

$\omega_{b/i}$: Angular velocity of UAV with respect to inertial frame F^i

ω_p : Propeller rotation speed

δ_a : Combined aileron deflection

δ_{a_l}, δ_{a_r} : Left and right aileron deflections, respectively

δ_a : Combined aileron deflection

δ_e : Elevator deflection

δ_{f_l}, δ_{f_r} : Left and right flap deflections, respectively

δ_r : Rudder deflection

δ_t : Throttle deflection

ρ : Air density

π : Pi number

LIST OF TABLES

Page

Table 2.1 : Aerodynamic coefficients. **23**
Table 4.1 : Saturation limits on actuators [2]. **45**
Table 4.2 : Trim targets with respect to flight scenarios [2]. **49**
Table 4.3 : References given along with the trim values for each flight scenario. **49**
Table 4.4 : Trim targets with respect to flight scenarios [2]. **57**
Table A.1 : Aircraft geometry [1]. **77**
Table A.2 : Moment of inertia data [1]. **77**
Table A.3 : Numerical values of aerodynamic coefficients [1]. **77**
Table A.4 : Trim points obtained for each flight scenario. **78**
Table A.5 : Trim points obtained for each flight scenario in case of presence of SW **79**
Table A.6 : Steady state errors in the nonlinear simulations. **120**
Table A.7 : Settling times in the nonlinear simulations. **121**
Table A.8 : Maximum overshoots in the nonlinear simulations. **122**
Table A.9 : Steady state errors in the PIL simulations. **123**
Table A.10: Settling times in the PIL simulations. **123**
Table A.11: Maximum overshoots in the PIL simulations. **123**

LIST OF FIGURES

Page

Figure 2.1 : Forces and moments in body axis of Ultra Stick 25E [1]. **7**
Figure 2.2 : Inertial and vehicle frames **8**
Figure 2.3 : Vehicle 1 frame **9**
Figure 2.4 : Vehicle 2 frame **9**
Figure 2.5 : Body frame **10**
Figure 2.6 : Stability frame **11**
Figure 2.7 : Wind frame **11**
Figure 2.8 : Wind triangle in horizontal plane **14**
Figure 2.9 : Wind triangle in vertical plane **14**
Figure 2.10: Longitudinal aerodynamic forces and moments [3]. **21**
Figure 2.11: Discrete WG profile [4]. **27**
Figure 2.12: Procedures for deriving linear decoupled models [1]. **31**
Figure 3.1 : MPC block diagram [5] **33**
Figure 3.2 : MPC concept [5]. **34**
Figure 3.3 : Prediction model [6] **35**
Figure 3.4 : State estimation model [6]. **36**
Figure 4.1 : Nonlinear fixed wing UAV model [2]. **46**
Figure 4.2 : Nonlinear closed loop model with the constrained lateral and longitudinal MIMO MPCs. **47**
Figure 4.3 : Structure of the constrained lateral and longitudinal MIMO MPCs. **48**
Figure 4.4 : Lateral response of straight and level in NL simulation. **50**
Figure 4.5 : Longitudinal response of straight and level in NL simulation. **50**
Figure 4.6 : Lateral response of level climb in NL simulation. **51**
Figure 4.7 : Longitudinal response of level climb in NL simulation. **51**
Figure 4.8 : Lateral response of level turn in NL simulation. **52**
Figure 4.9 : Longitudinal response of level turn in NL simulation. **52**
Figure 4.10: Lateral response of climbing turn in NL simulation. **53**
Figure 4.11: Longitudinal response of climbing turn in NL simulation. **53**
Figure 4.12: Lateral response of level steady heading sideslip in NL simulation. **54**
Figure 4.13: Longitudinal response of level steady heading sideslip in NL simulation. **54**
Figure 4.14: Schematic diagram of the hardware used in the PIL simulations. **58**
Figure 4.15: Structure of the PIL simulation. **59**
Figure 4.16: Lateral response of straight and level in PIL simulation. **60**
Figure 4.17: Longitudinal response of straight and level in PIL simulation. **60**
Figure 4.18: Lateral response of level climb in PIL simulation. **61**
Figure 4.19: Longitudinal response of level climb in PIL simulation. **61**

Figure 4.20: Lateral response of level turn in PIL simulation. **62**
Figure 4.21: Longitudinal response of level turn in PIL simulation. **62**
Figure 4.22: Lateral response of climbing turn in PIL simulation. **63**
Figure 4.23: Longitudinal response of climbing turn in PIL simulation. **63**
Figure 4.24: Lateral response of level steady heading sideslip in PIL simulation. **64**
Figure 4.25: Longitudinal response of level steady heading sideslip in PIL simulation. **64**

MODEL PREDICTIVE CONTROL
OF A FIXED WING UNMANNED AERIAL VEHICLE

SUMMARY

A model predictive control (MPC) strategy based on the lateral and longitudinal linear models is proposed for the flight control design. unmanned aerial vehicles (UAVs) are important to have a place for the usage in the various civil and military applications like battlefield and police surveillance, reconnaissance, combat, targeting, decoying, crop dusting, observations, TV broadcasting, photography, logistics etc. Thus the control of them is extremely important from the standpoint of carrying out their duties in a desired and controlled manner. MPC has been an important control technique in on-line applications. It has been able to be implemented to dynamic processes with smaller time scales such as aerospace by the help of modern computers.

The purpose of the thesis is a fixed wing UAV to undergo 5 flight scenarios as straight and level, level climb, level turn, climbing turn and level steady heading sideslip in a desired and controlled manner by means of constrained multi input multi output MPCs. Simulations are carried out for the nonlinear (NL) closed loop aircraft Simulink model available from the University of Minnesota UAV research group with the implemented MPCs designed in this thesis. The results of the NL simulations show that the MPCs can achieve satisfactory performance and flying qualities under 3 different test conditions in terms of existing unmeasured outputs and unmeasured output disturbances. The proposed MPC design provide more flexibility in terms of tracking complex trajectories comparing with the classical controllers in the literature. Besides they provide to change more than one references of the states at any time.

As another study of this thesis, the constrained multi input multi output lateral and longitudinal linear models based MPCs which are proposed and tested in the NL simulations are tested in the processor in the loop (PIL) simulations under windy conditions such as steady wind and wind gust. BeagleBone Black Rev C is used as a target hardware or processor in the PIL simulations. The same fixed wing UAV is targeted to perform PIL simulations for the same flight scenarios under the specified windy conditions in a desired and controlled manner.

The results of the PIL simulations show that the MPCs proposed in this thesis can achieve satisfactory performance and flying qualities for the all flight scenarios under the windy conditions. The proposed MPCs which are capable to provide more flexibility in terms of tracking complex trajectories are showed to be able to be implemented to hardware by means of the PIL simulations under the specified windy conditions which are difficult for performance tests. It can be clearly seen that the MPCs can be easily implemented to a low-cost and small-sized board like BeagleBone Black Rev C.

SABİT KANATLI BİR İNSANSIZ HAVA ARACININ MODEL ÖNGÖRÜLÜ KONTROLÜ

ÖZET

Tezde sabit kanatlı bir insansız hava aracının (İHA) model öngörülü kontrolü (MÖK) çalışılmıştır. Sivil ve askeri alanda İHA'ların kullanımı son yıllarda artmıştır. Günümüzde de keşif, muharebe, hedef tayini ve yanıltıcı amaçlı askeri alanda kullanılmakta olup; keşif, gözlem, TV yayını, fotoğrafçılık, lojistik ve ilaçlama amaçlı sivil alanda da kullanımı bulunmaktadır. Ulaşılması mümkün olamayan ve tehlikeli alanlarda kullanılabilir olması İHA'ların önemini artırmaktadır.

Tasarım formülasyonunun çok değişkenli bir yapıya sahip olması MÖK'ün en önemli özelliklerinden birisidir. Aynı zamanda kontrolcü tek giriş tek çıkışlı bir sistemden çok giriş çok çıkışlı bir sisteme genişletilebilir. Bir sistemin çevrimiçi optimize edilebilmesi, diğer tekniklere kıyasla tasarım yapısının kolaylığı ve mikro kontrolörler gibi basit sistemlere gömülebilmesi MÖK'ün önemli avantajlarından bir kaçı olarak sayılabilir.

Tezde önerilen yanal ve boylamsal çok giriş çok çıkışlı kısıtlı MÖK, çok giriş çok çıkışlı yanal ve boylamsal doğrusal durum uzay modellerine dayanmaktadır. Bu doğrusal modeller tam doğrusal durum uzay modelinin, yanal ve boylamsal modlara ait durum değişkenleri yardımıyla ikiye ayrılarak elde edilmektedir. Söz konusu ayırma işlemi uçuş dinamiğinde yaygın olarak kullanılan bir yöntemdir. Bu yöntem yanal ile boylamsal modların aralarındaki çapraz kuplaj etkisinin ihmal edilebilir olması varsayımıyla kullanılmaktadır. İHA'nın xz düzlemine göre simetrik olması ve kanatçık ile irtifa ve yön dümenleri gibi klasik kontrol yüzeylerine sahip olarak tasarlanmış olması durumunda bu varsayım geçerlidir. Tam doğrusal durum uzay modeli, Minnesota Üniversitesi İHA araştırma grubunun açık olarak sunmuş olduğu Ultra Stick 25e marka ve modelli İHA'ya ait doğrusal olmayan modelinin denge noktaları etrafında doğrusallaştırılmasıyla elde edilmektedir. Denge noktaları tezde ele alınan sürekli kanat-irtifa, sabit tırmanış, sabit irtifa - sürekli dönüş, sabit tırmanış - sürekli dönüş, sürekli kanat-irtifa - yana kayma uçuşları olmak üzere toplamda 5 uçuş senaryosuna dayanmaktadır. Söz konusu her uçuş senaryosu için ayrı ayrı denge noktaları hesaplanmaktadır. Tezin öncelikli amacı da söz konusu uçuş senaryoları için hesaplanan denge noktaları etrafında doğrusallaştırılarak elde edilen yanal ve boylamsal doğrusal durum uzay modellerine dayanan kısıtlı MÖK'ler sayesinde İHA'nın her uçuş senaryosunda dinamik denge konumunda kontrollü bir şekilde uçuşunu sağlamaktır.

Tezin ilk aşamasında, çok giriş çok çıkışlı yanal ve boylamsal doğrusal durum uzay modellerine dayanan kısıtlı MÖK'lerin yatış açısı pozisyonu, yunuslama açısı pozisyonu, istikamet açısı pozisyonu, irtifa, hız ve dönüş koordinasyonu kontrolü amaçlı dahil edildiği doğrusal olmayan kapalı çevrim simülasyonları gerçekleştirilmiştir. Bu simülasyonlarda yanal ve boylamsal MÖK'lerin bütün

girişlerine (yanal ve boylamsal doğrusal durum uzay modellerinin bütün çıkışlarına) ilk anda hesaplanan denge noktaları referans olarak verilmiştir. Bütün uçuş senaryolarında 5. saniyeden itibaren hava hızına denge noktası değerine ilaveten $1m/s$ referans verilmiştir. Sürekli kanat-irtifa uçuşunun 5. saniyesinde, irtifaya denge noktası değerine ilaveten $4.16m$ ve istikamet açısına ise denge noktası değerine ilaveten 4° referans verilmiştir. Sabit tırmanış uçuşunun 5. saniyesinde istikamet açısına denge noktası değerine ilaveten 4° referans verilmiştir. Sabit irtifa - sürekli dönüş ile sabit tırmanış - sürekli dönüş uçuşlarının 5. saniyelerinde yatış açısına denge noktası değerine ilaveten 4° referans verilmiştir. Sürekli kanat-irtifa - yana kayma uçuşunun 5. saniyesinde ise istikamet açısına denge noktası değerine ilaveten 4° referans verilmiştir. MÖK'lerin performansı 3 farklı şartlarda test edilmiştir. Öncelikle MÖK'ler nominal şartlarda, sonrasında boylamsal MÖK'ün girişlerinin (boylamsal doğrusal durum uzay modeli çıkışlarının) arasından sadece öteleme ivmeleri a_x ve a_z'nin ölçülemeyen çıkış olarak tayin edilmesi durumunda, son olarak ise tayin edilmiş olan söz konusu 2 çıkış ile birlikte yine boylamsal MÖK'ün girişlerinin (boylamsal doğrusal durum uzay modeli çıkışlarının) arasında yer alan hava hızının üzerine 1 büyüklüğünde rastgele basamak tarzında gürültü olacak şekilde bir ölçülemeyen çıkış bozucusu eklenmiştir.

Doğrusal olmayan simülasyonların sonucunda tasarlanan çok giriş çok çıkışlı MÖK'lerin her uçuş senaryosunda tatmin edici nitelikte uçuş performansı sağladığı gözlemlenmiştir. Tezde önerilen MÖK'ler, karmaşık yörüngeleri takip edebilmesi açısından literatürde yer alan klasik kontrolcülere kıyasla daha fazla esneklik sağlamıştır. Ayrıca çok giriş çok çıkışlı yanal ve boylamsal doğrusal durum uzay modellerine ait çıkışların, herhangi bir anda referans verilerek değişimlerine imkan vermektedir.

Tezin son aşamasında ise ilk aşamada önerilen ve performansları belirtilen 3 farklı şart altında test edilen çok giriş çok çıkışlı yanal ve boylamsal doğrusal durum uzay modellerine dayanan kısıtlı MÖK'lerin aynı şekilde dönüş koordinasyonu; hız; irtifa; yatış, yunuslama ve istikamet açısı pozisyonu kontrolü amaçlı performansı rüzgar koşullarında işlemci döngüsü simülasyonları ile test edilmiştir. Rüzgar şartları kontrolcülerin performansının testi için önemli parametrelerden birisidir. Çünkü kontrolcülerin rüzgar gibi önemli bir bozucuya karşı duyarsız olması istenir. Bu sebeple rüzgar etkisi kontrolcü tasarımında hesaba katılması gerekmektedir. Tezin bu aşamasında da düzenli rüzgarın bileşenleri İHA'nın dinamiğine dahil edilerek denge noktaları seti elde edilmiş ve böylece elde edilen doğrusal modellerin de düzenli rüzgar bilgisine sahip olması sağlanmıştır. Bu durum her uçuş senaryosunda MÖK'ün düzenli rüzgarın varlığından bilgisinin olmasını sağlayarak minimum hatayla İHA'nın kontrolünün gerçekleştirilmesine imkan vermiştir. İşlemci döngüsü simülasyonları, bir kontrolcü modelinden üretilen kodun gerçek bir hedef donanımda veya işlemcide donanım döngüsü simülasyonları ve/veya gerçek uçuş öncesi test edilmesi açısından oldukça önemlidir. İşlemci döngüsü simülasyonlarında kullanılan hedef donanım olarak BeagleBone Black Rev C marka ve modelli kontrol kartı kullanılmıştır. İlk aşamada kullanılmış olan İHA'ya ait doğrusal olmayan uçak modeli bu simülasyonlarda da herhangi bir farklılık olmadan ele alınmıştır. Simülasyonlarda ilk aşamadan farklı olarak yanal ve boylamsal MÖK'lerin bütün girişlerine (yanal ve boylamsal doğrusal durum uzay modellerinin bütün çıkışlarına) sadece hesaplanan denge noktaları referans olarak verilmiştir. Ayrıca MÖK'lerin girişine herhangi bir ölçülemeyen çıkış ve ölçülemeyen çıkış bozucusu dahil edilmemiş olup, düzenli

rüzgarın daimi olduğu ve 15. saniyede rüzgarın aniden değiştiği bir durum ele alınmıştır. Söz konusu İHA'nın işlemci döngüsü simülasyonlarında aynı 5 uçuş senaryosu için belirtilen rüzgar şartları altındaki dayanıklılığının test edilmesi amaçlanmıştır.

Tezde önerilen çok giriş çok çıkışlı yanal ve boylamsal kısıtlı MÖK'lerin ilk aşamada gerçekleştirilen doğrusal olmayan kapalı çevrim simülasyonlarında olduğu gibi belirtilen rüzgar koşulları altında işlemci döngüsü simülasyonlarında da her uçuş senaryosu için tatmin edici nitelikte uçuş performansı sağladığı gözlemlenmiştir. Karmaşık yörüngeleri takip edebilmesi açısından daha fazla esneklik sağladığı görülen MÖK'lerin, söz konusu işlemci döngüsü simülasyonları sayesinde hedef donanım olarak kullanılan BeagleBone Black Rev C gibi düşük maliyetli ve az yer kaplayan bir kontrol kartına gömülebileceği ve böylece donanım döngüsü simülasyonlarında ve/veya gerçek uçuş testlerinde kullanılabileceği sonucuna varılmıştır.

1. INTRODUCTION

Usage of UAVs have increased in the various civil and military applications in recent years. UAVs are used for battlefield surveillance, reconnaissance, combat, targeting and decoying on military applications. Also they are used in civilian applications for reconnaissance, crop dusting, observations, police surveillance, TV broadcasting, photography, logistics etc. The significance of their usage is extremely high in the way of being able to be used in inhospitable and hazardous environments.

The researches in the beginning of the last century were mostly on auto pilot systems. Altitude and heading holds could be designed before the classical control theory. Much more controllers were designed and implemented to the aircraft in order to assist the pilot in flying by the help of development of classical control theory and the introduction of the jet engine. Thus, control of aircraft has been investigated for a long time [7].

Researches on the recent technologies and controllers for autopilot systems are illustrated in detail by [8]. In practice, the use of PID controller is a popular control method since a zero steady state error and a fast time response can be obtained for a step input reference. PIDs to be unable to cope with the flight envelope is one of the most important disadvantages of their usage. Another disadvantage of PIDs is that they can not ensure enough robustness to model parametric uncertainties particularly occuring in small fixed-wing UAVs. Moreover, time varying properties of the environment have a large influence on nonlinear (NL) coupled dynamics of small sized UAVs. The uncertainties in modelling and external disturbances make the dynamics more challenging for control applications. Hence, recent researchers are focused on NL, intelligent adaptive and robust control laws providing satisfied performance over a large flight envelope even in presence of uncertainties [9]. A baseline and heading controller are publicly available by [2]. The baseline controller is a PI (Proportional–Integral) controller consisting of pitch and roll trackers as well as yaw damper. Similarly, heading controller consists of the same structure except

velocity, altitude and psi trackers as distinct from the baseline controller. Classical PID controllers are implemented and then roll angle controller is redesigned using both H_∞ and μ synthesis by [1]. [10] presents a new strategy to design robust PID controller for uncertain higher-order systems. [11] investigates the feasibility of H_2 and H_1 autopilots for longitudinal UAV control and [12] presents a combined adaptive control law based on shunting method and passification for an UAV autopilot homing guidance system.

Complex algorithms which cause high computational times require high capacity hardware. Also the hardware must not be big in size and expensive. Thus, the decreasing size and cost of microcontrollers besides increasing performance, [13] and [14], makes researchers possible to implement controllers designed to the hardware of UAVs. Implementation successfully to hardware is provided by [15–18]. Being able to change the flight condition from horizontal flight to hover is achieved by means of the proposed neural network adaptive controller [19]. A formation flight is performed by nonlinear dynamic inversion [20]. General adaptive, gain scheduling and intelligent adaptive controls are investigated in [21]. In addition, literature on neural networks for system identification and control are investigated. [22] presents the controller design methods applied to the altitude hold mode autopilot for a non-minimum phase UAV. Three autopilot configurations are proposed and compared in [9]. The first one combines traditional PID control with an H_1 loop shaping approach to assess the robustness characteristics achievable with the PID approach. This configuration limits the required computational power and eases the implementation procedure. The second one proposes an L_1 controller applied to a complete NL UAV aircraft model including model uncertainties and unmodeled dynamics. Application of the controller shows that the L_1 controller is robust to model changes and a gain retuning is not required. The last one presents an autopilot configuration for longitudinal and latero-directional fixed-wing UAV control based on the backstepping technique. The adaptation of an existing backstepping controller for generating an autopilot configuration suitable for mini-UAVs and implementing real-time on a microcontroller board are achieved as the goals of this controller.

In recent years, MPC has been an important control technique in online applications by the help of modern computers. Although MPC is mostly used to control large time scale factory processes such as petroleum refineries and power plants [23], it has been

implemented to dynamic processes with smaller time scales such as aerospace [24] and [25] and automotive industries [26].

The design formulation to have a completely multivariable framework where the performance parameters of the control system can be stated as engineering interests is one of the most important advantages of MPC. In this way, the operations done by the MPC controller can be monitored and evaluated during operation for a system model where the parameters are known and can be adjusted by the user. Also, the controller can be extended from a Single Input Single Output (SISO) controller to a MIMO controller [27]. In addition, MPC has the ability to implement hard and soft constraints on a multivariable system, which provides a system to operate close to its profit margins by placing constraints on the operation of a system [28]. Soft constraints are the simple constraints that would optimize the system but are not implemented at the cost of hard constraints, while hard constraints are the constraints must be adhered. A system to be able to be optimised on-line can be considered as another advantage of MPC. The simplicity of the design framework compared to other techniques is another important advantage. Hence, MPC can be implemented to simple systems such as microcontrollers [28].

Indirect adaptive control using MPC is utilised and tested for height control and autonomous hover of an unmanned helicopter by [23]. [29] presents another application of MPC for an unmanned helicopter with five different models linearized at trim conditions of hover, acceleration and flying up. Nonlinear Model Predictive Controllers (NMPCs) are proposed for fixed wing UAV path tracking [30, 31] and extreme maneuvers [32]. The authors of [30] propose an NMPC for fixed-wing UAV path tracking. The controller is successfully implemented in a dedicated onboard computer installed on an experimental fixed-wing UAV and tested with real-time hardware-in-the-loop simulations. An MPC control scheme is applied to the autopilot for the Aerosonde UAV model by [33]. There is not enough information about the structure of the MPC designed. In the study, only straight and level flight is handled as a flight scenario. Therefore, it is very difficult to have enough information about the performance of the MPC comparing with the MPCs designed in this thesis since they are tested under various flight scenarios. As another MPC application on fixed wing UAVs, [7] designed an MPC for the control of Ariel UAV. It is based on a MIMO Linear

Time Invariant (LTI) state space model derived from the steady wings-level flight trim condition. The inputs of the model are throttle, elevator, aileron and rudder while its outputs are chosen as airspeed and Euler angles. In the study, the bank or roll angle can not be changed by the MPC since the aileron is assumed to be stuck at its initial value. Even though it is not important for the steady wings-level flight, the aileron has to be active especially for turning flight scenarios. Therefore, the MPCs designed in this thesis can handle the flight scenarios including turning maneuver for a fixed wing UAV. Moreover, MPC is used for reference tracking in guidance and navigation applications. The MPCs proposed by [34] track altitude, airspeed and heading or yaw angle while the MPCs proposed by [35] track roll and pitch angles with their rates. However, the MPCs proposed in this thesis provide to track all outputs of linear and longitudinal linear models, which is explained in Chapter 4.

In this thesis, MPC is used as controller of the UAV on the strength of the advantages of MPC mentioned above for the following control objectives as pitch attitude hold, altitude hold, speed hold, roll-angle hold, turn coordination and heading hold. Lateral and longitudinal MIMO MPCs are designed based on lateral and longitudinal linear decoupled models. These linear decoupled models are prefered for the design of the MPCs due to the dynamics of the UAV is highly nonlinear and the cross-coupling effect between the lateral and longitudinal modes is negligible as a result of the UAV model used in the study to be symmetrical about xz plane and designed with conventional aileron, rudder and elevator control surfaces. The linear decoupled models are derived from linearizing the nonlinear model at trim operating points. The trim operating points are obtained for each flight condition by defining trim targets. Straight and level, level climb, level turn, climbing turn and level steady heading sideslip are the flight conditions considered in this thesis.

The performance of the MPCs applied to the NL UAV model is tested under different conditions. Firstly, the performance of them is tested under nominal conditions. Secondly, it is tested under 2 unmeasured outputs (UOs) as linear accelerations in x and z directions (a_x and a_z). Finally, it is tested under 1 unmeasured output disturbance (UOD) on airspeed V_a with a random step-like noise having a magnitude of 1 along with the 2 UOs. The results of the simulations are encouraging [36].

The MPCs designed in this thesis provide to give or change more than one references of the states at any time. In this way, the controller to provide more flexibility in terms of tracking or maneuvering complex trajectories is one of the most important advantages of MPC comparing with the classical controllers, i.e. baseline and heading controllers [2], given in the literature.

Windy conditions are one of the most important parameters in testing performance of controllers. Therefore, the effects of them must be taken into account in design of controllers and controllers must be insensitive or robust to disturbances like winds. A sliding mode controller is designed based on a full NL mathematical model of a fixed wing UAV that includes the stochastic wind effects by [37]. A disturbance observer-based path following controller for small UAVs in the presence of wind is proposed by [38]. [39] presents a simplified back-stepping control law to control the aircraft in case of existing both steady winds and significant discrete wind-gusts.

PIL simulation has an extreme significance on the test of the code generated from a controller model run on an actual target hardware or processor before an HIL simulation or actual flight test to be performed. [15] shows the good prediction to the closed-loop tracking performance obtained from flight tests to be provided by the software in the loop (SIL) and PIL testings. A C code developed for the control blocks is generated from developed model and verified using PIL co-simulation with RTDX by [40]. A PIL implementation is demonstrated on two targets, 127 a Texas Instruments Delfino microcontroller and an ARM Cortex 9 microprocessor by [41]. An embedded MPC to be able to be automatically generated, compiled, and implemented on cost effective off-the-shelf hardware in a short time is proved.

Another study of this thesis is about PIL simulations. The proposed MPCs are used as controller of the UAV for the same control objectives in terms of roll, pitch and yaw attitude, altitude and speed hold along with turn coordination. The performance of the MPCs without any UOs, UODs and measurement noises (MNs) applied to the NL UAV model is tested in the PIL simulations under the windy conditions such as SW and WG while SW components are taken into account to the dynamics of the UAV model in trim calculations. Robustness of the MPCs to the environment effects to be analyzed for each flight scenario and the MPCs to be able to be implemented to real system by means of the PIL simulations are the aim of this last study. It can be

clearly said that the results of the simulations are encouraging for each flight scenario as shown and discussed in Chapter 4.

2. UAV DYNAMICS

2.1 UAV platform

The fixed wing UAV whose nonlinear model used in this thesis is UltraStick 25E as shown in Figure 2.1. The plane has a conventional horizontal and vertical tail with rudder and elevator control surfaces. Also it uses a symmetrical airfoil wing and has both aileron and flap control surfaces [1]. Some important physical parameters are given in Table A.1.

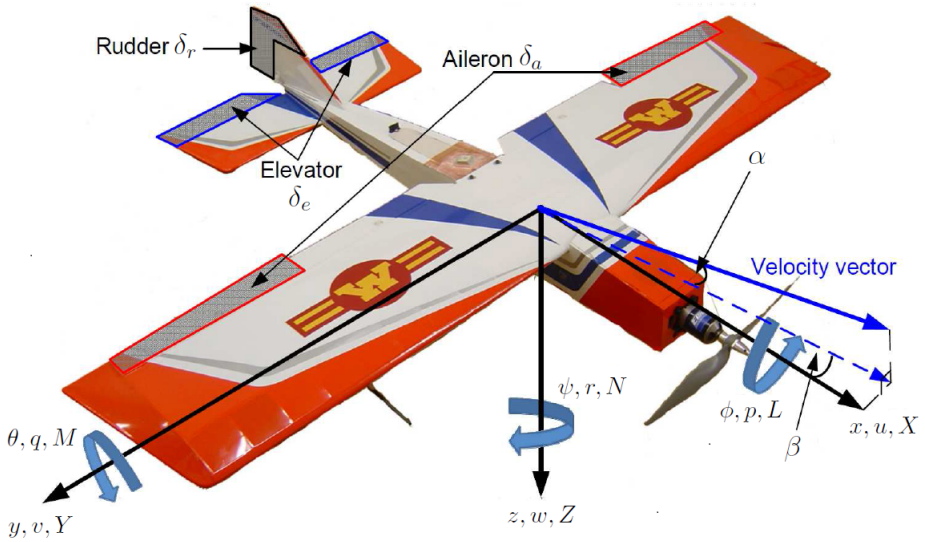

Figure 2.1 : Forces and moments in body axis of Ultra Stick 25E [1].

2.2 Coordinate Frames

Several coordinate systems are defined and described as the inertial frame, the vehicle frame, the vehicle-1 frame, the vehicle-2 frame, the body frame, the stability frame, and the wind frame [3]. A flat, non-rotating earth is assumed through the thesis.

2.2.1 Inertial frame

The inertial frame F^i which is earth-fixed with its origin at the defined home location is known as north-east-down (NED) reference frame. The unit vector $\mathbf{i}^i$ denotes the

north or inertial x direction, $\mathbf{j}^i$ denotes the east or inertial y direction, and $\mathbf{k}^i$ denotes the earth center or inertial z direction as shown in Figure 2.2.

2.2.2 Vehicle frame

The vehicle frame F^v whose origin is located at the center of mass of UAV is aligned with the axis of F^i as shown in Figure 2.2. It is clearly seen that there is a translational transformation between F^i and F^v.

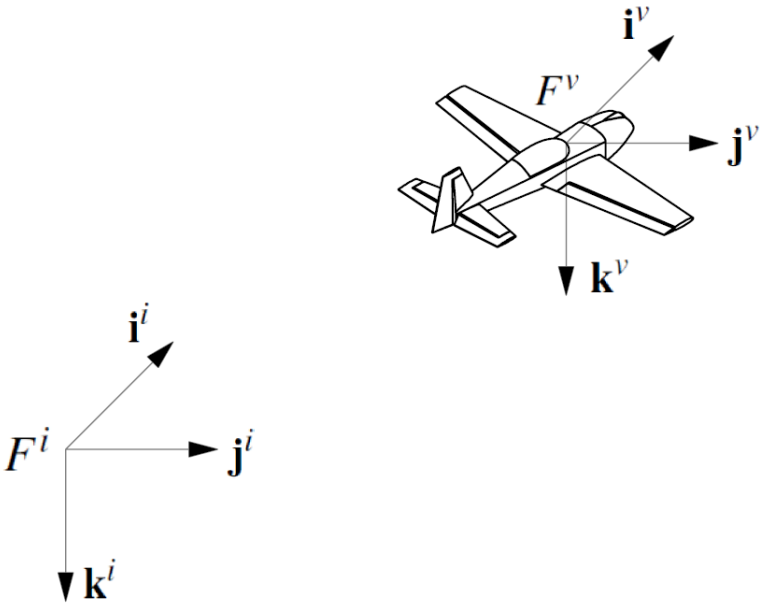

Figure 2.2 : Inertial and vehicle frames.

2.2.3 Vehicle 1 frame

The vehicle 1 frame F^{v1} whose origin is located at the center of mass of UAV is obtained by rotating F^v with the heading (or yaw) angle ψ in a positive right-handed rotation about $\mathbf{k}^v$ as shown in Figure 2.3. It is clearly seen that there is a rotational transformation between F^v and F^{v1} which can be given as follows:

$$\mathbf{p}^{v1} = R_v^{v1}(\psi)\mathbf{p}^v$$

where

$$R_v^{v1}(\psi) = \begin{pmatrix} \cos\psi & \sin\psi & 0 \\ -\sin\psi & \cos\psi & 0 \\ 0 & 0 & 1 \end{pmatrix}$$

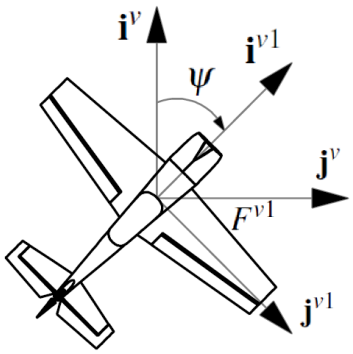

Figure 2.3 : Vehicle 1 frame.

2.2.4 Vehicle 2 frame

The vehicle 2 frame F^{v2} whose origin is located at the center of mass of UAV is obtained by rotating F^{v1} with the pitch angle θ in the positive right-handed direction about $\mathbf{j}^{v1}$ as shown in Figure 2.4. Similarly, there is a rotational transformation between F^{v1} and F^{v2} which can be given as follows:

$$\mathbf{p}^{v2} = R_{v1}^{v2}(\theta)\mathbf{p}^{v1}$$

where

$$R_{v1}^{v2}(\theta) = \begin{pmatrix} \cos\theta & 0 & -\sin\theta \\ 0 & 1 & 0 \\ \sin\theta & 0 & \cos\theta \end{pmatrix}$$

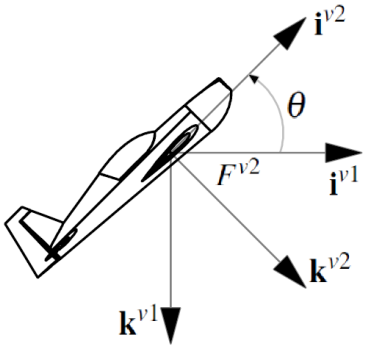

Figure 2.4 : Vehicle 2 frame.

2.2.5 Body frame

The body frame F^b whose origin is located at the center of mass of UAV is obtained by rotating F^{v2} with the roll angle ϕ in a positive right-handed rotation about $\mathbf{i}^{v2}$ as shown in Figure 2.5. Similarly, there is a rotational transformation between F^{v2} and F^b which can be given as follows:

$$\mathbf{p}^b = R^b_{v2}(\phi)\mathbf{p}^{v2}$$

where

$$R^b_{v2}(\phi) = \begin{pmatrix} 1 & 0 & 0 \\ 0 & \cos\phi & \sin\phi \\ 0 & -\sin\phi & \cos\phi \end{pmatrix}$$

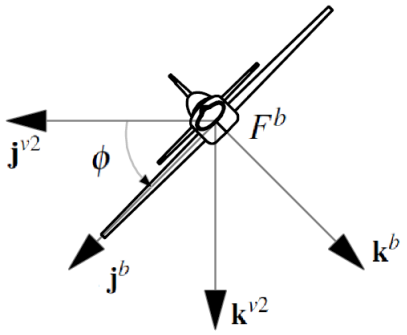

Figure 2.5 : Body frame.

The transformation from F^v to F^b can be given by the following relationship:

$$\begin{aligned} R^b_v(\phi,\theta,\psi) =& R^b_{v2}(\phi)R^{v2}_{v1}(\theta)R^{v1}_v(\psi) \\ =& \begin{pmatrix} 1 & 0 & 0 \\ 0 & \cos\phi & \sin\phi \\ 0 & -\sin\phi & \cos\phi \end{pmatrix} \begin{pmatrix} \cos\theta & 0 & -\sin\theta \\ 0 & 1 & 0 \\ \sin\theta & 0 & \cos\theta \end{pmatrix} \begin{pmatrix} \cos\psi & \sin\psi & 0 \\ -\sin\psi & \cos\psi & 0 \\ 0 & 0 & 1 \end{pmatrix} \\ =& \begin{pmatrix} c\theta c\psi & c\theta s\psi & -s\theta \\ s\phi s\theta c\psi - c\phi s\psi & s\phi s\theta s\psi + c\phi c\psi & s\phi c\theta \\ c\phi s\theta c\psi + s\phi s\psi & c\phi s\theta s\psi - s\phi c\psi & c\phi c\theta \end{pmatrix} \end{aligned} \tag{2.1}$$

where $c_x \triangleq \cos x$ and $s_x \triangleq \sin x$ are used for the shorthand notation. ϕ, θ and ψ are the roll, pitch and yaw angles as the body attitude Euler angles, respectively. They are important to be used for representing the orientation of a body in three dimensions.

2.2.6 Stability frame

The stability frame F^s whose origin is located at the center of mass of UAV is obtained by rotating F^b with the angle of attack α in a left-handed rotation about $\mathbf{j}^b$ as shown in Figure 2.6. Similarly, there is a rotational transformation between F^b and F^s which can be given as follows:

$$\mathbf{p}^s = R^s_b(\alpha)\mathbf{p}^b$$

where

$$R_b^s(\alpha) = \begin{pmatrix} \cos\alpha & 0 & \sin\alpha \\ 0 & 1 & 0 \\ -\sin\alpha & 0 & \cos\alpha \end{pmatrix}$$

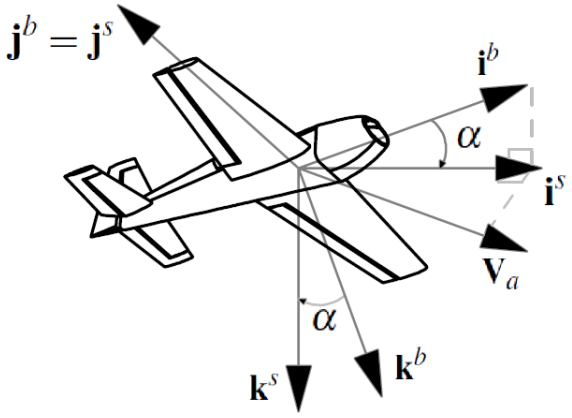

Figure 2.6 : Stability frame.

2.2.7 Wind frame

The wind frame F^w whose origin is located at the center of mass of UAV is obtained by rotating F^s with the side-slip angle β in a right-handed rotation about $\mathbf{k}^s$ as shown in Figure 2.7. Similarly, there is a rotational transformation between F^s and F^w which can be seen as follows:

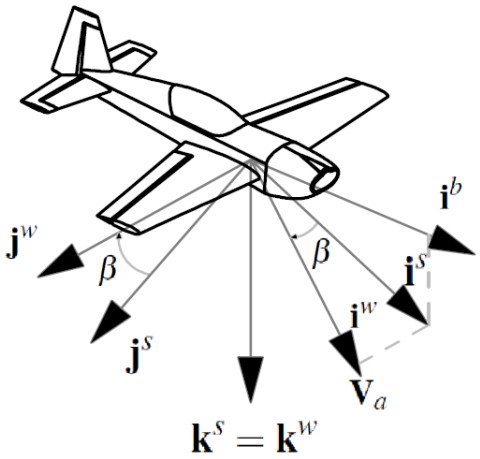

Figure 2.7 : Wind frame.

$$\mathbf{p}^w = R_s^w(\beta)\mathbf{p}^s$$

where

$$R_s^w(\beta) = \begin{pmatrix} \cos\beta & \sin\beta & 0 \\ -\sin\beta & \cos\beta & 0 \\ 0 & 0 & 1 \end{pmatrix}$$

The transformation from F^b to F^w can be expressed as the rotational matrix in Equation 2.2 or from F^w to F^b in Equation 2.3:

$$\begin{aligned} R_b^w(\alpha,\beta) =& R_s^w(\beta)R_b^s(\alpha) \\ =& \begin{pmatrix} \cos\beta & \sin\beta & 0 \\ -\sin\beta & \cos\beta & 0 \\ 0 & 0 & 1 \end{pmatrix} \begin{pmatrix} \cos\alpha & 0 & \sin\alpha \\ 0 & 1 & 0 \\ -\sin\alpha & 0 & \cos\alpha \end{pmatrix} \\ =& \begin{pmatrix} \cos\beta\cos\alpha & \sin\beta & \cos\beta\sin\alpha \\ -\sin\beta\cos\alpha & \cos\beta & -\sin\beta\sin\alpha \\ -\sin\alpha & 0 & \cos\alpha \end{pmatrix} \end{aligned} \tag{2.2}$$

$$R_w^b(\alpha,\beta) = (R_b^w)^T(\alpha,\beta) = \begin{pmatrix} \cos\beta\cos\alpha & -\sin\beta\cos\alpha & -\sin\alpha \\ \sin\beta & \cos\beta & 0 \\ \cos\beta\sin\alpha & -\sin\beta\sin\alpha & \cos\alpha \end{pmatrix} \tag{2.3}$$

2.3 UAV Speeds

The rotational matrices obtained so far is important from the standpoint of the inertial forces generated by the UAV to be a function of velocities and accelerations relative to the F^i, while the aerodynamic forces to be a function of the velocity of the airframe relative to the surrounding air F^w. The relationship between airspeed $\mathbf{V}_a$, ground speed $\mathbf{V}_g$ and wind speed $\mathbf{V}_w$, which is called as wind triangle, can be given as follows [3]:

$$\mathbf{V}_a = \mathbf{V}_g - \mathbf{V}_w \tag{2.4}$$

where $\mathbf{V}_a$ is the velocity of UAV with respect to the surrounding air F^w as in Equation 2.5, $\mathbf{V}_g$ is the velocity of UAV with respect to F^i, and $\mathbf{V}_w$ is the velocity of wind with respect to F^i, which is in the range of 20-50 % of $\mathbf{V}_a$, as in Equation 2.6.

$$\mathbf{V}_a^w = \begin{pmatrix} V_a \\ 0 \\ 0 \end{pmatrix} \tag{2.5}$$

$$\mathbf{V}_w^v = \begin{pmatrix} w_n \\ w_e \\ w_d \end{pmatrix} \tag{2.6}$$

$\mathbf{V}_g$ and $\mathbf{V}_w$ can be expressed in F^b as follows:

$$\mathbf{V}_g^b = \begin{pmatrix} u \\ v \\ w \end{pmatrix} \tag{2.7}$$

$$\mathbf{V}_w^b = \begin{pmatrix} u_w \\ v_w \\ w_w \end{pmatrix} = R_v^b(\phi, \theta, \psi) \begin{pmatrix} w_n \\ w_e \\ w_d \end{pmatrix} \tag{2.8}$$

Substituting Equation 2.7 and 2.8 into 2.4, $\mathbf{V}_a$ can be obtained in F^b in terms of u_r, v_r and w_r as follows:

$$\begin{aligned} \mathbf{V}_a^b = \begin{pmatrix} u_r \\ v_r \\ w_r \end{pmatrix} = \begin{pmatrix} u - u_w \\ v - v_w \\ w - w_w \end{pmatrix} &= R_w^b(\alpha, \beta) \begin{pmatrix} V_a \\ 0 \\ 0 \end{pmatrix} \\ &= \begin{pmatrix} \cos\beta\cos\alpha & -\sin\beta\cos\alpha & -\sin\alpha \\ \sin\beta & \cos\beta & 0 \\ \cos\beta\sin\alpha & -\sin\beta\sin\alpha & \cos\alpha \end{pmatrix} \begin{pmatrix} V_a \\ 0 \\ 0 \end{pmatrix} \\ &= V_a \begin{pmatrix} \cos\beta\cos\alpha \\ \sin\beta \\ \cos\beta\sin\alpha \end{pmatrix} \end{aligned} \tag{2.9}$$

The aerodynamic forces and moments are calculated by the help of u_r, v_r and w_r. u, v and w which are the states of UAV are obtained from the solution of the equations of motion. u_w, v_w and w_w which are the speed components of a wind model are the inputs of the equations of motion. From the Equation 2.9, the following expressions can be obtained:

$$V_a = \sqrt{u_r^2 + v_r^2 + w_r^2} \tag{2.10}$$

$$\alpha = \tan^{-1}\left(\frac{w_r}{u_r}\right) \tag{2.11}$$

$$\beta = \sin^{-1}\left(\frac{v_r}{\sqrt{u_r^2 + v_r^2 + w_r^2}}\right) \tag{2.12}$$

When there is a wind whose speed is different from zero, the course angle χ and the inertial (referenced) flight path angle γ are the angles which are used to specify the direction of $\mathbf{V}_g$ vector. χ is defined as the angle between true north $\mathbf{i}^i$ and $\mathbf{V}_g$ as can be seen in Figure 2.8. It is the direction of travel of UAV relative to the earth's surface. γ is the angle between the horizontal plane and $\mathbf{V}_g$ as in Figure 2.9. It is very significant to provide the information about where the UAV is heading in vertical plane [42].

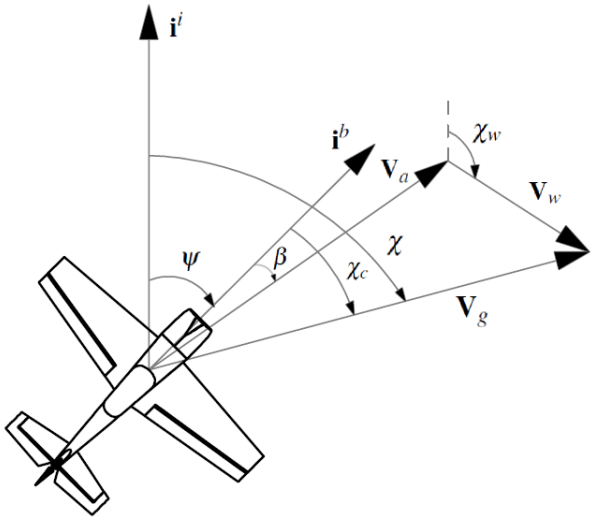

Figure 2.8 : Wind triangle in horizontal plane.

The crab angle χ_c, which is the angle between χ and ψ as shown in Equation 2.13, and χ_w, which is the angle between true north $\mathbf{i}^i$ and $\mathbf{V}_w$, both occur when there is a constant wind. If not, they are zero.

$$\chi_c \triangleq \chi - \psi \tag{2.13}$$

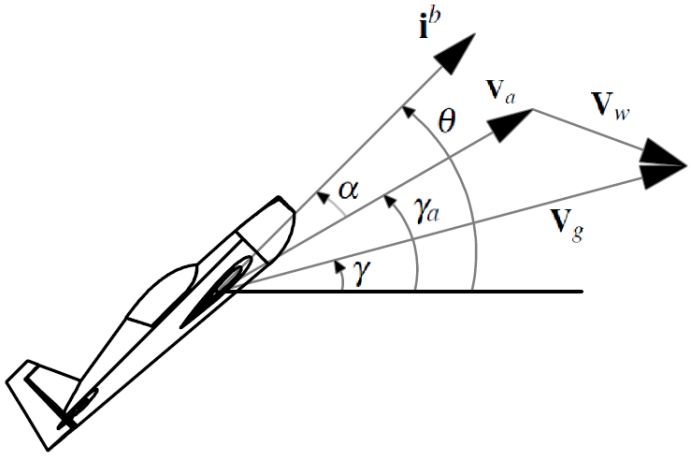

Figure 2.9 : Wind triangle in vertical plane.

As can be seen in Figure 2.9, air-mass-referenced flight-path angle γ_a which is the angle between the horizontal plane and $\mathbf{V}_a$ occurs in case of presence of a down component of wind. It can be simply expressed as follows:

$$\gamma_a = \theta - \alpha \tag{2.14}$$

$\mathbf{V}_g$ and $\mathbf{V}_a$ in F^i can be written as follows:

$$\begin{aligned}\mathbf{V}_g^i = R_{v1}^v(\chi)R_{v2}^{v1}(\gamma)\mathbf{V}_g^b &= \begin{pmatrix}\cos\chi & -\sin\chi & 0\\ \sin\chi & \cos\chi & 0\\ 0 & 0 & 1\end{pmatrix}\begin{pmatrix}\cos\gamma & 0 & \sin\gamma\\ 0 & 1 & 0\\ -\sin\gamma & 0 & \cos\gamma\end{pmatrix}\begin{pmatrix}V_g\\ 0\\ 0\end{pmatrix}\\ &= V_g\begin{pmatrix}\cos\chi\cos\gamma\\ \sin\chi\cos\gamma\\ -\sin\gamma\end{pmatrix}\end{aligned} \tag{2.15}$$

$$\begin{aligned}\mathbf{V}_a^i = R_{v1}^v(\psi)R_{v2}^{v1}(\gamma_a)\mathbf{V}_a^b &= \begin{pmatrix}\cos\psi & -\sin\psi & 0\\ \sin\psi & \cos\psi & 0\\ 0 & 0 & 1\end{pmatrix}\begin{pmatrix}\cos\gamma_a & 0 & \sin\gamma_a\\ 0 & 1 & 0\\ -\sin\gamma_a & 0 & \cos\gamma_a\end{pmatrix}\begin{pmatrix}V_a\\ 0\\ 0\end{pmatrix}\\ &= V_a\begin{pmatrix}\cos\psi\cos\gamma_a\\ \sin\psi\cos\gamma_a\\ -\sin\gamma_a\end{pmatrix}\end{aligned} \tag{2.16}$$

The wind triangle can be obtained in F^i from Equation 2.15 and 2.16 as follows:

$$\begin{aligned}\mathbf{V}_a^i &= \mathbf{V}_g^i - \mathbf{V}_w^i\\ V_a\begin{pmatrix}\cos\psi\cos\gamma_a\\ \sin\psi\cos\gamma_a\\ -\sin\gamma_a\end{pmatrix} &= V_g\begin{pmatrix}\cos\chi\cos\gamma\\ \sin\chi\cos\gamma\\ -\sin\gamma\end{pmatrix} - \begin{pmatrix}w_n\\ w_e\\ w_d\end{pmatrix}\end{aligned} \tag{2.17}$$

γ_a is obtained by solving the equation above as follows:

$$\gamma_a = \arcsin\left(\frac{V_g\sin\gamma + w_d}{V_a}\right) \tag{2.18}$$

Alternatively, γ_a and γ can be expressed in the presence of wind as follows [42]:

$$\gamma_a = -\arcsin\left(\frac{V_a}{V_g}\left(-\sin\theta\cos\alpha\cos\beta + \sin\phi\cos\theta\sin\beta + \cos\phi\cos\theta\sin\alpha\cos\beta\right)\right) \tag{2.19}$$

$$\gamma = -\arcsin\left(\frac{V_a}{V_g}\left(-\sin\theta\cos\alpha\cos\beta + \sin\phi\cos\theta\sin\beta + \cos\phi\cos\theta\sin\alpha\cos\beta + w_d\right)\right) \tag{2.20}$$

As it can be easily seen from Equations 2.19 and 2.20 along with Figure 2.9 that $\gamma = \gamma_a$ in case of the absence of wind.

2.4 Kinematics

The translational velocity of the UAV is commonly expressed in terms of the velocity in F^b while the translational position of the UAV, p_n, p_e and p_d, is usually measured and expressed in F^i. Therefore differentiation and a rotational transformation from F^b to F^v is required for obtaining the velocity in F^i as shown in the following expression [3]:

$$\begin{aligned} \frac{d}{dt}\begin{pmatrix} p_n \\ p_e \\ p_d \end{pmatrix} &= \left(R_v^b\right)^T \begin{pmatrix} u \\ v \\ w \end{pmatrix} \\ \begin{pmatrix} \dot{p_n} \\ \dot{p_e} \\ \dot{p_d} \end{pmatrix} &= \begin{pmatrix} c_\theta c_\psi & s_\phi s_\theta c_\psi - c_\phi s_\psi & c_\phi s_\theta c_\psi + s_\phi s_\psi \\ c_\theta s_\psi & s_\phi s_\theta s_\psi + c_\phi c_\psi & c_\phi s_\theta s_\psi - s_\phi c_\psi \\ -s_\theta & s_\phi c_\theta & c_\phi c_\theta \end{pmatrix} \begin{pmatrix} u \\ v \\ w \end{pmatrix} \end{aligned} \tag{2.21}$$

The following navigation equations can be written from Equation 2.21 as follows:

$$\dot{p_n} = u(c_\theta c_\psi) + v(s_\phi s_\theta c_\psi - c_\phi s_\psi) + w(c_\phi s_\theta c_\psi + s_\phi s_\psi) \tag{2.22}$$

$$\dot{p_e} = u(c_\theta s_\psi) + v(s_\phi s_\theta s_\psi + c_\phi c_\psi) + w(c_\phi s_\theta s_\psi - s_\phi c_\psi) \tag{2.23}$$

$$\dot{p_d} = -\dot{h} = -u(s_\theta) + v(s_\phi c_\theta) + w(c_\phi c_\theta) \tag{2.24}$$

There is a relationship between Euler angles (angular positions), which are defined in F^b, F^{v2} and F^{v1}, and angular rates, which are defined in F^b. Thus, angular rates are expressed in terms of the derivative of Euler angles in F^b as follows:

$$\begin{aligned} \begin{pmatrix} p \\ q \\ r \end{pmatrix} &= \begin{pmatrix} \dot{\phi} \\ 0 \\ 0 \end{pmatrix} + R_{v2}^b(\phi) \begin{pmatrix} 0 \\ \dot{\theta} \\ 0 \end{pmatrix} + R_{v2}^b(\phi) R_{v1}^{v2}(\theta) \begin{pmatrix} 0 \\ 0 \\ \dot{\psi} \end{pmatrix} \\ &= \begin{pmatrix} \dot{\phi} \\ 0 \\ 0 \end{pmatrix} + \begin{pmatrix} 1 & 0 & 0 \\ 0 & \cos\phi & \sin\phi \\ 0 & -\sin\phi & \cos\phi \end{pmatrix} \begin{pmatrix} 0 \\ \dot{\theta} \\ 0 \end{pmatrix} \\ &\quad + \begin{pmatrix} 1 & 0 & 0 \\ 0 & \cos\phi & \sin\phi \\ 0 & -\sin\phi & \cos\phi \end{pmatrix} \begin{pmatrix} \cos\theta & 0 & -\sin\theta \\ 0 & 1 & 0 \\ \sin\theta & 0 & \cos\theta \end{pmatrix} \begin{pmatrix} 0 \\ 0 \\ \dot{\psi} \end{pmatrix} \\ &= \begin{pmatrix} 1 & 0 & -\sin\theta \\ 0 & \cos\phi & \sin\phi\cos\theta \\ 0 & -\sin\phi & \cos\phi\cos\theta \end{pmatrix} \begin{pmatrix} \dot{\phi} \\ \dot{\theta} \\ \dot{\psi} \end{pmatrix} \end{aligned} \tag{2.25}$$

or

$$\begin{pmatrix} \dot{\phi} \\ \dot{\theta} \\ \dot{\psi} \end{pmatrix} = \begin{pmatrix} 1 & \sin\phi\tan\theta & \cos\phi\tan\theta \\ 0 & \cos\phi & -\sin\phi \\ 0 & \sin\phi\sec\theta & \cos\phi\sec\theta \end{pmatrix} \begin{pmatrix} p \\ q \\ r \end{pmatrix} \tag{2.26}$$

The following kinematic equations can be written from Equation 2.26 as follows:

$$\dot{\phi} = p + \tan\theta(q\sin\phi + r\cos\phi) \tag{2.27}$$

$$\dot{\theta} = q\cos\phi - r\sin\phi \tag{2.28}$$

$$\dot{\psi} = \frac{q\sin\phi + r\cos\phi}{\cos\phi} \tag{2.29}$$

2.5 Dynamics

Newton's 2^{nd} law is applied to derive the equations of motion of UAV. Motion of UAV is referenced to a fixed reference frame, which means inertial reference frame. Also it can be referenced to other frames like body frame particularly used for $\mathbf{V}_g^b$ [3].

2.5.1 Translational motion

A UAV which is in translational motion can be expressed with respect to the Newton's 2^{nd} law as follows:

$$m\left(\frac{d\mathbf{V}_g}{dt}\right)_i = \mathbf{f} \tag{2.30}$$

where $\mathbf{f}$ is the total external forces acting on UAV including gravity, aerodynamic and propulsion forces. $\left(\frac{d}{dt}\right)_i$ is the time derivative with respect to F^i. Thus, derivative of V_g with respect to F^i can be obtained in terms of the derivative in body frame and angular velocity as follows:

$$\left(\frac{d\mathbf{V}_g}{dt}\right)_i = \left(\frac{d\mathbf{V}_g}{dt}\right)_b + \omega_{b/i} \times \mathbf{V}_g \tag{2.31}$$

where $\omega_{b/i}$ is the angular velocity of UAV with respect to F^i. The following equation can be obtained by substituting Equation 2.31 into Equation 2.30:

$$m\left(\left(\frac{d\mathbf{V}_g}{dt}\right)_b + \omega_{b/i} \times \mathbf{V}_g\right) = \mathbf{f} \tag{2.32}$$

Newton's 2^{nd} law can be rewritten in F^b by means of $\mathbf{V}_g$, $\omega_{b/i}$ and $\mathbf{f}$ in F^b as follows:

$$m\left(\left(\frac{d\mathbf{V}_g^b}{dt}\right)_b + \omega_{b/i}^b \times \mathbf{V}_g^b\right) = \mathbf{f}^b \tag{2.33}$$

where $\mathbf{V}_g^b = (u,v,w)^T$, $\omega_{b/i}^b = (p,q,r)^T$ and $\mathbf{f}^b = (X,Y,Z)^T$. Lastly, Equation 2.33 can be rewritten as follows:

$$\begin{gathered}\frac{d}{dt}\begin{pmatrix}u\\v\\w\end{pmatrix} + \begin{pmatrix}p\\q\\r\end{pmatrix} \times \begin{pmatrix}u\\v\\w\end{pmatrix} = \frac{1}{m}\begin{pmatrix}X\\Y\\Z\end{pmatrix} \\ \begin{pmatrix}\dot{u}\\\dot{v}\\\dot{w}\end{pmatrix} = \begin{pmatrix}rv-qw\\pw-ru\\qu-pv\end{pmatrix} + \frac{1}{m}\begin{pmatrix}X\\Y\\Z\end{pmatrix}\end{gathered} \tag{2.34}$$

2.5.2 Rotational motion

Newton's 2^{nd} law can be expressed in terms of angular momentum $\mathbf{h}$ and total external moments about center of UAV $\mathbf{m}$ in F^i as follows:

$$\left(\frac{d\mathbf{h}}{dt}\right)_i = \mathbf{m} \tag{2.35}$$

Similarly, the Newton's 2^{nd} law expression for rotational motion above can be obtained with respect to F^b as follows:

$$\left(\frac{d\mathbf{h}^b}{dt}\right)_b + \omega_{b/i}^b \times \mathbf{h}^b = \mathbf{m}^b \tag{2.36}$$

where $\mathbf{m}^b \triangleq (L,M,N)^T$ and $\mathbf{h}^b \triangleq \mathbf{J}\omega_{b/i}^b$ along with $\mathbf{J}$ which is inertia matrix can be given as follows:

$$\mathbf{J} = \begin{pmatrix} J_x & -J_{xy} & -J_{xz} \\ -J_{xy} & J_y & -J_{yz} \\ -J_{xz} & -J_{yz} & J_z \end{pmatrix} \tag{2.37}$$

where the diagonal terms J_x, J_y and J_z are the moment of inertia. The remaining terms are called as product of inertia. $\mathbf{J}$ is calculated by using UAV CAD model or determined by using bifilar pendulum method ([43] and [44]). UAV is assumed to be symmetrical about the plane spanned by $\mathbf{i}^b$ and $\mathbf{k}^b$ which provides $J_{xy} = J_{yz} = 0$ and makes Equation 2.37 simplified as in Equation 2.38. Thus, inverse of $\mathbf{J}$ is obtained as

can be seen in Equation 2.39.

$$\mathbf{J} = \begin{pmatrix} J_x & 0 & -J_{xz} \\ 0 & J_y & 0 \\ -J_{xz} & 0 & J_z \end{pmatrix} \tag{2.38}$$

$$\mathbf{J}^{-1} = \begin{pmatrix} \frac{J_z}{\Gamma} & 0 & \frac{J_{xz}}{\Gamma} \\ 0 & \frac{1}{J_y} & 0 \\ \frac{J_{xz}}{\Gamma} & 0 & \frac{J_x}{\Gamma} \end{pmatrix} \tag{2.39}$$

where $\Gamma = J_x J_z - J_{xz}^2$. Substituting $\mathbf{h}^b \triangleq \mathbf{J}\omega_{b/i}^b$ and $\mathbf{m}^b \triangleq (L,M,N)^T$ into Equation 2.36:

$$\begin{aligned} \left(\frac{d\left(\mathbf{J}\omega_{b/i}^b\right)}{dt}\right)_b + \omega_{b/i}^b \times \mathbf{J}\omega_{b/i}^b &= \mathbf{m}^b \\ \omega_{b/i}^b \cancelto{0}{\left(\frac{d\mathbf{J}}{dt}\right)_b} + \mathbf{J}\left(\frac{d\omega_{b/i}^b}{dt}\right)_b + \omega_{b/i}^b \times \mathbf{J}\omega_{b/i}^b &= \mathbf{m}^b \\ \mathbf{J}\left(\frac{d}{dt}\begin{pmatrix} p \\ q \\ r \end{pmatrix}\right)_b + \begin{pmatrix} p \\ q \\ r \end{pmatrix} \times \mathbf{J}\begin{pmatrix} p \\ q \\ r \end{pmatrix} &= \begin{pmatrix} L \\ M \\ N \end{pmatrix} \\ \mathbf{J}^{-1}\left(\begin{pmatrix} L \\ M \\ N \end{pmatrix} - \begin{pmatrix} p \\ q \\ r \end{pmatrix} \times \mathbf{J}\begin{pmatrix} p \\ q \\ r \end{pmatrix}\right) &= \begin{pmatrix} \dot{p} \\ \dot{q} \\ \dot{r} \end{pmatrix} \end{aligned} \tag{2.40}$$

The following expression of $(\dot{p},\dot{q},\dot{r})^T$ can be obtained by substituting Equation 2.38 and 2.39 into 2.40:

$$\begin{aligned} \begin{pmatrix} \dot{p} \\ \dot{q} \\ \dot{r} \end{pmatrix} &= \begin{pmatrix} \frac{J_z}{\Gamma} & 0 & \frac{J_{xz}}{\Gamma} \\ 0 & \frac{1}{J_y} & 0 \\ \frac{J_{xz}}{\Gamma} & 0 & \frac{J_x}{\Gamma} \end{pmatrix} \left(\begin{pmatrix} L \\ M \\ N \end{pmatrix} - \begin{pmatrix} p \\ q \\ r \end{pmatrix} \times \begin{pmatrix} J_x & 0 & -J_{xz} \\ 0 & J_y & 0 \\ -J_{xz} & 0 & J_z \end{pmatrix} \begin{pmatrix} p \\ q \\ r \end{pmatrix}\right) \\ &= \begin{pmatrix} \frac{J_z}{\Gamma} & 0 & \frac{J_{xz}}{\Gamma} \\ 0 & \frac{1}{J_y} & 0 \\ \frac{J_{xz}}{\Gamma} & 0 & \frac{J_x}{\Gamma} \end{pmatrix} \left(\begin{pmatrix} J_{xz}pq + (J_y - J_z)qr \\ J_{xz}(r^2 - p^2) + (J_z - J_x)pr \\ (J_x - J_y)pq - J_{xz}qr \end{pmatrix} + \begin{pmatrix} L \\ M \\ N \end{pmatrix}\right) \\ &= \begin{pmatrix} \Gamma_1 pq - \Gamma_2 qr + \Gamma_3 L + \Gamma_4 N \\ \Gamma_5 pr - \Gamma_6(p^2 - r^2) + \frac{1}{J_y}M \\ \Gamma_7 pq - \Gamma_1 qr + \Gamma_4 L + \Gamma_8 N \end{pmatrix} \end{aligned} \tag{2.41}$$

where

$$\Gamma_1 = \frac{J_{xz}(J_x - J_y + J_z)}{\Gamma} \quad \Gamma_2 = \frac{J_z(J_z - J_y) + J_{xz}^2}{\Gamma}$$

$$\Gamma_3 = \frac{J_z}{\Gamma} \quad \Gamma_4 = \frac{J_{xz}}{\Gamma}$$

$$\Gamma_5 = \frac{J_z - J_x}{J_y} \quad \Gamma_6 = \frac{J_{xz}}{J_y}$$

$$\Gamma_7 = \frac{J_x(J_x - J_y) + J_{xz}^2}{\Gamma} \quad \Gamma_8 = \frac{J_x}{\Gamma}$$

The nominal, lower and upper bound values for the moment of inertia of the UAV and the propulsion system can be found in Table A.2.

2.5.3 Forces and moments

Forces have three components in terms of gravitational $\mathbf{f}_g$, aerodynamic $\mathbf{f}_a$ and propulsion $\mathbf{f}_p$ while moments have 2 components in terms of aerodynamic $\mathbf{m}_a$ and propulsion $\mathbf{m}_p$.

2.5.4 Gravitational force

Gravitational force $\mathbf{f}_g$ which is a function of m and gravitational acceleration g acts in the direction of $\mathbf{k}^i$ in F^v as expressed below:

$$\mathbf{f}_g^v = \begin{pmatrix} 0 \\ 0 \\ mg \end{pmatrix} \tag{2.42}$$

Since $\mathbf{f}$ is expressed in F_b, $\mathbf{f}_g^v$ must be written in F_b by means of rotation from F_v to F_b as follows:

$$\begin{aligned} \mathbf{f}_g^b = R_v^b \begin{pmatrix} 0 \\ 0 \\ mg \end{pmatrix} &= \begin{pmatrix} c\theta c\psi & c\theta s\psi & -s\theta \\ s\phi s\theta c\psi - c\phi s\psi & s\phi s\theta s\psi + c\phi c\psi & s\phi c\theta \\ c\phi s\theta c\psi + s\phi s\psi & c\phi s\theta s\psi - s\phi c\psi & c\phi c\theta \end{pmatrix} \begin{pmatrix} 0 \\ 0 \\ mg \end{pmatrix} \\ &= \begin{pmatrix} -mg\sin\theta \\ mg\cos\theta\sin\phi \\ mg\cos\theta\cos\phi \end{pmatrix} \end{aligned} \tag{2.43}$$

2.5.5 Aerodynamic forces and moments

Aerodynamic forces are lift and drag forces which are used to define the effect of the pressure acting on the body of UAV. They are the functions of aerodynamic pressure $\overline{q}$, planform area of the UAV S and aerodynamic coefficients and can be expressed along

with aerodynamic moment as follows:

$$\begin{aligned} F_{lift} &= \overline{q}SC_L = \frac{1}{2}\rho V_a^2 SC_L \\ F_{drag} &= \overline{q}SC_D = \frac{1}{2}\rho V_a^2 SC_D \\ M_a &= \overline{q}ScC_m = \frac{1}{2}\rho V_a^2 ScC_m \end{aligned} \tag{2.44}$$

where ρ is air density. C_L, C_D and C_m are the nondimensional aerodynamic coefficients which may be able to be specified in F^w and F^b. They are essentially dependent on α and β along with their rates, p, q, r, V_a, surface deflections, engine power level, configuration effects and ground-proximity effects [45].

Aerodynamic forces and moments are decomposed into longitudinal and lateral. Longitudinal forces involve lift and drag forces which act in the direction of $\mathbf{i}^b$ and $\mathbf{k}^b$, respectively as indicated in Figure 2.10. There is one component of longitudinal moment acting about $\mathbf{j}^b$ axis. Lateral force acts in the direction of $\mathbf{j}^b$ while moments about $\mathbf{i}^b$ and $\mathbf{k}^b$ axes.

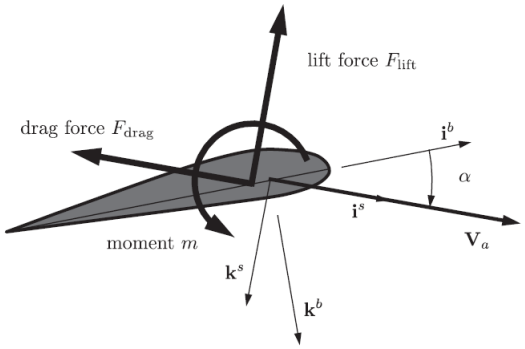

Figure 2.10 : Longitudinal aerodynamic forces and moments [3].

2.5.5.1 Longitudinal aerodynamic forces and moment

The motion is in $\mathbf{i}^b - \mathbf{k}^b$ plane which is called as pitch plane in case of acting longitudinal aerodynamic forces and moment on UAV. The lift and drag forces which are in F^s along with the pitch moment as can be seen in Figure 2.10 can be expressed as follows:

$$\begin{aligned} F_{lift} &= \frac{1}{2}\rho V_a^2 SC_L \\ F_{drag} &= \frac{1}{2}\rho V_a^2 SC_D \\ M_a &= \frac{1}{2}\rho V_a^2 ScC_m \end{aligned} \tag{2.45}$$

The forces and moment in Equation 2.45 are mostly nonlinear. They can be linearised by using Taylor series approximations under the assumption of the flow over the wing

to remain laminar and be attached for small α. For instance, lift force can be linearised as follows:

$$F_{lift} = \frac{1}{2}\rho V_a^2 S\left(C_{L_0} + \frac{\partial C_L}{\partial \alpha}\alpha + \frac{\partial C_L}{\partial \dot{\alpha}}\dot{\alpha} + \frac{\partial C_L}{\partial q}q + \frac{\partial C_L}{\partial \delta_e}\delta_e\right) \tag{2.46}$$

where δ_e is elevator deflection. The nondimensional aerodynamic coefficient C_{L_0} is the value of the C_L in case of $\alpha = \dot{\alpha} = q = \delta_e = 0$. C_L, α and δ_e are nondimensional since their units are in radians while $\dot{\alpha}$ and q are not since their units are in rad/s. Therefore $\frac{c}{2V_a}$ is used as a common unit factor to nondimensionalise the related terms. Rewriting the Equation 2.46 with respect to this phenomena gives the following equation [1]:

$$F_{lift} = \frac{1}{2}\rho V_a^2 S\left(C_{L_0} + C_{L_\alpha}\alpha + C_{L_{\delta_e}}\delta_e + \frac{c}{2V_a}\left(C_{L_{\dot{\alpha}}}\dot{\alpha} + C_{L_q}q\right)\right) \tag{2.47}$$

where $C_{L_\alpha} \triangleq \frac{\partial C_L}{\partial \alpha}$, $C_{L_{\delta_e}} \triangleq \frac{\partial C_L}{\partial \delta_e}$, $C_{L_{\dot{\alpha}}} \triangleq \frac{\partial C_L}{\partial \frac{c}{2V_a}}$ and $C_{L_q} \triangleq \frac{\partial C_L}{\partial \frac{c}{2V_a}}$. Similarly, all nondimensional aerodynamic coefficients are obtained by the same method. Drag force and moment can be obtained in the same way as follows:

$$F_{drag} = \frac{1}{2}\rho V_a^2 S\left(C_{D_0} + C_{D_{\delta e}}\delta e + C_{D_{\delta r}}\delta r + \frac{(C_L - C_{L_{min}})}{\pi.e.AR}\right) \tag{2.48}$$

$$M_a = \frac{1}{2}\rho V_a^2 Sc\left(C_{m_0} + C_{m_\alpha}\alpha + C_{m_{\delta_e}}\delta_e + \frac{c}{2V_a}\left(C_{m_{\dot{\alpha}}}\dot{\alpha} + C_{m_q}q\right)\right) \tag{2.49}$$

where δ_r is rudder deflection and e is the Oswald efficiency factor having a value of 0.75 in this thesis. AR is the wing aspect ratio with $\frac{1}{\pi.e.AR} = 0.0815$ [46].
The lift and drag forces obtained in Equation 2.47 and 2.48 must be expressed in F^b by means of a rotation about α from F^s as follows:

$$\begin{aligned}\begin{pmatrix} X_a \\ Z_a \end{pmatrix} &= \begin{pmatrix} \cos\alpha & -\sin\alpha \\ \sin\alpha & \cos\alpha \end{pmatrix}\begin{pmatrix} -F_{drag} \\ -F_{lift} \end{pmatrix} \\ &= \frac{1}{2}\rho V_a^2 S\begin{pmatrix} C_X \\ C_Z \end{pmatrix}\end{aligned} \tag{2.50}$$

where

$$\begin{aligned} C_X &= C_L\sin\alpha - C_D\cos\alpha \\ C_Z &= -C_D\sin\alpha - C_L\cos\alpha \end{aligned} \tag{2.51}$$

in terms of C_L and C_D below:

$$\begin{aligned} C_L &= C_{L_0} + C_{L_\alpha}\alpha + C_{L_{\delta_e}}\delta_e + \frac{c}{2V_a}\left(C_{L_{\dot{\alpha}}}\dot{\alpha} + C_{L_q}q\right) \\ C_D &= C_{D_0} + C_{D_{\delta e}}\delta e + C_{D_{\delta r}}\delta r + \frac{(C_L - C_{L_{min}})}{\pi.e.AR} \end{aligned} \tag{2.52}$$

2.5.5.2 Lateral aerodynamic force and moments

The type of motion is translational which occurs in case of acting lateral aerodynamic force and moments on UAV . The lateral force F_{a_y} and moments L and N can be expressed as follows:

$$\begin{aligned} Y_a &= \frac{1}{2}\rho V_a^2 S C_Y \\ &= \frac{1}{2}\rho V_a^2 S \left(C_{Y_\beta}\beta + C_{Y_{\delta r}}\delta_r + \frac{b}{2V_a}\left(C_{Y_p}p + C_{Y_r}r\right)\right) \end{aligned} \tag{2.53}$$

$$\begin{aligned} L_a &= \frac{1}{2}\rho V_a^2 S b C_l \\ &= \frac{1}{2}\rho V_a^2 S b \left(C_{l_\beta} + C_{l_{\delta_a}}\delta_a + C_{l_{\delta_r}}\delta_r + \frac{b}{2V_a}\left(C_{l_p}p + C_{l_r}r\right)\right) \end{aligned} \tag{2.54}$$

$$\begin{aligned} N_a &= \frac{1}{2}\rho V_a^2 S b C_n \\ &= \frac{1}{2}\rho V_a^2 S b \left(C_{n_\beta} + C_{n_{\delta_a}}\delta_a + C_{n_{\delta_r}}\delta_r + \frac{b}{2V_a}\left(C_{n_p}p + C_{n_r}r\right)\right) \end{aligned} \tag{2.55}$$

where δ_a is combined aileron deflection. The nondimensional aerodynamic coefficients are summarized in Table 2.1. They are necessary for modeling of the UAV, i.e. Ultrastick 25e used in this thesis. Their numerical values can be found in Table A.3.

Table 2.1 : Aerodynamic coefficients.

Lift Force	Drag Force	Side Force	Roll moment	Pitch moment	Yaw moment
C_{L_0}	C_{D_0}	C_{Y_β}	C_{l_β}	C_{m_0}	C_{n_β}
C_{L_α}	$C_{D_{\delta e}}$	$C_{Y_{\delta r}}$	$C_{l_{\delta r}}$	C_{m_α}	$C_{n_{\delta r}}$
$C_{L_{\dot{\alpha}}}$	$C_{D_{\delta r}}$	C_{Y_p}	C_{l_p}	$C_{m_{\delta e}}$	C_{n_p}
C_{L_q}		C_{Y_r}	C_{l_r}	$C_{m_{\dot{\alpha}}}$	C_{n_r}
$C_{L_{min}}$			$C_{l_{\delta a}}$	C_{m_q}	
$C_{L_{\delta e}}$					

The aerodynamic forces can be combined from Equation 2.50 and 2.53 as follows:

$$\mathbf{f}_a^b = \begin{pmatrix} X_a \\ Y_a \\ Z_a \end{pmatrix} = \frac{1}{2}\rho V_a^2 S \begin{pmatrix} C_X \\ C_Y \\ C_Z \end{pmatrix} \tag{2.56}$$

Similarly, the aerodynamic moments can be combined from Equation 2.54, 2.49 and 2.55 as follows:

$$\mathbf{m}_a^b = \begin{pmatrix} L_a \\ M_a \\ N_a \end{pmatrix} = \frac{1}{2}\rho V_a^2 S \begin{pmatrix} bC_l \\ cC_m \\ bC_n \end{pmatrix} \tag{2.57}$$

2.5.5.3 Propulsion force and moment

The relationship between the dynamics of electric motor and propeller is investigated in propulsion system. The dynamics of the propulsion system is expressed in terms of the propeller rotation speed, ω_p. The torque generated by the propeller, T_p, makes flight dynamics of small-sized UAVs having a propeller propulsion system sensitive to the dynamics of propulsion system. Because the propeller used in small UAVs is larger than its size. That's why, the torque is taken into account for obtaining total moment in the simulations. Considering the conservation of angular momentum, the propulsion dynamics can given as follows [1]:

$$\begin{aligned} (J_m + J_p)\dot{\omega}_p &= T_m - T_p \\ \dot{\omega}_p &= \frac{T_m - T_p}{J_m + J_p} \end{aligned} \tag{2.58}$$

where J_m is moment of inertia of rotating motor body with a value of $1.30 \times 10^{-4} kgm^2$ in this thesis, J_p is moment of inertia of propeller and T_m is output torque at motor shaft. T_m in terms of output power P_o is given by:

$$T_m = \frac{P_o}{\omega_p} \tag{2.59}$$

The propeller rotating by the help of T_m generates the thrust providing to propel the UAV forward. ω_p depends the input torque and V_a flowing into the propeller disk. In general, advance ratio J_{ar}, coefficient of thrust C_T and coefficient of power C_P have an effect on the performance of propeller as indicated in the following expressions:

$$J_{ar} = \frac{\pi V_a}{D_p \omega_p} \tag{2.60}$$

$$C_T = \frac{F_p(\pi)^2}{4\rho(D_p)^4(\omega_p)^2} \tag{2.61}$$

$$C_P = \frac{T_p(\pi)^3}{4\rho(D_p)^5(\omega_p)^2} \tag{2.62}$$

where D_p is the propeller diameter. F_p and T_p are the propeller thrust and torque, respectively. It is assumed that F_p acts along the x direction in F^b and through the center of gravity as indicated in Equation 2.63 [47]. With this assumption, the angular

momentum $\mathbf{h}_p$ of the rotating mass in F^b is expressed in Equation 2.64.

$$\mathbf{f}_p^b = \begin{pmatrix} T \\ 0 \\ 0 \end{pmatrix} \tag{2.63}$$

$$\mathbf{h}_p = \begin{pmatrix} J_p\omega_p \\ 0 \\ 0 \end{pmatrix} \tag{2.64}$$

If ω_p is constant, then $J_p\dot{\omega}_p = 0$, and the gyroscopic moment from the rotating mass is expressed as follows:

$$\begin{aligned} \mathbf{m}_p^b = \frac{d}{dt}\mathbf{h}_p = \omega_p \times \mathbf{h}_p &= \begin{pmatrix} 0 & -r & q \\ r & 0 & -p \\ -q & p & 0 \end{pmatrix} \begin{pmatrix} J_p\omega_p \\ 0 \\ 0 \end{pmatrix} \\ &= \begin{pmatrix} 0 \\ J_p\omega_p r \\ -J_p\omega_p q \end{pmatrix} \end{aligned} \tag{2.65}$$

The total forces acting on UAV can be obtained by means of Equation 2.43, 2.56 and 2.63 as follows:

$$\begin{aligned} \mathbf{f}^b &= \mathbf{f}_g^b + \mathbf{f}_a^b + \mathbf{f}_p^b \\ \begin{pmatrix} X \\ Y \\ Z \end{pmatrix} &= \begin{pmatrix} -mg\sin\theta \\ mg\cos\theta\sin\phi \\ mg\cos\theta\cos\phi \end{pmatrix} + \frac{1}{2}\rho V_a^2 S \begin{pmatrix} C_X \\ C_Y \\ C_Z \end{pmatrix} + \begin{pmatrix} T \\ 0 \\ 0 \end{pmatrix} \end{aligned} \tag{2.66}$$

Substituting Equation 2.66 into 2.34, the following force equations are obtained:

$$\begin{pmatrix} \dot{u} \\ \dot{v} \\ \dot{w} \end{pmatrix} = \begin{pmatrix} rv - qw \\ pw - ru \\ qu - pv \end{pmatrix} + \frac{1}{m}\left(\begin{pmatrix} -mg\sin\theta \\ mg\cos\theta\sin\phi \\ mg\cos\theta\cos\phi \end{pmatrix} + \overline{q}S \begin{pmatrix} C_X \\ C_Y \\ C_Z \end{pmatrix} + \begin{pmatrix} T \\ 0 \\ 0 \end{pmatrix} \right)$$

$$\dot{u} = rv - qw + \frac{\overline{q}S}{m}C_X - g\sin\theta + \frac{T}{m} \tag{2.67}$$

$$\dot{v} = pw - ru + \frac{\overline{q}S}{m}C_Y - g\cos\theta\sin\phi \tag{2.68}$$

$$\dot{w} = qu - pv + \frac{\overline{q}S}{m}C_Z - g\cos\theta\cos\phi \tag{2.69}$$

Low-cost sensors like inertial measurement unit (IMU) measure p, q and r and translational accelerations a_x, a_y and a_z in x, y and z axis directions, respectively, due to

applied forces, except gravity [47, 48]. Equating Equation 2.66 to 2.33, the following expression is obtained:

$$\begin{gathered} m\left(\left(\frac{d\mathbf{V}_g^b}{dt}\right)_b + \omega_{b/i}^b \times \mathbf{V}_g^b\right) = \mathbf{f}_g^b + \mathbf{f}_a^b + \mathbf{f}_p^b \\ \underbrace{\left(\left(\frac{d\mathbf{V}_g^b}{dt}\right)_b + \omega_{b/i}^b \times \mathbf{V}_g^b\right) - \frac{1}{m}\mathbf{f}_g^b}_{\mathbf{a}} = \frac{1}{m}(\mathbf{f}_a^b + \mathbf{f}_p^b) \end{gathered} \tag{2.70}$$

a_x, a_y and a_z can be obtained in scalar form as follows:

$$\begin{aligned} a_x &= \dot{u} - rv + qw + g\sin\theta \\ a_y &= \dot{v} - pw + ru - g\cos\theta\sin\phi \\ a_z &= \dot{w} - qu + pv - g\cos\theta\cos\phi \end{aligned} \tag{2.71}$$

Similarly, the total moments acting on UAV can be obtained by means of Equation 2.57 and 2.65 as follows:

$$\begin{gathered} \mathbf{m}^b = \mathbf{m}_a^b + \mathbf{m}_p^b \\ \begin{pmatrix} L \\ M \\ N \end{pmatrix} = \frac{1}{2}\rho V_a^2 S \begin{pmatrix} bC_l \\ cC_m \\ bC_n \end{pmatrix} + \begin{pmatrix} 0 \\ J_p\omega_p r \\ -J_p\omega_p q \end{pmatrix} \end{gathered} \tag{2.72}$$

Substituting Equation 2.72 into 2.41, the following moment equations are obtained:

$$\begin{pmatrix} \dot{p} \\ \dot{q} \\ \dot{r} \end{pmatrix} = \begin{pmatrix} \frac{J_z}{\Gamma} & 0 & \frac{J_{xz}}{\Gamma} \\ 0 & \frac{1}{J_y} & 0 \\ \frac{J_{xz}}{\Gamma} & 0 & \frac{J_x}{\Gamma} \end{pmatrix} \left(\begin{pmatrix} J_{xz}pq + (J_y - J_z)qr \\ J_{xz}(r^2 - p^2) + (J_z - J_x)pr \\ (J_x - J_y)pq - J_{xz}qr \end{pmatrix} + \frac{1}{2}\rho V_a^2 S \begin{pmatrix} bC_l \\ cC_m \\ bC_n \end{pmatrix} + \begin{pmatrix} 0 \\ J_p\omega_p r \\ -J_p\omega_p q \end{pmatrix} \right)$$

$$\dot{p} - \frac{J_{xz}}{J_x}\dot{r} = \frac{\overline{q}Sb}{J_x}C_l - \frac{J_z - J_y}{J_x}qr + \frac{J_{xz}}{J_x}qp \tag{2.73}$$

$$\dot{q} = \frac{\overline{q}S\overline{c}}{J_y}C_m - \frac{J_x - J_z}{J_y}pr - \frac{J_{xz}}{J_y}(p^2 - r^2) + \frac{J_p}{J_y}\omega_p r \tag{2.74}$$

$$\dot{r} - \frac{J_{xz}}{J_z}\dot{p} = \frac{\overline{q}Sb}{J_z}C_n - \frac{J_y - J_x}{J_z}pq + \frac{J_{xz}}{J_z}qr - \frac{J_p}{J_z}\omega_p q \tag{2.75}$$

2.5.6 Wind models

In this thesis, steady wind (SW) and wind gust (WG) are considered as environment model. An SW is continuous and assumed to act parallel to the surface of the earth [49]

which means to be horizontal and simply defined by a speed and direction as follows [50]:

$$\begin{aligned} u_{w_s} &= U_{w_s} \sin(\theta_{w_s}) \\ v_{w_s} &= U_{w_s} \cos(\theta_{w_s}) \end{aligned} \tag{2.76}$$

where u_{w_s} is the axial and v_{w_s} is the lateral components of the SW while U_{w_s} is the absolute magnitude and θ_{w_s} is the angle of the SW. U_{w_s} is chosen as 20 % of V_a, which is equal to $3.4 m/s$, and θ_{w_s} is chosen as $45°$.

Discrete WG model in Matlab is used as a WG model. It has a "1-cosine" shape as can be seen in Figure 2.11 and an expression in Equation 2.77.

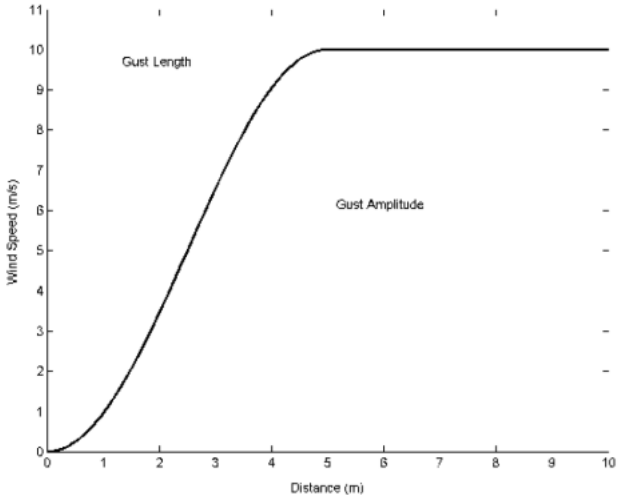

Figure 2.11 : Discrete WG profile [4].

$$V_{w_g} = \begin{cases} 0 & x_m < 0 \\ \frac{V_m}{2}\left(1 - \cos\left(\frac{\pi x_m}{d_m}\right)\right) & 0 \leq x_m \leq d_m \\ V_m & x_m > d_m \end{cases} \tag{2.77}$$

where V_m is the amplitude and d_m is the length of the gust, x_m is the distance traveled and V_{w_g} is the WG velocity in F^b. V_m and d_m are chosen from [3] under consideration of the conditions of low altitude with light turbulence. V_m consists of three components as $1.06, 1.06, 0.7 (m/s)$ and also d_m consists of three components as $200, 200, 50 (m)$.

In the simulations total wind vector can be assumed as follows:

$$\mathbf{V}_w = \mathbf{V}_{w_s} + \mathbf{V}_{w_g} \tag{2.78}$$

where $\mathbf{V}_{w_s}$ which is a constant vector is SW and $\mathbf{V}_{w_g}$ which is usually not constant due to the stochastic process represents WG and other atmospheric disturbances. SW is typically expressed in the F^i as follows:

$$\mathbf{V}_{w_s}^i = \begin{pmatrix} w_{n_s} \\ w_{e_s} \\ w_{d_s} \end{pmatrix} \tag{2.79}$$

where w_{n_s}, w_{e_s} and w_{d_s} are the speed of the SW in north, east and down directions in F^i, respectively. Since the atmospheric effects occur in the direction of the forward motion of UAV at a higher frequency than in the lateral and down directions, the wind gust is expressed in F^b as follows:

$$\mathbf{V}_{w_g}^b = \begin{pmatrix} u_{w_g} \\ v_{w_g} \\ w_{w_g} \end{pmatrix} \tag{2.80}$$

In the simulations, SW components are added to WG components after rotating from F^i to F^b. Thus total wind vector is obtained as follows:

$$\begin{aligned} \mathbf{V}_w^b &= R_v^b(\phi, \theta, \psi) \begin{pmatrix} w_{n_s} \\ w_{e_s} \\ w_{d_s} \end{pmatrix} + \begin{pmatrix} u_{w_g} \\ v_{w_g} \\ w_{w_g} \end{pmatrix} \\ &= \begin{pmatrix} u_{w_s} \\ v_{w_s} \\ w_{w_s} \end{pmatrix} + \begin{pmatrix} u_{w_g} \\ v_{w_g} \\ w_{w_g} \end{pmatrix} \end{aligned} \tag{2.81}$$

Equating Equation 2.81 and 2.8, the following relation is obtained:

$$\begin{pmatrix} u_w \\ v_w \\ w_w \end{pmatrix} = \begin{pmatrix} u_{w_s} + u_{w_g} \\ v_{w_s} + v_{w_g} \\ w_{w_s} + w_{w_g} \end{pmatrix} \tag{2.82}$$

2.5.7 Trim

Trim can be simply defined as an aircraft or UAV to be in equilibrium is said to be in trim in the aerodynamics literature [3]. The general nonlinear equations of motion of a UAV can be defined as follows [51]:

$$\dot{x} = f(x, u) \tag{2.83}$$

where $x \in \mathbb{R}^n$ is state vector having n element and $u \in \mathbb{R}^m$ is control or input vector having m element. The system is said to be in trim or equilibrium at the state x_e and input u_e if the following condition is provided:

$$f(x_e, u_e) = 0$$

The expression above is a minimization problem which provides the nonlinear set of equations to be solved by a numerical approach.

In a trimmed flight condition the rate of change of the state vector is zero in F^i and the resultant of the applied forces and moments is zero. A UAV in a trimmed trajectory to be accelerated by means of non-zero resultant aerodynamic and gravitational forces and moments is balanced by centrifugal and gyroscopic inertial forces and moments. Therefore, motion of UAV is uniform in F^i under trim condition [52]. h, u, v, w, ϕ, θ, ψ, p, q and r are all constant or $\dot{u} = \dot{v} = \dot{w} = \dot{p} = \dot{q} = \dot{r} = 0$ as UAV is in constant-altitude, wings-level steady flight. However, trim conditions may include states inconstant. $\dot{h}$ is constant and h increases linearly in steady-climb, wings-level flight while $\dot{\psi}$ is constant and ψ increases linearly in a constant turn. That's why, the conditions for trim to be given as follows would be better for generalization:

$$\dot{x_e} = f(x_e, u_e)$$

Computing trim states and inputs are the objective if UAV simultaneously satisfies the traveling at a constant V_{a_e} and orbit of radius R_e along with climbing at a constant γ_e. The related parameters are inputs to the trim calculations. Trimmed flight is independent of position since the right-hand side of equations are not dependent of p_n, p_e and p_d. Also it is independent of ψ since $\dot{p_n}$ and $\dot{p_d}$ are dependent on it.

Control inputs are evaluated in order to keep the output state vector at desired values. When there is an oppurtunity to measure the wind speed disturbing the autonomous flight, the measured values can be included in Equation 2.83. The effects of wind disturbance to be able to be included in the simulation model by adding the wind speed components to $\mathbf{V}_w^b$ as in Equation 2.81 is assumed [51]. In this thesis, this assumption is considered as SW components to be taken into account during trim calculations.

Trim calculations are performed in Matlab with two steps. Firstly, a trim condition is specified by using *operspec* function. Then, the inputs required to trim based on specified initial conditions are calculated by *findop* function. Linearization can be performed after triming by using *linearize* function in order to obtain a linear model around the trim operating point [53].

2.5.8 Linear models

The linear model given in Equation 2.84 is derived from linearizing the nonlinear model about trim operating point which is obtained for each flight scenario by trimming the UAV at a desired flight operating envelop [1]. In Matlab, the full linear model is linearised by *linearize* function.

$$\begin{aligned} \dot{x}_f &= A_f x_f + B_f u_f \\ y_f &= C_f x_f + D_f u_f \end{aligned} \tag{2.84}$$

where A_f, B_f, C_f and D_f are the system, input, output and feedforward matrices of the full linearised state space model, respectively. The expressions of the state vector x_f, input vector u_f and output vector y_f can be given as follows:

$$\begin{aligned} x_f &= \begin{pmatrix} \phi & \theta & \psi & p & q & r & u & v & w & p_n & p_e & p_d & \omega_p \end{pmatrix}^T \\ u_f &= \begin{pmatrix} \delta_t & \delta_e & \delta_r & \delta_{a_l} & \delta_{a_r} & \delta_{f_l} & \delta_{f_r} & \delta_a \end{pmatrix}^T \\ y_f &= \begin{pmatrix} V_a & \beta & \alpha & h & \phi & \theta & \psi & p & q & r & \gamma & a_x & a_z \end{pmatrix}^T \end{aligned}$$

where δ_t is the throttle, δ_{a_l} and δ_{a_r} left and right aileron, δ_{f_l} and δ_{f_r} left and right flap deflections. $h = -p_d$ is the altitude above ground level.

Decoupling the linearized model into lateral and longitudinal models is a widespread method in flight dynamics under the assumption that the cross-coupling effect between the two modes is negligible. This assumption is considered valid when the UAV model is symmetrical about xz plane and designed with conventional aileron, rudder and elevator control surfaces. In this thesis, linear decoupled models given in Equation 2.85 and 2.86 are utilised for MPC design. They are obtained by means of the full linear model to be decoupled into lateral and longitudinal-directional modes by taking the states related with the each mode. Figure 2.12 shows the whole procedure step by step. In Matlab lateral and longitudinal linear models are obtained by using *modred* function which provides to reduce the order of the full linear state-space model. In order to perform this process, required variables of state, input and output vectors are selected.

$$\begin{aligned} \dot{x}_{lon} &= A_{lon} x_{lon} + B_{lon} u_{lon} \\ y_{lon} &= C_{lon} x_{lon} + D_{lon} u_{lon} \end{aligned} \tag{2.85}$$

$$\begin{aligned} \dot{x}_{lat} &= A_{lat}x_{lat} + B_{lat}u_{lat} \\ y_{lat} &= C_{lat}x_{lat} + D_{lat}u_{lat} \end{aligned} \tag{2.86}$$

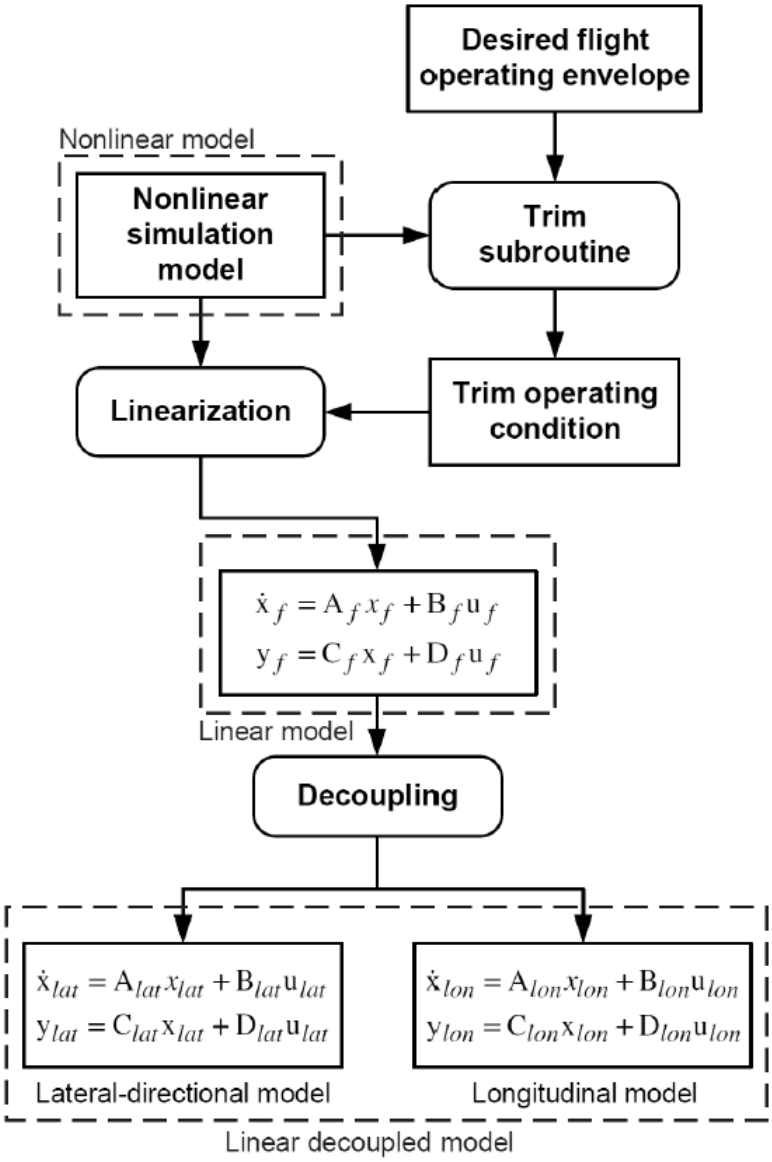

Figure 2.12 : Procedures for deriving linear decoupled models [1].

where A_{lon}, B_{lon}, C_{lon} and D_{lon} are the system, input, output and feedforward matrices of the linear longitudinal state space model, respectively. Similarly, A_{lat}, B_{lat}, C_{lat} and D_{lat} are the ones of the linear lateral state space model, respectively. The expressions of the state vectors, x_{lon} corresponding to Equations 2.67, 2.69, 2.74, 2.28 2.24, 2.58 and x_{lat} corresponding to Equations 2.68, 2.73, 2.75, 2.27, 2.29; input

vectors, u_{lon} and u_{lat}; and output vectors, y_{lon} and y_{lat}, can be given as follows:

$$x_{lon} = \begin{pmatrix} u & w & q & \theta & p_d & \omega_p \end{pmatrix}^T$$
$$u_{lon} = \begin{pmatrix} \delta_e & \delta_t \end{pmatrix}^T$$
$$y_{lon} = \begin{pmatrix} V_a & \alpha & q & \theta & h & a_x & a_z \end{pmatrix}^T$$

$$x_{lat} = \begin{pmatrix} v & p & r & \phi & \psi \end{pmatrix}^T$$
$$u_{lat} = \begin{pmatrix} \delta_a & \delta_r \end{pmatrix}^T = \begin{pmatrix} \delta_{a_l} & \delta_{a_r} & \delta_r \end{pmatrix}^T$$
$$y_{lat} = \begin{pmatrix} \beta & p & r & \phi & \psi \end{pmatrix}^T$$

3. MODEL PREDICTIVE CONTROL

3.1 MPC Concept

The MPC strategy can be seen in the block diagram in Figure 3.1. The current values of the output variables are predicted by a process model. The residuals also known as prediction model errors are the differences between the actual and predicted outputs. They are directly fed to the prediction block as feedback signals. In the set-point calculations block also known as optimizer block and control calculations block also known as controller block, the related calculations including inequality constraints such as upper and lower limits on the input and output variables are performed by the help of the predictions at each sampling period [5].

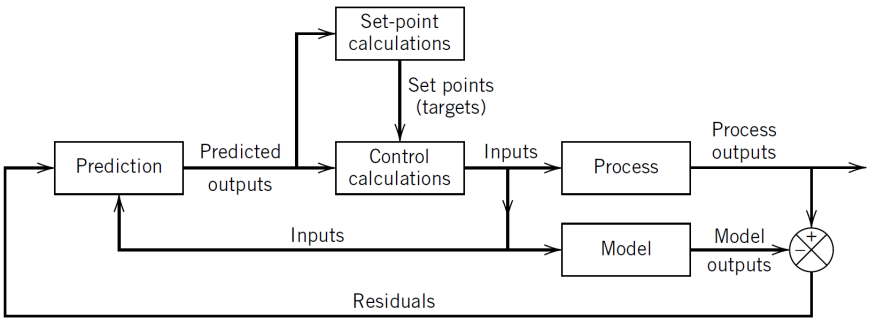

Figure 3.1 : MPC block diagram [5].

Targets or set-points are calculated by optimization which is traditionally based on a linear steady-state model and aimed to minimize a cost function. The inequality constraint changes due to variations in process conditions, equipment and instrumentation result in change in the optimum values of targets. As soon as the control calculations are performed, the targets are calculated at each sampling period.

The current measurements and predictions of the future values of the outputs underlie the MPC calculations whose objective is to determine a sequence of control moves or manipulated input changes in order that the predicted response moves to the target in an optimal manner. Figure 3.2 indicates the actual output y, predicted

output $\hat{y}$ and manipulated input u for SISO control. A set of m_h values of the input $[u(k+i-1), i=1,2,...,m_h]$ which consists of the current input $u(k)$ and m_h-1 future inputs are calculated by the MPC strategy. After the m_h control moves which is known as control horizon, the input is kept constant. They are calculated in order that a set of p_h predicted outputs $[\hat{y}(k+i), i=1,2,...,p_h]$ reaches the target in an optimal manner. The number of predictions p_h is called as prediction horizon. The significant point is the control calculations to be performed in terms of optimizing an objective function.

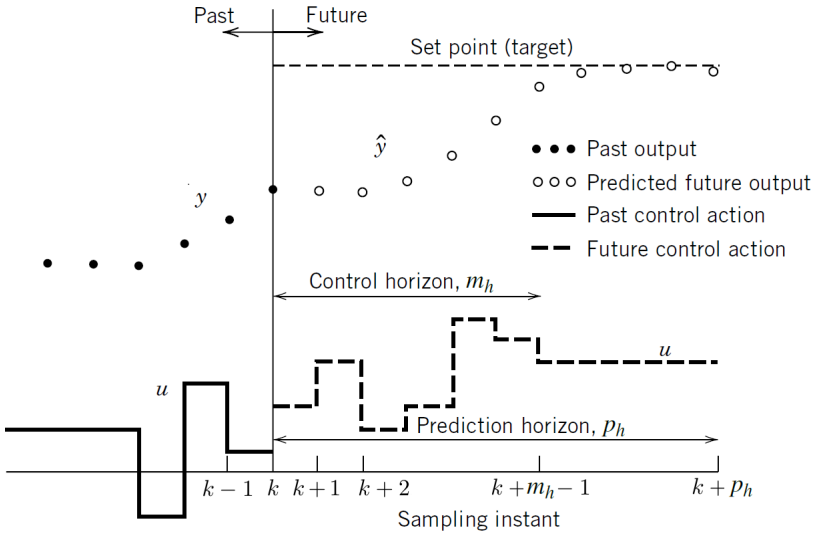

Figure 3.2 : MPC concept [5].

The values of u at the next m_h sampling instants, $[u(k), u(k+1), ..., u(k+m_h-1)]$ are calculated at sampling period k by optimizing a cost function so as to provide the process to become very close to the reference trajectory. Then, the first control move $u(k)$ is implemented at the same sampling period. When new measurements are available, a new sequence is calculated at the next sampling period $k+1$ and similar to the previous step only the first control move $u(k+1)$ is implemented. The same steps are repeated at each sampling period. As a summary, only first control move is implemented even though a sequence of m_h control moves is calculated at each sampling period by solving quadratic programming (QP) problem in order to minimize the predicted deviations from the reference trajectory over the next p_h sampling periods. This procedure is called as receding horizon approach. It is one of the distinct feature of MPC strategy.

3.2 Prediction Model

A linear time-invariant (LTI) plant model which is shown in Figure 3.3 is used by MPC [6].

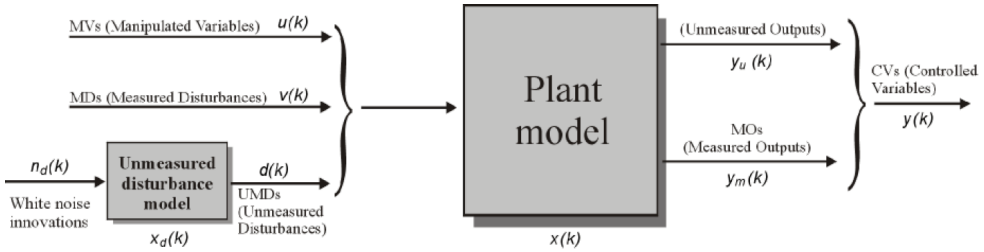

Figure 3.3 : Prediction model [6].

It can be described by the following linear state space equations:

$$\begin{aligned} x(k+1) &= Ax(k) + B_u u(k) + B_v v(k) + B_d d(k) \\ y_m(k) &= C_{mo} x(k) + D_{vm} v(k) + D_{dm} d(k) \\ y_u(k) &= C_u x(k) + D_{vu} v(k) + D_{du} d(k) + D_u u(k) \end{aligned} \tag{3.1}$$

where

$x(k)$ n_x- dimensional plant state vector

$u(k)$ n_u- dimensional manipulated variables (MV) vector

$v(k)$ n_v- dimensional measured disturbances (MD) vector

$d(k)$ n_d- dimensional unmeasured disturbances (UD) vector which consists of both state disturbances ($B_d \neq 0$) and output disturbances ($D_d \neq 0$)

$y_m(k)$ measured outputs (MO) vector

$y_u(k)$ unmeasured outputs (UO) vector

A system matrix

B_u input control matrix

B_v measured disturbance matrix

B_d unmeasured disturbance matrix

C_{mo} measured output matrix

C_u unmeasured output matrix

D_u feedthrough input control matrix

D_{vm} feedthrough measured disturbance matrix of measured output

D_{vu} feedthrough measured disturbance matrix of unmeasured output

D_{dm} feedthrough unmeasured disturbance matrix of measured output

D_{du} feedthrough unmeasured disturbance matrix of unmeasured output

3.3 State Estimation

A state estimator which is based on the model in Figure 3.4 predict $x(k)$, $x_d(k)$ when they are not directly measurable.

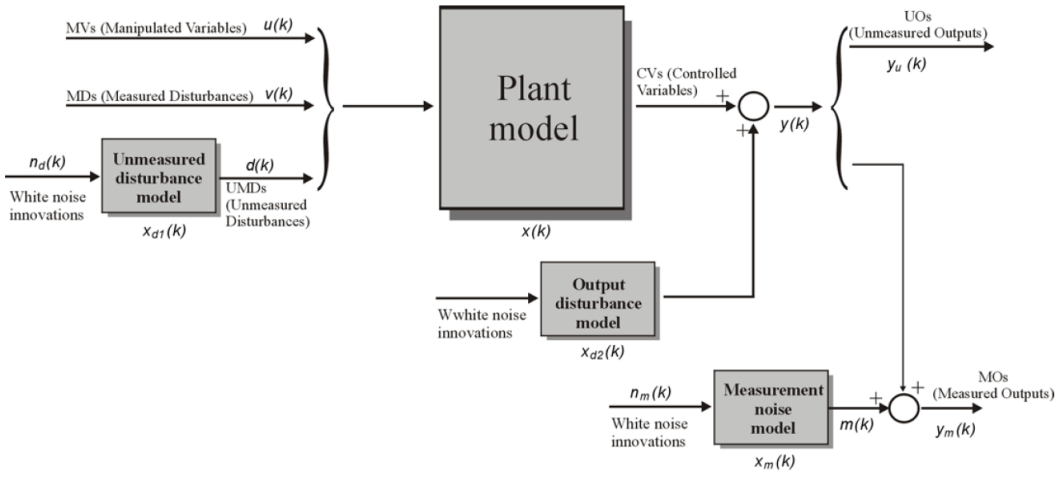

Figure 3.4 : State estimation model [6].

3.3.1 Unmeasured disturbance model

Unmeasured input disturbance model which allows to model random disturbances entering the plant affects $x(k)$ and/or $y(k)$. The combination of plant and disturbance models to be observable is the key point for defining the model which can be stated in terms of $d(k)$ as follows:

$$\begin{aligned} x_d(k+1) &= \overline{A}x_d(k) + \overline{B}n_d(k) \\ d(k) &= \overline{C}x_d(k) + \overline{D}n_d(k) \end{aligned} \tag{3.2}$$

where

$x_d(k)$ state vector of unmeasured input disturbance model

$n_d(k)$ random Gaussian noise with zero mean and unit covariance matrix

$\overline{A}$ system matrix of unmeasured input disturbance model

$\overline{B}$ unmeasured disturbance matrix of unmeasured input disturbance model

$\overline{C}$ output matrix of unmeasured input disturbance model

$\overline{D}$ feedthrough unmeasured disturbance matrix of unmeasured input disturbance model

Unmeasured output disturbance model is a collection of integrators which are excited by random Gaussian noise and added for each measured output on condition that there is not any violation of observability.

3.3.2 Measurement noise model

$y_m(k)$ to be corrupted by a measurement noise $m(k)$ which is the output of the measurement noise model in Equation 3.3 is assumed. However, the measurement noise model to be integrated into the prediction model given in Equation 3.1 is unnecessary since the objective of MPC is to provide $y_u(k)$ and $(y_m(k)\breve{}m(k))$ to become very close to the reference vector $r(k)$.

$$\begin{aligned} x_m(k+1) &= \tilde{A}x_m(k) + \tilde{B}n_m(k) \\ m(k) &= \tilde{C}x_m(k) + \tilde{D}n_m(k) \end{aligned} \tag{3.3}$$

where

$x_m(k)$ state vector of measurement noise model

$n_m(k)$ random Gaussian noise with zero mean and unit covariance matrix

$\tilde{A}$ system matrix of measurement noise model

$\tilde{B}$ unmeasured disturbance matrix of measurement noise model

$\tilde{C}$ output matrix of measurement noise model

$\tilde{D}$ feedthrough unmeasured disturbance matrix of measurement noise model

3.3.3 State observer

A state observer is used for reducing the prediction error by updating $x(k)$, $x_d(k)$ and $x_m(k)$ at each sampling instant. State estimator can be used providing that the models used in the design of the MPC are observable [6]. The output of the system is estimated before the states of the system in terms of the known parameters as follows [6]:

$$\hat{y}(k) = C\hat{x}(k \mid k-1) + D_v v(k) + D_d \overline{C}\hat{x}_d(k \mid k-1) + \tilde{C}\hat{x}_m(k \mid k-1) \tag{3.4}$$

As can be seen from Eqn (3.4) that the estimated output $\hat{y}(k)$ is calculated from the models and the states estimated at the previous sampling instant $\hat{x}(k \mid k-1)$. Then, the states at the current sampling instant can be calculated from $\hat{y}(k)$ as follows:

$$\begin{pmatrix} \hat{x}(k \mid k) \\ \hat{x}_d(k \mid k) \\ \hat{x}_m(k \mid k) \end{pmatrix} = \begin{pmatrix} \hat{x}(k \mid k-1) \\ \hat{x}_d(k \mid k-1) \\ \hat{x}_m(k \mid k-1) \end{pmatrix} + K_{ob}(y(k) - \hat{y}(k)) \tag{3.5}$$

where K_{ob} is the observer gain obtained by Kalman filtering techniques, which indicates that the current states are estimated from the states estimated at the previous sampling instant and a correction term. The estimated states based on the error between the measured output $y(k)$ and the estimated output $\hat{y}(k)$ are updated by the correction term. The estimated states in Eqn (3.5) are used in the calculation of the optimal control. Also, the estimated states are used for estimating the state at the next sampling instant as follows [6]:

$$\begin{pmatrix} \hat{x}(k+1 \mid k) \\ \hat{x}_d(k+1 \mid k) \\ \hat{x}_m(k+1 \mid k) \end{pmatrix} = \begin{pmatrix} A\hat{x}(k \mid k) + B_u u(k) + B_v v(k) + B_d \overline{C}\hat{x}_d(k \mid k) \\ \overline{A}\hat{x}_d(k \mid k) \\ \tilde{A}\hat{x}_m(k \mid k) \end{pmatrix} \tag{3.6}$$

The estimates obtained in Eqn (3.6) are used as the estimates of the previous states $\hat{x}(k \mid k-1)$ in Eqn (3.5) at the next sampling period.

3.4 Optimization Problem

MPC comprises an optimization problem which is solved by QP method. The MPC control action with the estimates of $x(k)$ and $x_d(k)$ at time k is obtained by solving the

optimization problem as follows [6]:

$$\triangle u(k \mid k), ..., \min_{\triangle u(m_h-1+k|k)} \{ \sum_{i=0}^{p_h-1} (\sum_{j=1}^{n_y} \mid w^{y}_{i+1,j}(y_j(k+i+1 \mid k) - r_j(k+i+1)) \mid^2 + \sum_{j=1}^{n_u} \mid w^{\triangle u}_{i,j} \triangle u_j(k+i \mid k) \mid^2 + \sum_{j=1}^{n_u} \mid w^{u}_{i,j}(u_j(k+i \mid k) \mid^2 - u_{jtarget}(k+i)) \mid^2) \} \tag{3.7}$$

subject to the following constraints:

$$\begin{aligned} u_{j,min}(i) \leq u_j(k+i \mid k) \leq u_{j,max}(i) \\ \triangle u_{j,min}(i) \leq \triangle u_j(k+i \mid k) \leq \triangle u_{j,max}(i) \\ y_{j,min}(i) \leq y_j(k+i+1 \mid k) \leq y_{j,max}(i) \\ \triangle u(k+h \mid k) = 0 \\ h = m, ..., p_h - 1 \\ i = 0, ..., p_h - 1 \end{aligned}$$

where

$()_j$ $j-th$ component of an input-output vector

$(k+i \mid k)$ value predicted for time $k+i$ based on the information available as time k

$w^{\triangle u}_{i,j}$ nonnegative weight of $\triangle u$

$w^{u}_{i,j}$ nonnegative weight of u

$w^{y}_{i,j}$ nonnegative weight of y

n_y number of plant output variables

n_u number of manipulated variables

p_h prediction horizon which is the number of future control intervals that is evaluated with prediction as the MVs are optimized at control interval k [6].

m_h control horizon which is the number of moves of MV to be optimized at k [6].

the sequence of input increments is $\triangle u(k \mid k), ..., \triangle u(m_h - 1 + k \mid k)$ with its final value $u(k) = u(k-1) + \triangle u(k \mid k)^*$. $\triangle u(k \mid k)^*$ is the 1^{st} element of the optimal sequence. w to be smaller means the behaviour of the corresponding variable to the overall performance to be the less important. $u_{jtarget}(k+i)$ is the set-point vector for the input vector.

The following matrices are used in order to solve the optimization problem as indicated in Equation 3.7:

$$\begin{aligned} \begin{pmatrix} x \\ x_d \end{pmatrix} &\rightarrow x \\ \begin{pmatrix} A & B_d\overline{C} \\ 0 & \overline{A} \end{pmatrix} &\rightarrow A \\ \begin{pmatrix} B_u \\ 0 \end{pmatrix} &\rightarrow B_u \\ \begin{pmatrix} B_d\overline{D} \\ \overline{B} \end{pmatrix} &\rightarrow B_d \\ \begin{pmatrix} C & D_d\overline{C} \end{pmatrix} &\rightarrow C \end{aligned} \tag{3.8}$$

The prediction model in Equation 3.1 can be rewritten in the following equation in terms of $y(k)$ under the assumption of $d(k) = n_d(k)$ along with the assumptions as made in Equation 3.8.

$$\begin{aligned} x(k+1) &= Ax(k) + B_u u(k) + B_v v(k) + B_d n_d(k) \\ y(k) &= Cx(k) + D_v v(k) + D_d n_d(k) \end{aligned} \tag{3.9}$$

where

$y(k)$ overall output vector which is the summation of $y_m(k)$ and $y_u(k)$

C overall output matrix which consists of C_m and C_u

D_v overall feedthrough measured disturbance matrix which consists of D_{vm} and D_{vu}

D_d overall feedthrough unmeasured disturbance matrix which consists of D_{dm} and D_{du}

If the problem of predicting the future trajectories of the model is considered to be performed at time $k = 0$ and $n_d(i)$ to be set to zero for all prediction periods i, the

following expression is obtained [6]:

$$y(i \mid 0) = C[A^i x(0) + \sum_{h=0}^{i-1} (A^{i-1} B_u (u(-1) + \sum_{j=0}^{h} \triangle u(j)) + B_v v(h))] + D_v v(i) \quad (3.10)$$

which gives the following solution [6]:

$$\begin{pmatrix} y(1) \\ \cdots \\ y(p_h) \end{pmatrix} = S_x x(0) + S_{u1} u(-1) + S_u \begin{pmatrix} \Delta u(0) \\ \cdots \\ \Delta u(p_h - 1) \end{pmatrix} + H_v \begin{pmatrix} v(0) \\ \cdots \\ v(p_h) \end{pmatrix} \quad (3.11)$$

where

$$S_x = \begin{pmatrix} CA \\ CA^2 \\ \cdots \\ CA^{p_h} \end{pmatrix} \in \mathbb{R}^{p_h n_y \times n_x}, \quad S_{u1} = \begin{pmatrix} CB_u \\ CB_u + CAB_u \\ \cdots \\ \sum_{h=0}^{p_h-1} CA^h B_u \end{pmatrix} \in \mathbb{R}^{p_h n_y \times n_u}$$

$$S_u = \begin{pmatrix} CB_u & 0 & \cdots & 0 \\ CB_u + CAB_u & CB_u & \cdots & 0 \\ \cdots & \cdots & \cdots & \cdots \\ \sum_{h=0}^{p_h-1} CA^h B_u & \sum_{h=0}^{p_h-2} CA^h B_u & \cdots & CB_u \end{pmatrix} \in \mathbb{R}^{p_h n_y \times p_h n_u}$$

$$H_v = \begin{pmatrix} CB_v & D_v & 0 & \cdots & 0 \\ CAB_v & CB_v & D_v & \cdots & 0 \\ \cdots & \cdots & \cdots & \cdots & \cdots \\ CA^{p_h-1} B_v & CA^{p_h-2} B_v & CA^{p_h-3} B_v & \cdots & D_v \end{pmatrix} \in \mathbb{R}^{p_h n_y \times (p_h+1) n_v}$$

where

n_x number of plant state variables

n_v number of measured disturbances

$u_{j,min}$ lower bound on u

$u_{j,max}$ upper bound on u

$\triangle u_{j,min}$ lower bound on $\triangle u$

$\triangle u_{j,max}$ upper bound on $\triangle u$

$y_{j,min}$ lower bound on y

$y_{j,max}$ upper bound on y

When $zo = [zo_0; \ldots; zo_{m_h-1}]$ is considered to be the free optimization variables of the optimization problem ($zo_0; \ldots; zo_{m_h-1}$ are scalars in case of any systems to have single manipulated variables), the cost function to be optimized becomes as follows:

$$\begin{aligned} J(zo) = & \left(\begin{pmatrix} u(0) \\ \cdots \\ u(p_h-1) \end{pmatrix} - \begin{pmatrix} u_{target}(0) \\ \cdots \\ u_{target}(p_h-1) \end{pmatrix} \right)^T W_u^2 \left(\begin{pmatrix} u(0) \\ \cdots \\ u(p_h-1) \end{pmatrix} - \begin{pmatrix} u_{target}(0) \\ \cdots \\ u_{target}(p_h-1) \end{pmatrix} \right) \\ & + \begin{pmatrix} \Delta u(0) \\ \cdots \\ \Delta u(p_h-1) \end{pmatrix}^T W_{\Delta u}^2 \begin{pmatrix} \Delta u(0) \\ \cdots \\ \Delta u(p_h-1) \end{pmatrix} \\ & + \left(\begin{pmatrix} y(1) \\ \cdots \\ y(p_h) \end{pmatrix} - \begin{pmatrix} r(1) \\ \cdots \\ r(p_h) \end{pmatrix} \right)^T W_y^2 \left(\begin{pmatrix} y(1) \\ \cdots \\ y(p_h) \end{pmatrix} - \begin{pmatrix} r(1) \\ \cdots \\ r(p_h) \end{pmatrix} \right) \end{aligned} \tag{3.12}$$

where

$$W_u = \begin{pmatrix} w_{0,1}^u & 0 & \ldots & \ldots & \ldots & \ldots & \ldots & \ldots & 0 \\ 0 & w_{0,2}^u & 0 & \ldots & \ldots & \ldots & \ldots & \ldots & 0 \\ \vdots & 0 & \ddots & 0 & \ldots & \ldots & \ldots & \ldots & 0 \\ \vdots & \vdots & 0 & w_{0,n_u}^u & 0 & \ldots & \ldots & \ldots & 0 \\ \vdots & \vdots & \vdots & 0 & \ddots & 0 & \ldots & \ldots & 0 \\ \vdots & \vdots & \vdots & \vdots & 0 & w_{p_h-1,1}^u & 0 & \ldots & 0 \\ \vdots & \vdots & \vdots & \vdots & \vdots & 0 & w_{p_h-1,2}^u & 0 & 0 \\ \vdots & \vdots & \vdots & \vdots & \vdots & \vdots & 0 & \ddots & 0 \\ 0 & 0 & 0 & 0 & 0 & 0 & 0 & 0 & w_{p_h-1,n_u}^u \end{pmatrix}$$

$$W_{\Delta u} = \begin{pmatrix} w_{0,1}^{\Delta u} & 0 & \ldots & \ldots & \ldots & \ldots & \ldots & \ldots & 0 \\ 0 & w_{0,2}^{\Delta u} & 0 & \ldots & \ldots & \ldots & \ldots & \ldots & 0 \\ \vdots & 0 & \ddots & 0 & \ldots & \ldots & \ldots & \ldots & 0 \\ \vdots & \vdots & 0 & w_{0,n_u}^{\Delta u} & 0 & \ldots & \ldots & \ldots & 0 \\ \vdots & \vdots & \vdots & 0 & \ddots & 0 & \ldots & \ldots & 0 \\ \vdots & \vdots & \vdots & \vdots & 0 & w_{p_h-1,1}^{\Delta u} & 0 & \ldots & 0 \\ \vdots & \vdots & \vdots & \vdots & \vdots & 0 & w_{p_h-1,2}^{\Delta u} & 0 & 0 \\ \vdots & \vdots & \vdots & \vdots & \vdots & \vdots & 0 & \ddots & 0 \\ 0 & 0 & 0 & 0 & 0 & 0 & 0 & 0 & w_{p_h-1,n_u}^{\Delta u} \end{pmatrix}$$

$$W_y = \begin{pmatrix} w^y_{1,1} & 0 & \dots & \dots & \dots & \dots & \dots & \dots & 0 \\ 0 & w^y_{1,2} & 0 & \dots & \dots & \dots & \dots & \dots & 0 \\ \vdots & 0 & \ddots & 0 & \dots & \dots & \dots & \dots & 0 \\ \vdots & \vdots & 0 & w^y_{1,n_y} & 0 & \dots & \dots & \dots & 0 \\ \vdots & \vdots & \vdots & 0 & \ddots & 0 & \dots & \dots & 0 \\ \vdots & \vdots & \vdots & \vdots & 0 & w^y_{p_h,1} & 0 & \dots & 0 \\ \vdots & \vdots & \vdots & \vdots & \vdots & 0 & w^y_{p_h,2} & 0 & 0 \\ \vdots & \vdots & \vdots & \vdots & \vdots & \vdots & 0 & \ddots & 0 \\ 0 & 0 & 0 & 0 & 0 & 0 & 0 & 0 & w^y_{p_h,n_y} \end{pmatrix}$$

The limits on inputs, input increments, and outputs can be expressed as follows:

$$\begin{pmatrix} y_{min}(1) \\ \dots \\ y_{min}(p_h) \\ u_{min}(0) \\ \dots \\ u_{min}(p_h-1) \\ \Delta u_{min}(0) \\ \dots \\ \Delta u_{min}(p_h-1) \end{pmatrix} \leq \begin{pmatrix} y(1) \\ \dots \\ y(p_h) \\ u(0) \\ \dots \\ u(p_h-1) \\ \Delta u(0) \\ \dots \\ \Delta u(p_h-1) \end{pmatrix} \leq \begin{pmatrix} y_{max}(1) \\ \dots \\ y_{max}(p_h) \\ u_{max}(0) \\ \dots \\ u_{max}(p_h-1) \\ \Delta u_{max}(0) \\ \dots \\ \Delta u_{max}(p_h-1) \end{pmatrix}$$

When $u(k)$, $\Delta u(k)$ and $y(k)$ are substituted, the following expression are obtained:

$$M_{zo} zo \leq M_{lim} + \begin{pmatrix} v(0) \\ \dots \\ v(p_h) \end{pmatrix} + M_u u(-1) + M_x x(0) \tag{3.13}$$

where matrices M_{zo}, M_{lim}, M_v, M_u and M_x are obtained from the upper and lower bounds. Therefore, the optimization problem can be solved at each sampling period.

The optimal solution can be computed by solving Equation 3.12 and 3.13 using a QP solver which solves the following convex program:

$$\min_x \left(f^T x + \frac{1}{2} x^T H zo \right) \tag{3.14}$$

such that

$$A_c x \leq b$$

where H is the Hessian and A_c linear constraint coefficients matrix, which are

constants. $x^T = zo^T$ is the decision, b and f are time-varying vectors. The corresponding matrices and vectors are computed during initialization and retrieved from computer memory by the controller. At the beginning of each control instant, the b and f are computed.

4. NONLINEAR AND PROCESSOR IN THE LOOP SIMULATIONS

4.1 Nonlinear Simulations

The NL model available from the University of Minnesota UAV research group [2] as shown in Figure 4.1 is used for obtaining the linear model and running closed loop simulations [36]. The closed loop NL model with the integrated constrained lateral and longitudinal MIMO MPCs in Figure 4.2 is simulated $100s$ with the solver used as Fourth-order Runge-Kutta fixed step integration method with a time step of $0.02s$ in Matlab for the 5 different flight scenarios as straight and level, level climb, level turn, climbing turn and level steady heading sideslip. The MPCs whose structure is shown in Figure 4.3 are designed including actuator saturation limits as indicated in Table 4.1 for each flight scenario. They are based on the linear lateral and longitudinal models in Eqns (2.85) and (2.86) which are derived from the NL model at trim operating point by using *mpc* and *linearize* commands in Matlab. Trim operating points are obtained with respect to the flight scenarios as shown in Table 4.2 by the help of *findop* command in Matlab. The performance of the MPCs is tested under 3 different conditions. Firstly, the performance of them is tested under nominal conditions. Secondly, it is tested under 2 UOs as a_x and a_z. Finally, it is tested under 1 UOD on V_a with a random step-like noise having a magnitude of 1 along with the 2 UOs.

Table 4.1 : Saturation limits on actuators [2].

Actuator	Lower Limit	Upper Limit
Throttle	0	1
Elevator	-25°	25°
Rudder	-25°	25°
Ailerons	-25°	25°

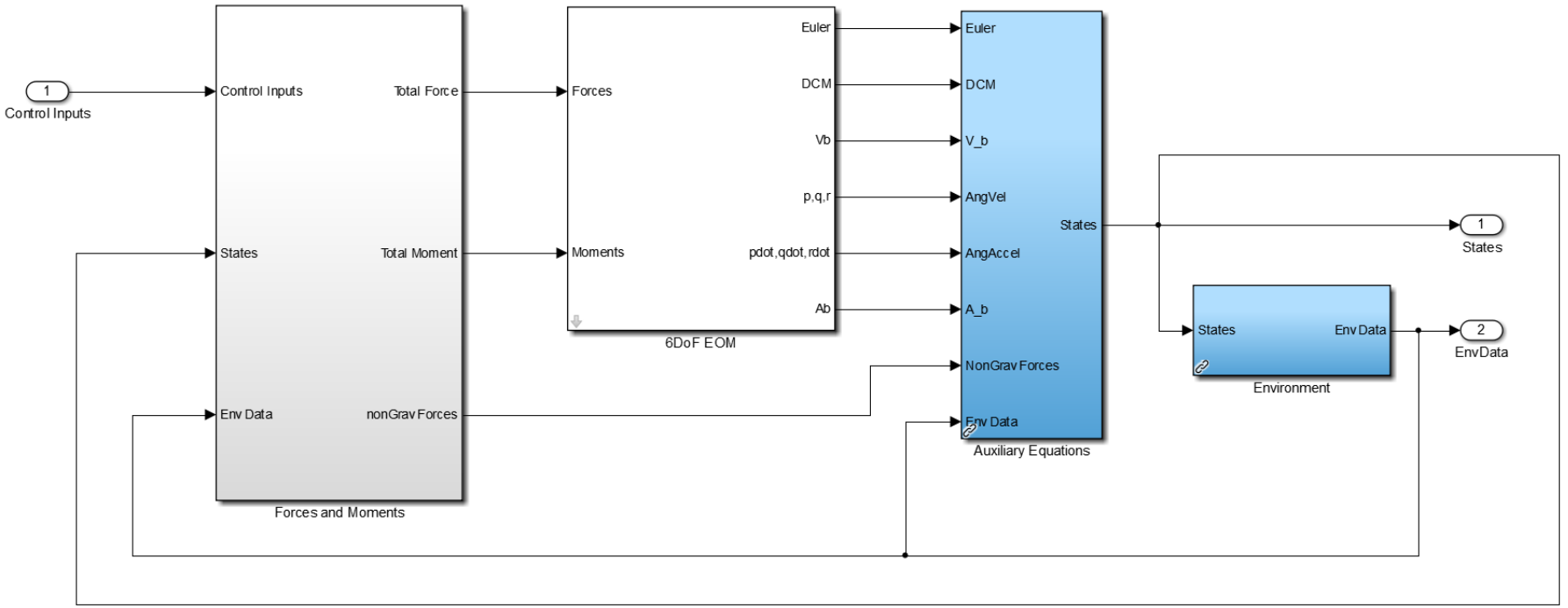

Figure 4.1 : Nonlinear fixed wing UAV model [2].

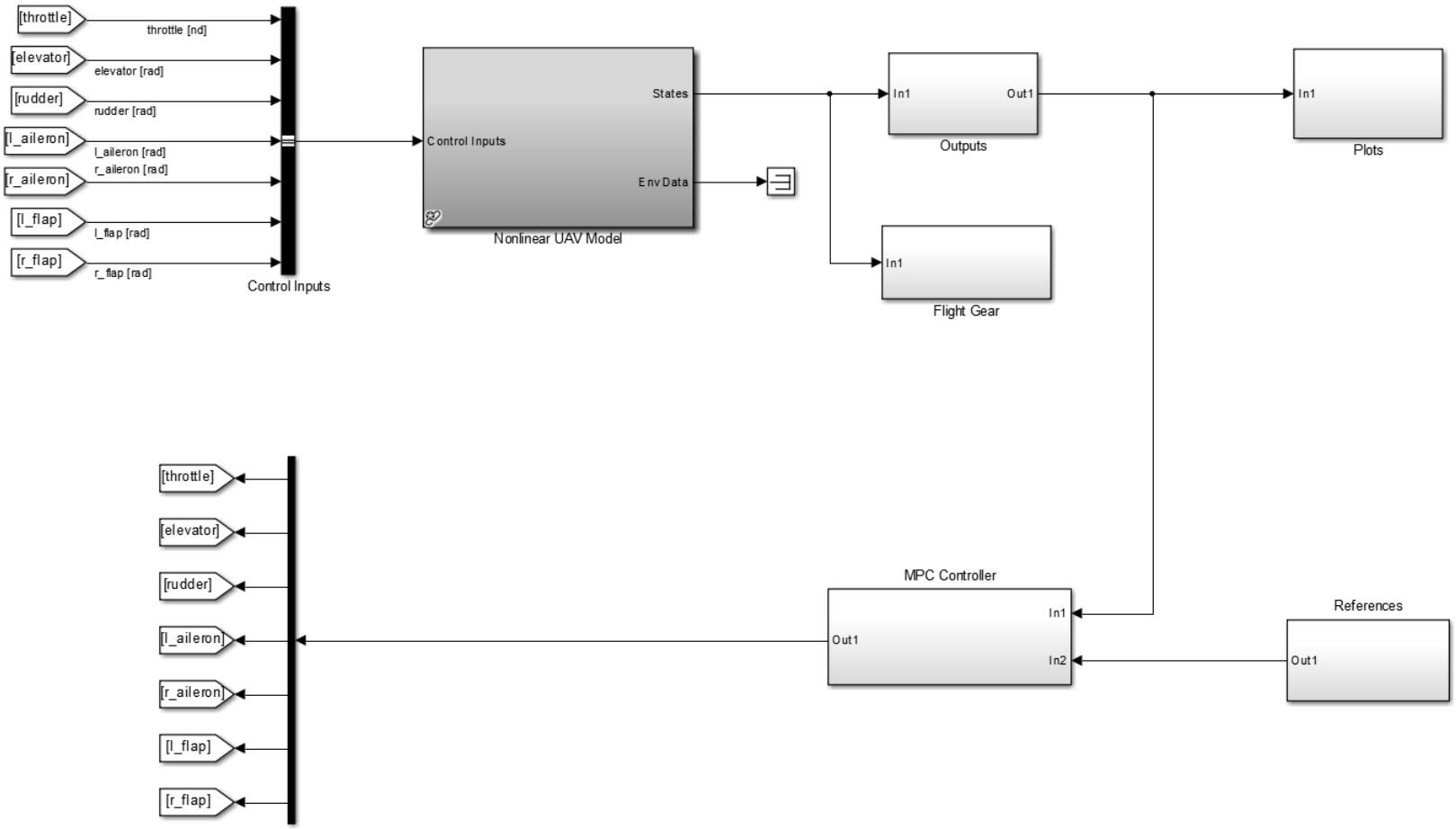

Figure 4.2 : Nonlinear closed loop model with the constrained lateral and longitudinal MIMO MPCs.

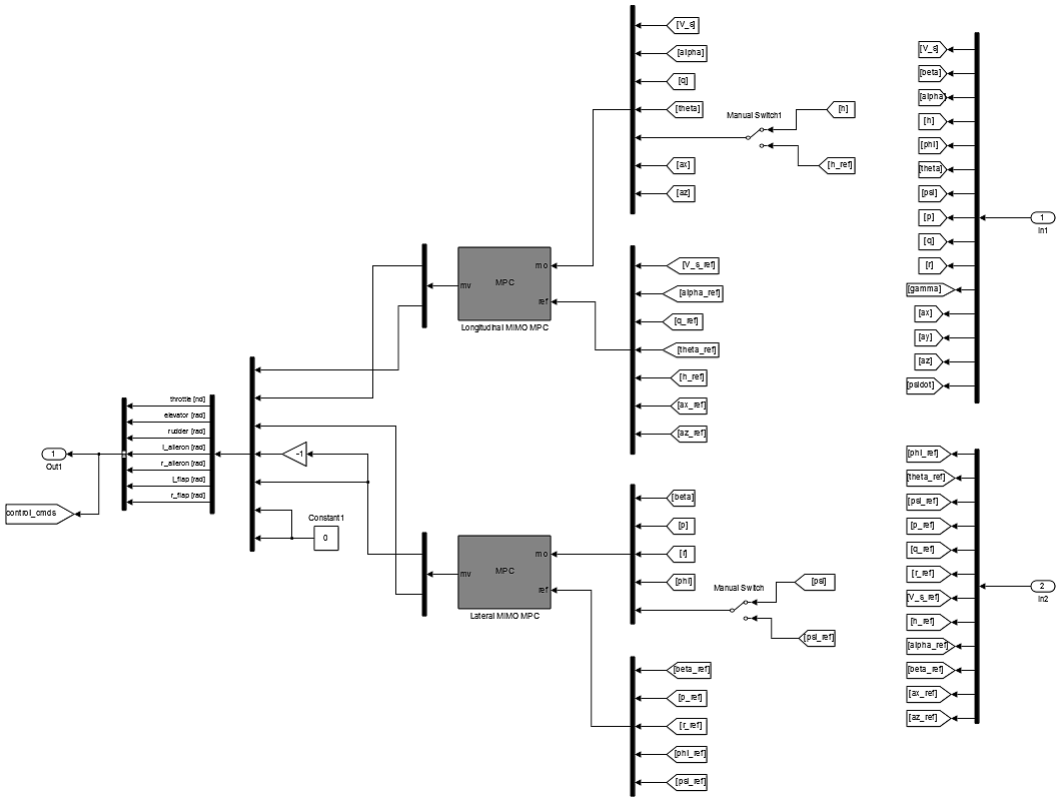

Figure 4.3 : Structure of the constrained lateral and longitudinal MIMO MPCs.

The MPCs are designed based on the linear lateral and longitudinal models which are decoupled from full linear model in Equation (2.84). The matrices of the all linear models with their numerical values can be seen in Appendix A. The full linear model is derived from the NL model at trim operating points obtained as in Table A.4 by using trim target of each flight scenario from Table 4.2.

There are some tricks in designing the MPCs for some flight scenarios. The key point for designing the MPCs in level climb is setting the altitude h free. The yaw angle ψ to be set free is the another key point for the MPCs in level turn. In parallel with these, both h and ψ are set free for climbing turn. In order to achieve climbing for level climb and climbing turn, h is required to change with time. On the other hand, ψ is required to change for level turn and climbing turn. Therefore the controllers must not make an effort for these control inputs to reach their reference value. As a result, h for level climb and climbing turn and ψ for level turn and climbing turn are set free by means of feeding their reference value through the constrained lateral and longitudinal MIMO MPCs instead of their instant value for each sampling period.

Table 4.2 : Trim targets with respect to flight scenarios [2].

Flight Scenario	Trim Target
Straight and Level	$V_a = 17m/s$, $\gamma = 0^\circ$
Level Climb	$V_a = 17m/s$, $\gamma = 5^\circ$
Level Turn	$V_a = 17m/s$, $\gamma = 0^\circ$, $\dot{\psi} = 20^\circ/s$
Climbing Turn	$V_a = 17m/s$, $\gamma = 5^\circ$, $\dot{\psi} = 20^\circ/s$
Level Steady Heading Sideslip	$V_a = 17m/s$, $\gamma = 0^\circ$, $\beta = 5^\circ$

Table 4.3 : References given along with the trim values for each flight scenario.

Flight Scenario	Reference given along with the trim value			
	$V_a(m/s)$	$h(m)$	$\phi(^\circ)$	$\psi(^\circ)$
Straight and Level	1	4.16	$\cdots$	4°
Level Climb	1	$\cdots$	$\cdots$	4°
Level Turn	1	$\cdots$	4°	$\cdots$
Climbing Turn	1	$\cdots$	4°	$\cdots$
Level Steady Heading Sideslip	1	$\cdots$	$\cdots$	4°

The simulations are carried out by exciting the closed loop NL model by means of giving trim values of each state as references except the ones in Table 4.3 at $5^{th}s$ of the simulation. An extra 4° reference is given to ψ in straight and level and level climb scenarios different from the article [36] in order to point out the effect of the controller in controlling the lateral dynamics despite of the longitudinal flights. The graphs for the NL simulations of all flight scenarios can be seen in the following figures [36]:

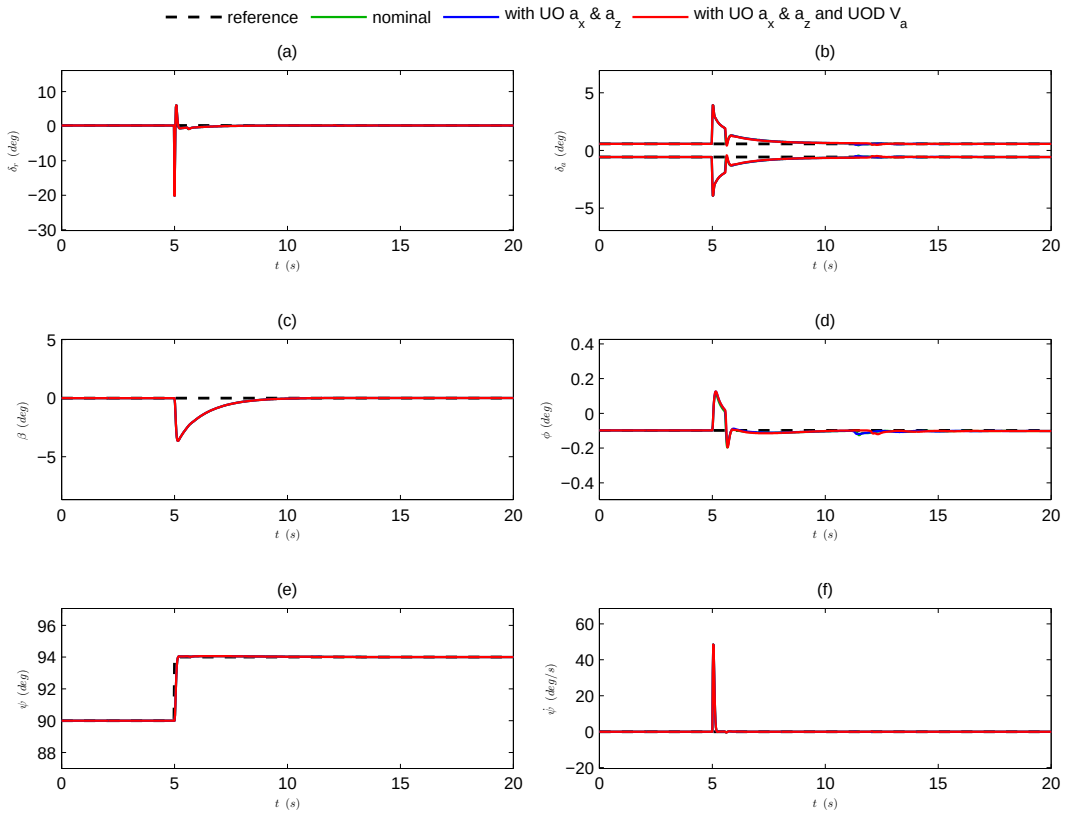

Figure 4.4 : Lateral response of straight and level in NL simulation.

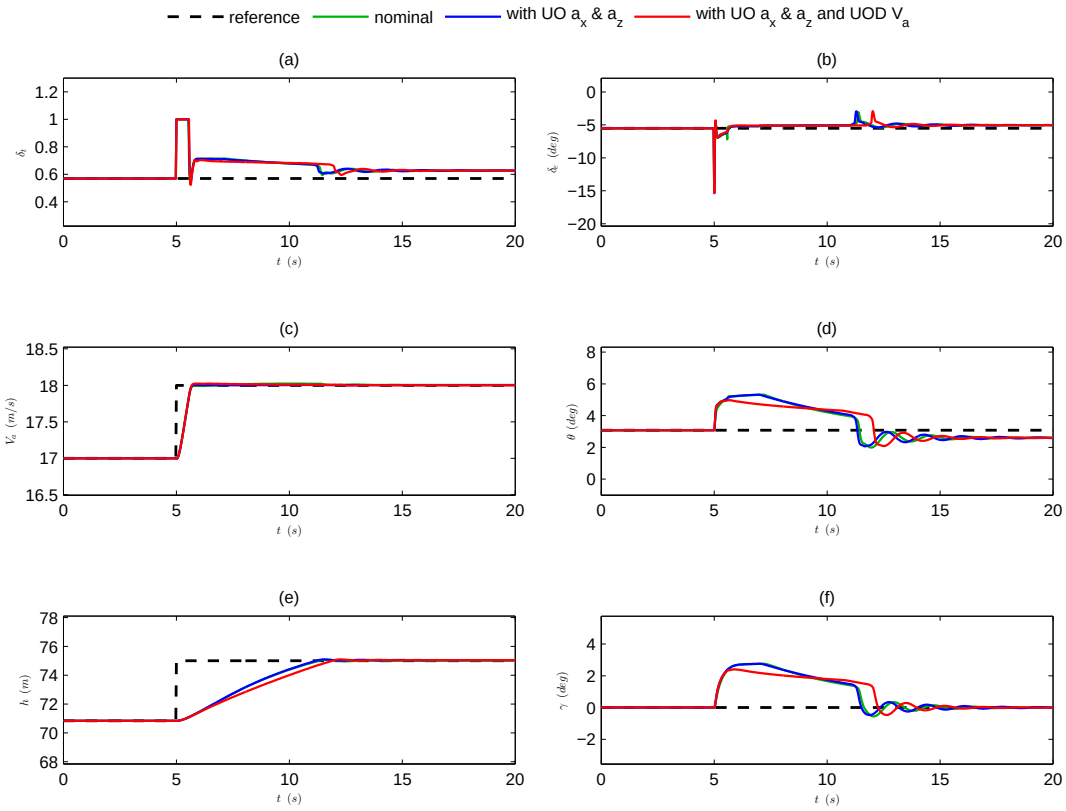

Figure 4.5 : Longitudinal response of straight and level in NL simulation.

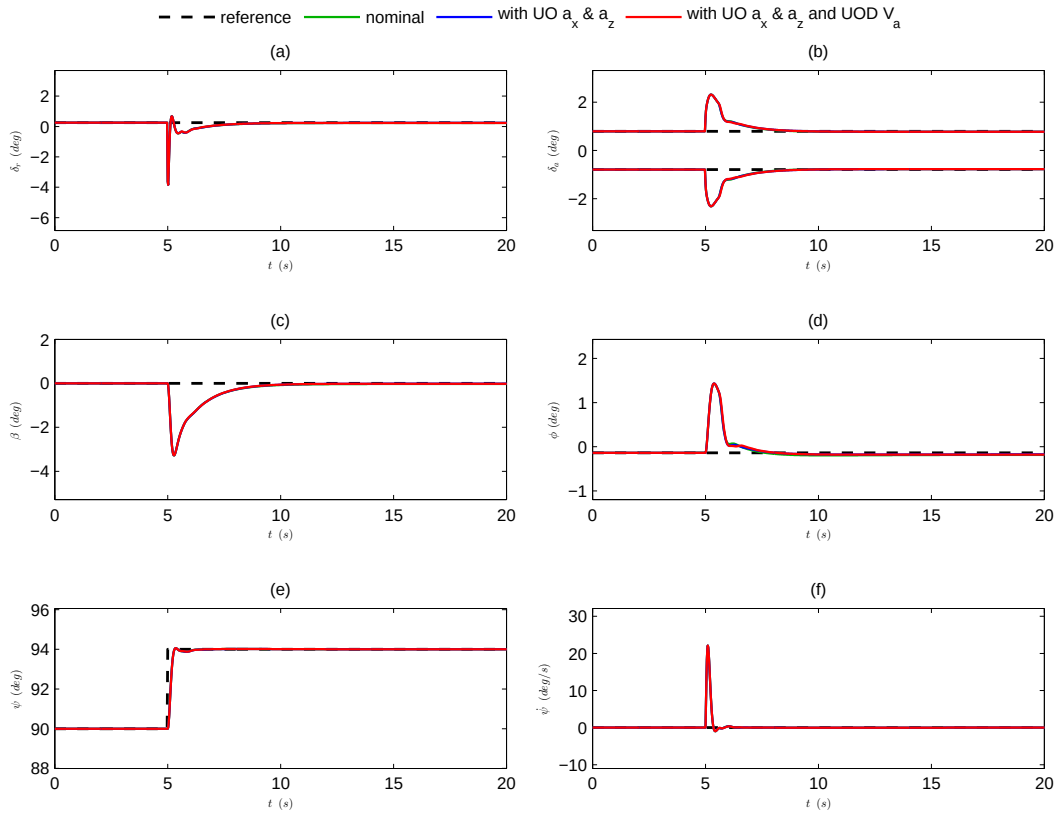

Figure 4.6 : Lateral response of level climb in NL simulation.

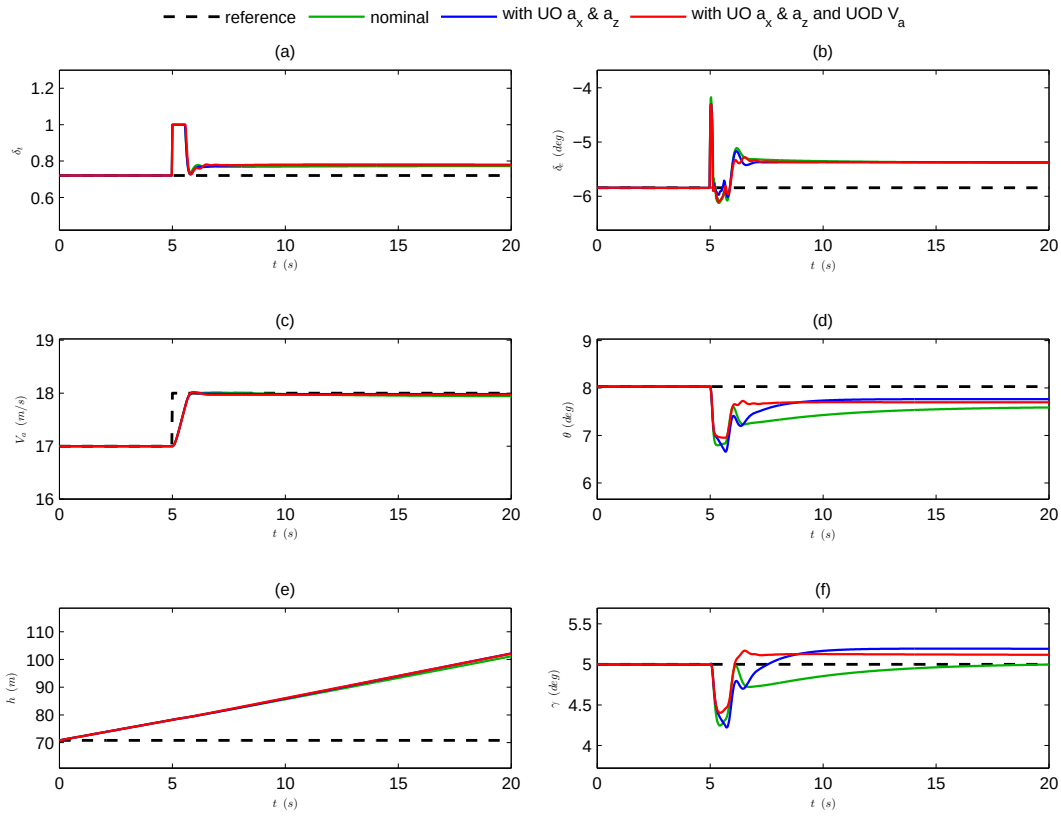

Figure 4.7 : Longitudinal response of level climb in NL simulation.

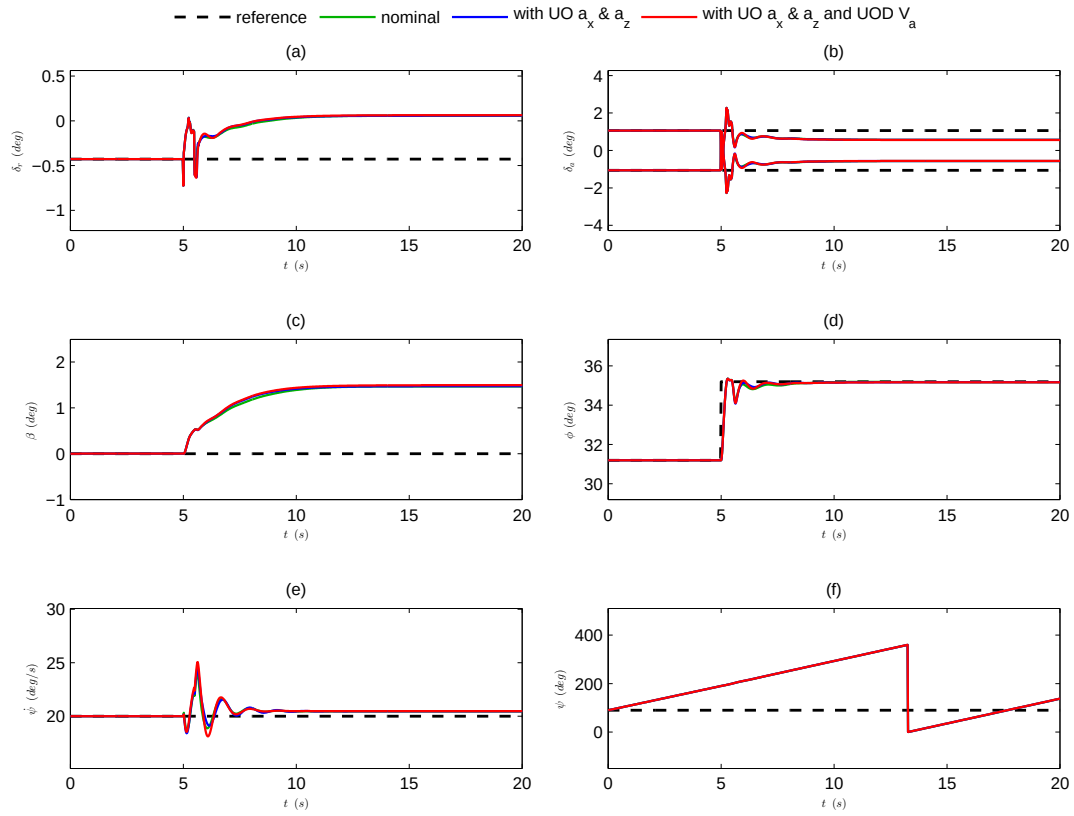

Figure 4.8 : Lateral response of level turn in NL simulation.

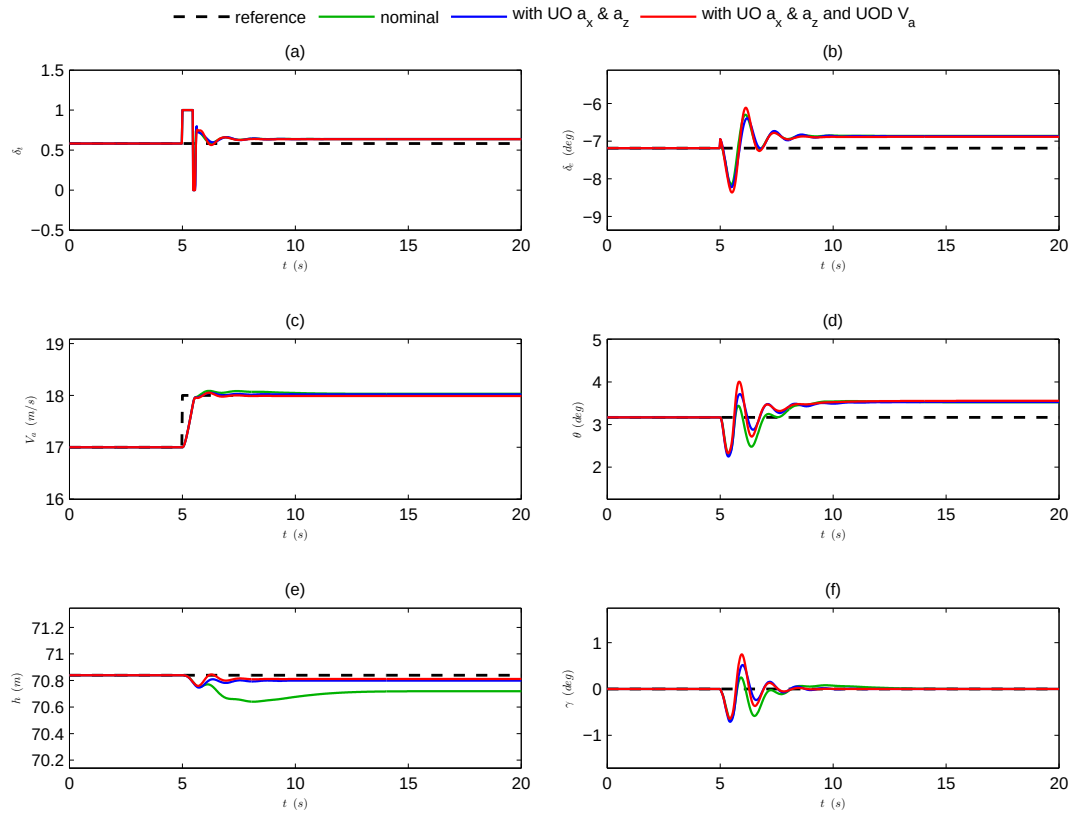

Figure 4.9 : Longitudinal response of level turn in NL simulation.

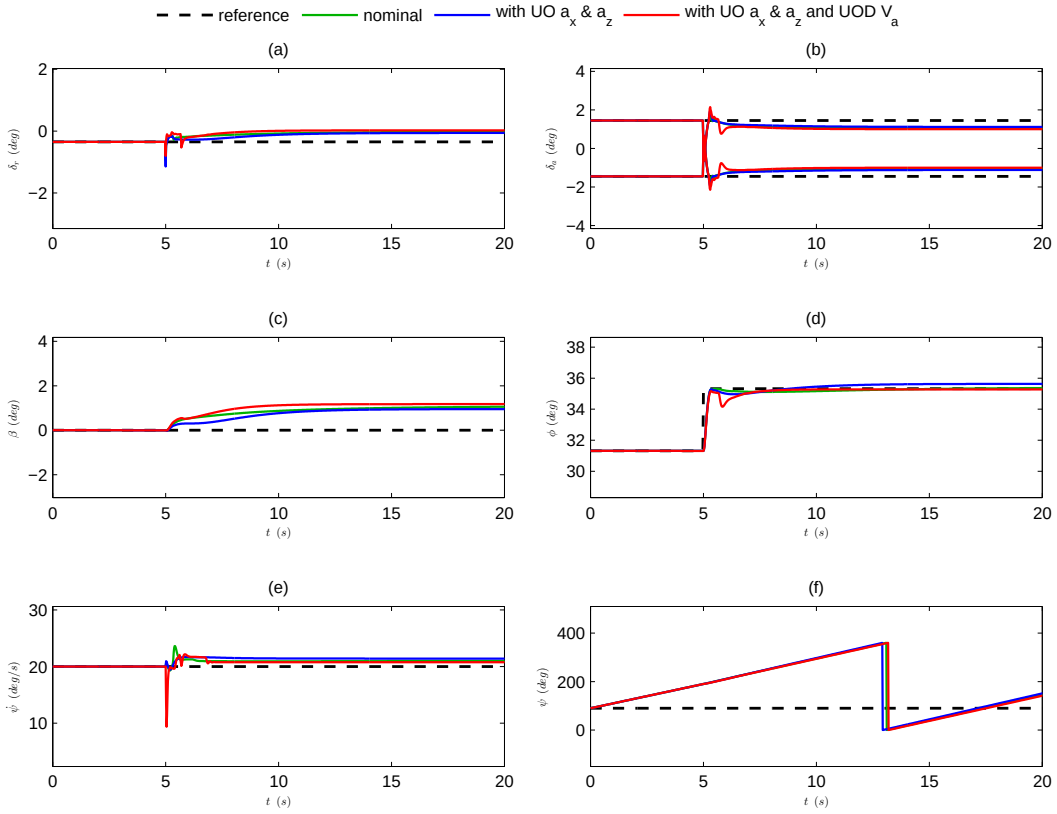

Figure 4.10 : Lateral response of climbing turn in NL simulation.

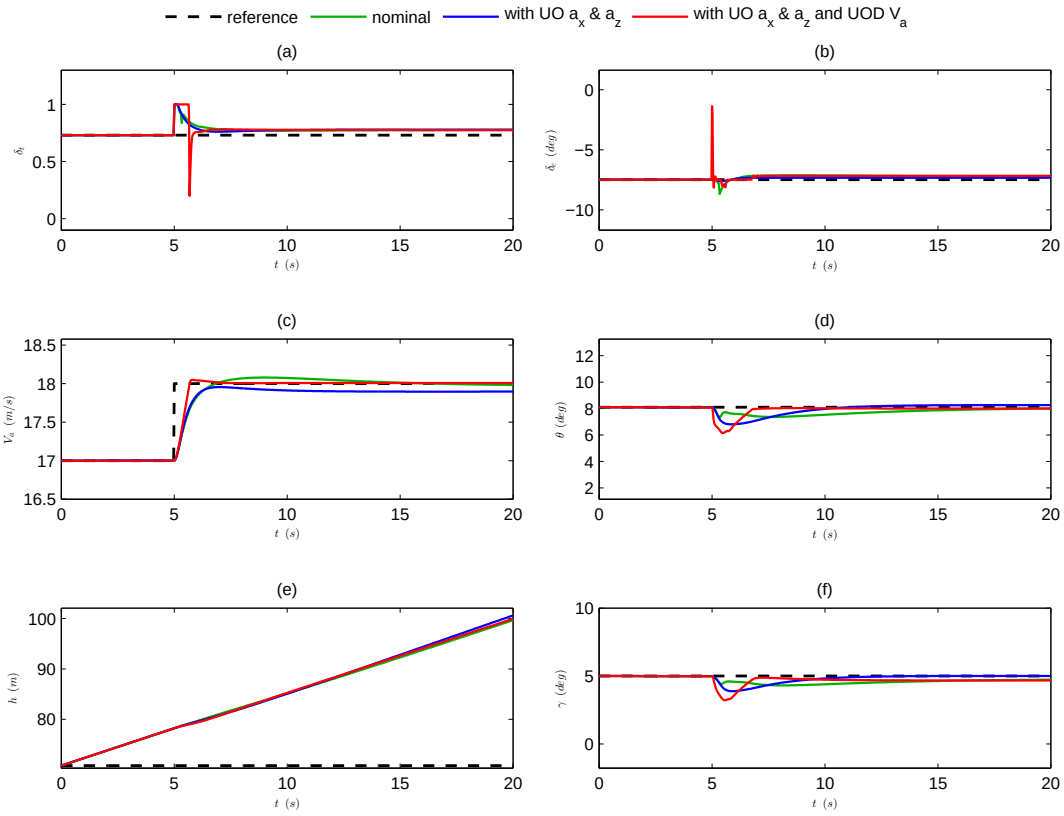

Figure 4.11 : Longitudinal response of climbing turn in NL simulation.

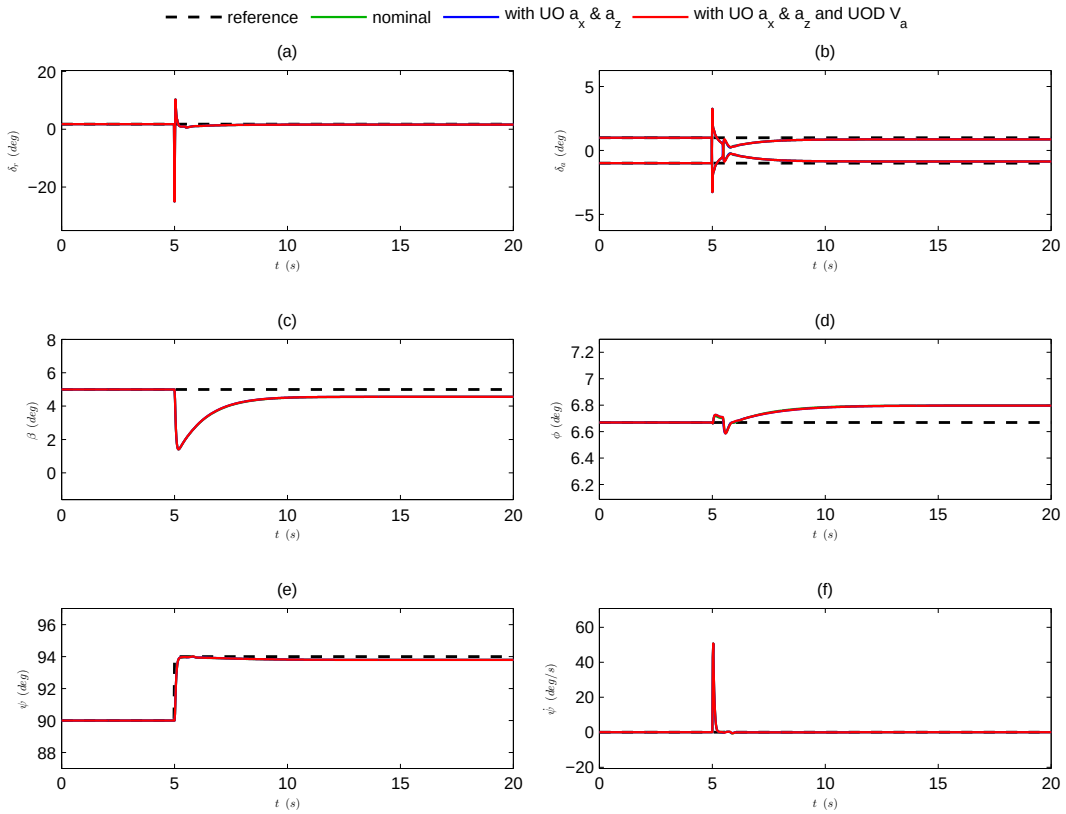

Figure 4.12 : Lateral response of level steady heading sideslip in NL simulation.

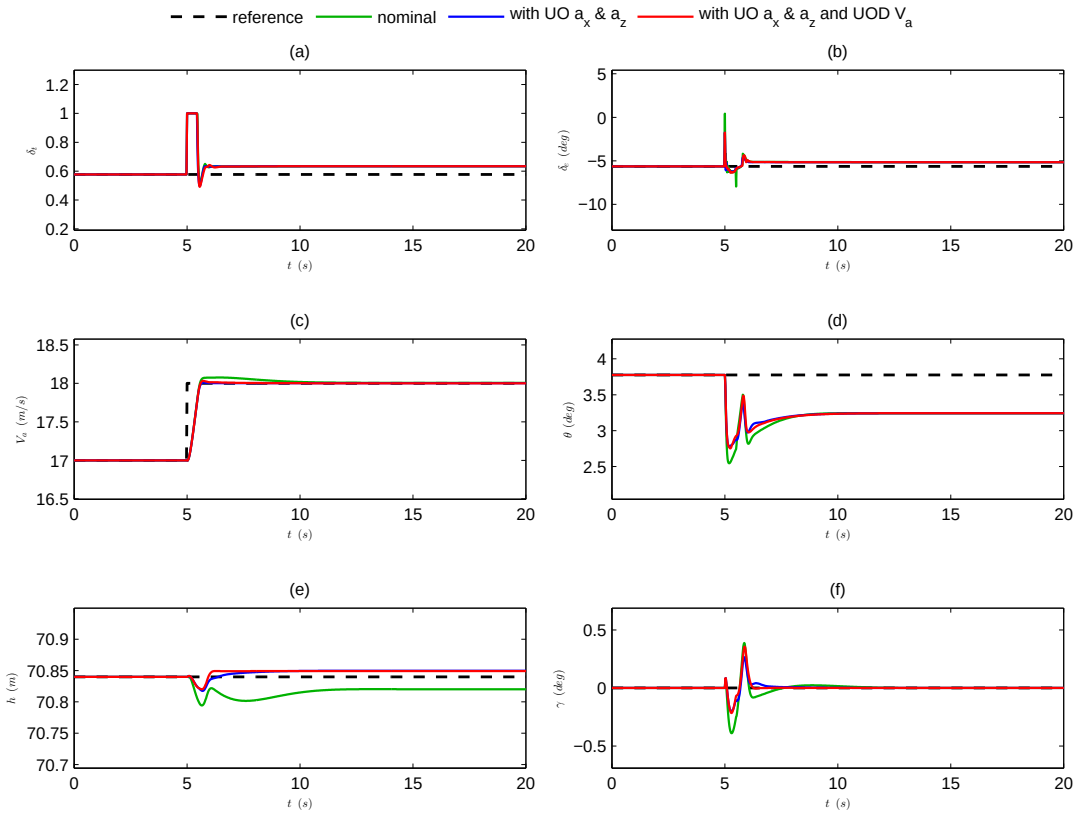

Figure 4.13 : Longitudinal response of level steady heading sideslip in NL simulation.

where UO and UOD denote the unmeasured output and unmeasured output disturbance, respectively, as mentioned in Chapter 1.

The constrained lateral and longitudinal MIMO MPCs generate input signals all time and change their values different from the trim values of each dependent on the references within the saturation limits in Table 4.1 as seen in all Figures from 4.4(a,b) to 4.13(a,b). Thus, they provide the all states to track the trim values along with the related states to track the references given at $5^{th}s$ as seen in Table 4.3. However, δ_t saturates for a while in Figures 4.5(a), 4.7(a), 4.9(a), 4.11(a), 4.13(a) in order to increase the airspeed V_a from trim point $17m/s$ to $18m/s$ due to the references given at $5^{th}s$ of the all simulations.

As can be seen in Figure 4.4 to 4.13 that the states track the trim values with nearly no steady state errors (SSEs) until $5^{th}s$. At steady state region, the states track the references with small SSEs as shown in Table A.6.

In the simulations of straight and level, oscillations starts to occur especially in Figures 4.5(d) and 4.5(f) with bigger amplitude than those of the others as a result of the references given to V_a and altitude h at $5^{th}s$. Due to the step reference with a magnitude of $4.16m$ along with its trim value given to h, flight path and pitch angles γ and θ oscillate much more in order h to reach the new reference value, $75m$, right away. Therefore, the biggest maximum percentage overshoot (MPO) is observed in θ for straight and level flight as can be seen in Table A.8 because of this short-time change of the flight scenario from straight and level to level climb. Similarly, oscillations are observed in Figures 4.7(d), 4.7(f), 4.13(d) and 4.13(f) with bigger amplitude than those of the others in the graphs of the simulations for level climb and level steady heading sideslip by means of the reference given to V_a at $5^{th}s$ in order V_a to reach the new reference value, $18m/s$, right away.

Considering the simulations of level turn and climbing turn, oscillations are observed especially in Figure 4.8(e) and 4.10(e) with bigger amplitude than those of the others by means of the references given to V_a and roll angle ϕ at $5^{th}s$, since yaw rate $\dot{\psi}$ is a function of V_a and ϕ [54]. A maximum SSE on sideslip angle β for level turn occur due to the decrease in level turn radius, which is a function of V_a and ϕ [55]. In climbing

turn, the SSEs on β and ψ occur due to the decrease in climbing turn radius, which is a function of V_a, ϕ and γ, as well [55].

On the other hand, maximum settling time is obtained in γ and θ for climbing turn as can be seen in Table A.7. Increasing the roll reference provides the UAV to lose altitude along with the decreasing turning radius in lateral motion. Thus, a little undershoot occurs in Figure 4.11(e) at $5^{th}s$ which means the UAV to start to lose altitude as a result of the undershoot in Figures 4.11(d) and 4.11(f). The longitudinal MIMO MPC provides γ and θ to track the reference value of each which means the UAV to climb in the same trajectory over time.

Modelling errors due to the linearization of the NL model at trim operating points are compensated by the help of Kalman state observer as a result of assigning a_x and a_z among the NL model outputs as unmeasured and adding a unit step as UOD to the V_a. Thus, steady state and especially transient state response of the simulations are improved in most cases comparing with the nominal condition as can be clearly seen in Tables A.6, A.7 and A.8.

4.2 Processor In The Loop Simulations

PIL simulations are performed for the same NL model of Ultra Stick 25E as in NL simulations. They are conducted in case of the 5 same flight scenarios under the windy conditions such as SW and WG in a desired and controlled manner by means of the deployed constrained lateral and longitudinal MIMO MPCs with no UOs, UODs and MNs on BeagleBone Black Rev C as the actual target hardware. The same NL model is used for obtaining the linear model and closed loop simulations. The closed loop NL model with the MPCs is simulated $100s$ with the solver used as Fourth-order Runge-Kutta fixed step integration method with a time step of $0.02s$ in Matlab for the same flight scenarios as mentioned before. The MPCs with the same structure as shown in Figure 4.3 are designed including the same actuator saturation limits as indicated in Table 4.1 for each flight scenario. They are based on the linear lateral and longitudinal models in Equations (2.85) and (2.86) which are obtained by decoupling the full linear model. The full linear model is derived from the NL model at trim operating obtained with respect to the trim targets of each flight scenario as shown in Table 4.4.

Table 4.4 : Trim targets with respect to flight scenarios [2].

Flight Scenario	Trim Target
Straight and Level	$V_a = 17m/s$, $\gamma = 0^\circ$, $h = 50m$
Level Climb	$V_a = 17m/s$, $\gamma = 5^\circ$, $h = 50m$
Level Turn	$V_a = 17m/s$, $\gamma = 0^\circ$, $h = 50m$, $\dot{\psi} = 20^\circ/s$
Climbing Turn	$V_a = 17m/s$, $\gamma = 5^\circ$, $h = 50m$, $\dot{\psi} = 20^\circ/s$
Level Steady Heading Sideslip	$V_a = 17m/s$, $\gamma = 0^\circ$, $h = 50m$, $\beta = 5^\circ$

Similarly, in PIL simulations, The MPCs are designed one by one for each flight scenario based linear lateral and longitudinal models whose matrices with numerical values can be found in Appendix A. The trim operating points obtained for each flight scenario in numerical values can be seen in Table A.5. SW components to be taken into account to the dynamics of the UAV model in trim calculations different from the NL simulations causes a small increase in θ with a magnitude of 0.4° in climbing type scenarios such as level climb and climbing turn, which provides to minimize the SSE. As mentioned before that the MPCs must not make an effort for altitude in climbing and yaw angle for turning scenarios. Therefore, the altitude is set free in climbing scenarios while the yaw angle is set free in turning scenarios by means of feeding their reference value through the longitudinal and lateral MIMO MPCs instead of their instant value for each sampling period in the related simulations.

PIL simulation consists of a laptop to simulate the NL plant to be controlled and the target hardware or processor which the MPCs are deployed as can be seen in Figure 4.14. Communication between them is done via a USB-serial link.

Actual target hardware used in this thesis is BeagleBone Black Rev C. It is a low-cost and small-sized board based on an AM335x ARM Cortex-A8 processor running at 1GHz with 512MB DDR3 RAM, 4GB 8-bit eMMC on-board flash storage and connection ports such as USB, Ethernet and HDMI [56].

The behaviour of a candidate control algorithm on target hardware or processor can be evaluated by PIL simulation, where the actual target processor is fully involved. The restrictions and requirements that the hardware imposes, such as limited memory resources or behavior of target-specific optimized code are not taken into account in ordinary simulations. PIL simulation provides to test the object code with using test vectors developed and applied to the Simulink model as the object code is deployed

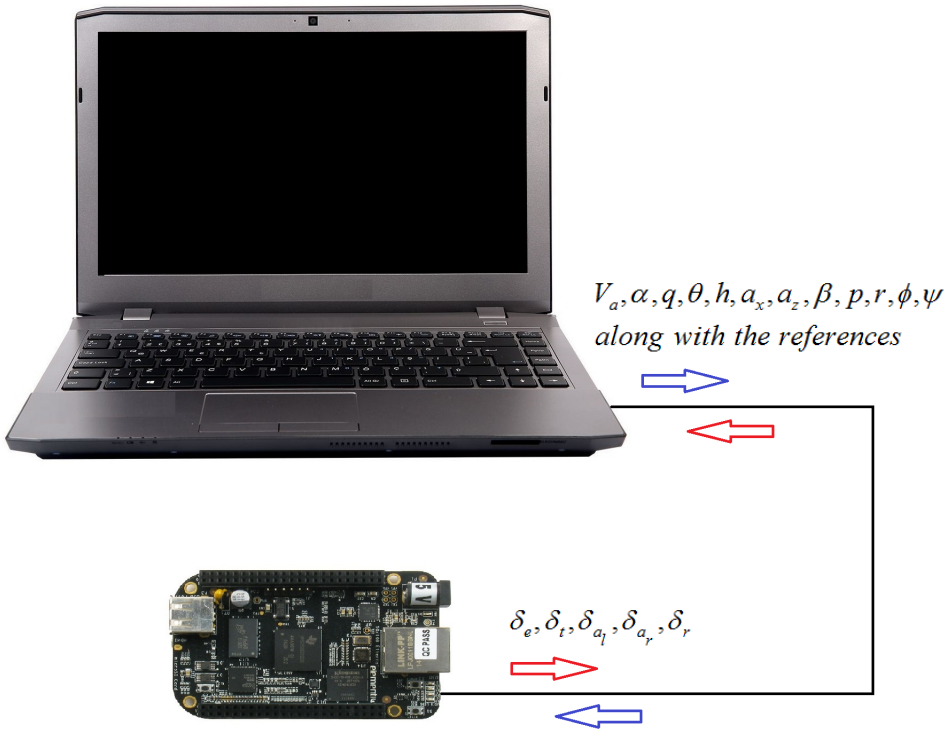

Figure 4.14 : Schematic diagram of the hardware used in the PIL simulations.

on the actual target hardware. Real code behavior can be verified on the actual target hardware and code coverage along with execution time can be obtained [57].

In Matlab, the PIL block is only available with the Embedded IDE Link product. It can be automatically created from a complete model or a subsystem to test the code which is generated or cross-compiled for the target hardware and runs on the target platform by means of the Embedded IDE Link product used with Real-Time Workshop Embedded Coder [57]. Thus, it runs the MATLAB generated C code on the actual target hardware. The process steps of PIL simulation in Matlab can be explained as follows:

- Firstly, stimulus signals to the code on the actual target hardware is sent by Simulink for each sample interval of the simulation through a communication channel.
- Then, the actual target hardware executes the PIL algorithm for one sample step.
- Finally, the PIL algorithm sends output signals computed in this process to Simulink through the channel.

One sample cycle of the simulation is said to be completed at the end of the above steps. Simulink proceeds to the next sample interval and these steps repeat during the

simulation. The most important point in PIL simulations is them not to run in real time. Simulink and the object code exchange all I/O data at each sample period [57]. Therefore, communications delay is much more important than the computation time [41]. Also, potential differences between the model and the object code can be checked if any deviations in the performance exist due to the compilation process by the help of PIL simulation as shown in Figure 4 [40].

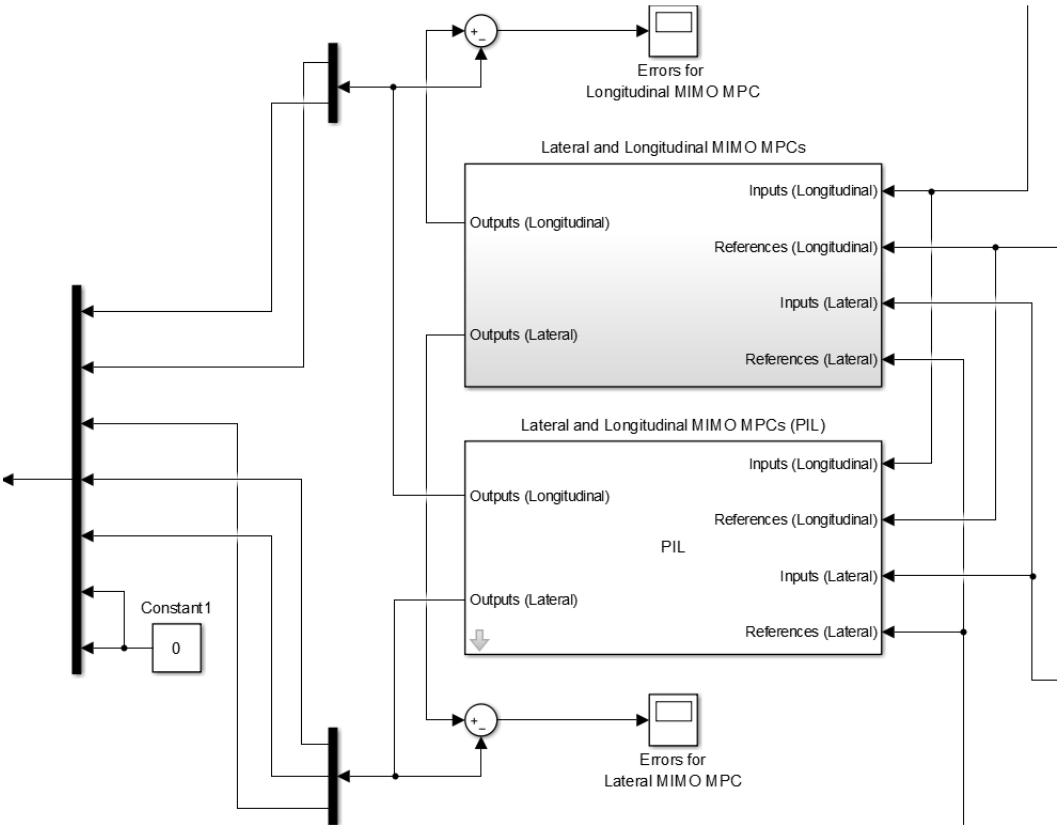

Figure 4.15 : Structure of the PIL simulation.

In NL simulations, the performance of the MPCs are tested with the change of the UO and UOD of the MPCs and some references of the states. Thus, robustness of the MPCs in case of these conditions are successfully tested. However, the performance of them are not tested in windy conditions and the application to the real hardware is not tested. Therefore, in the PIL simulations these conditions are tested in a successful way. The PIL simulations are carried out by exciting the closed loop NL model by means of giving trim values of the all outputs of both the lateral and longitudinal linear models as references. The graphs for the simulations of all flight scenarios can be seen in the following figures:

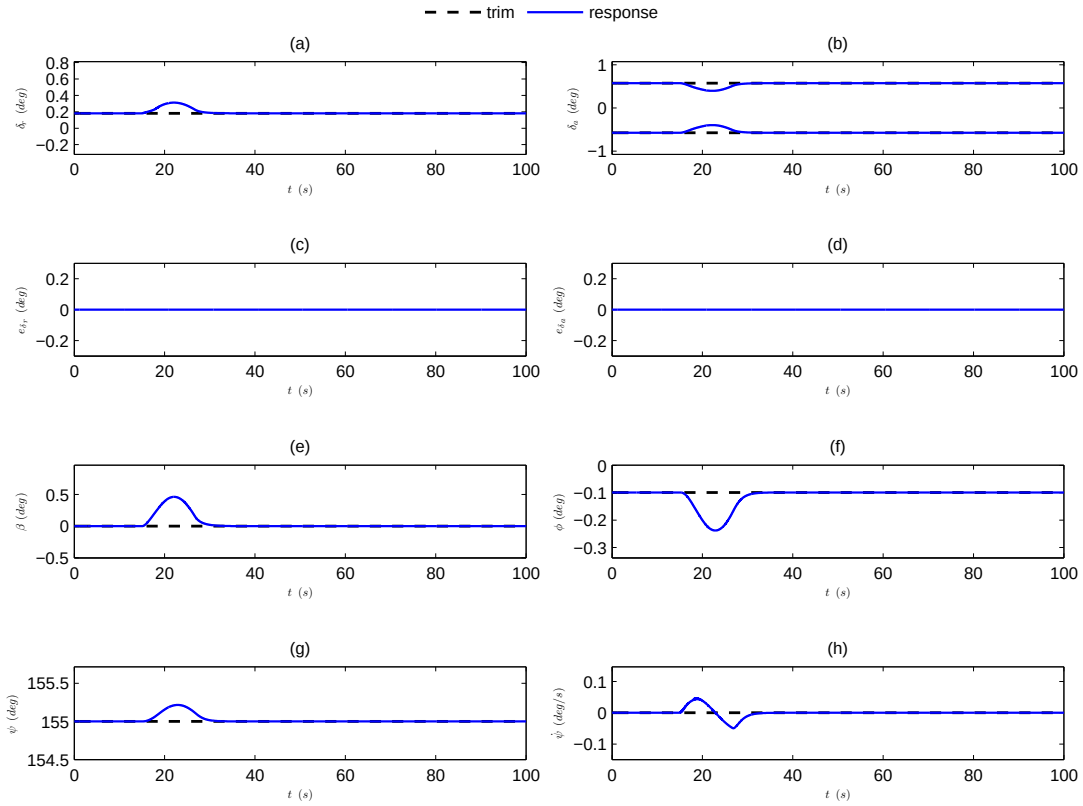

Figure 4.16 : Lateral response of straight and level in PIL simulation.

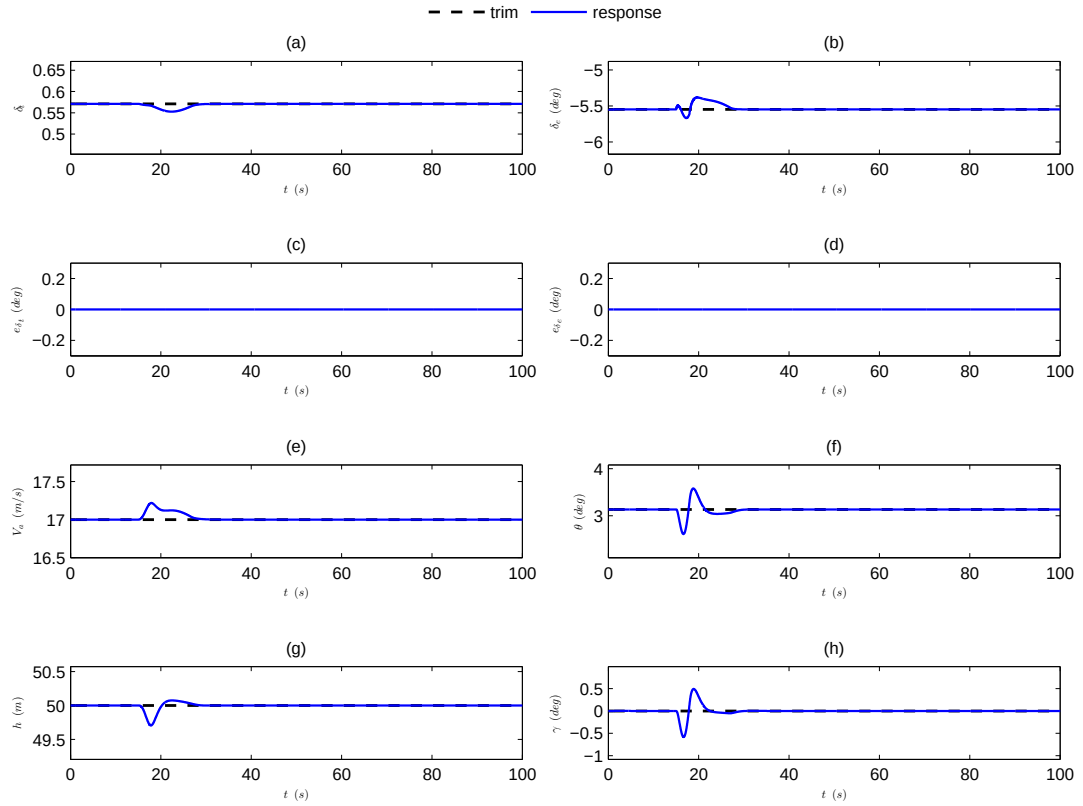

Figure 4.17 : Longitudinal response of straight and level in PIL simulation.

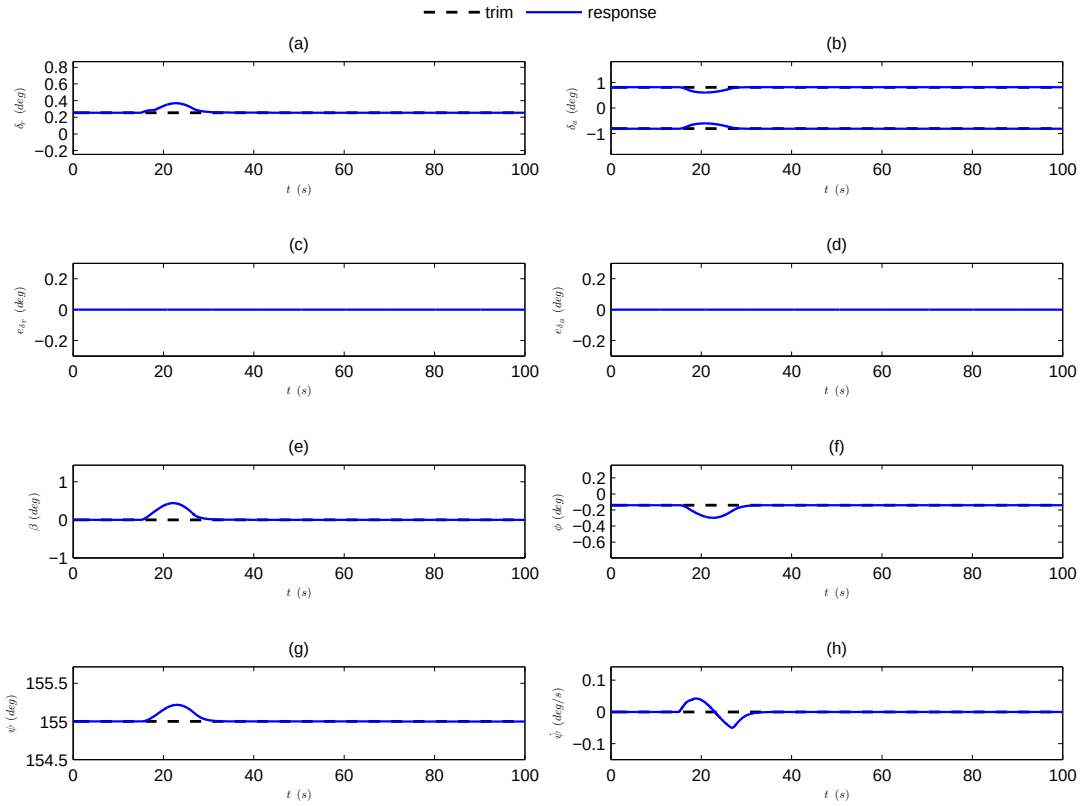

Figure 4.18 : Lateral response of level climb in PIL simulation.

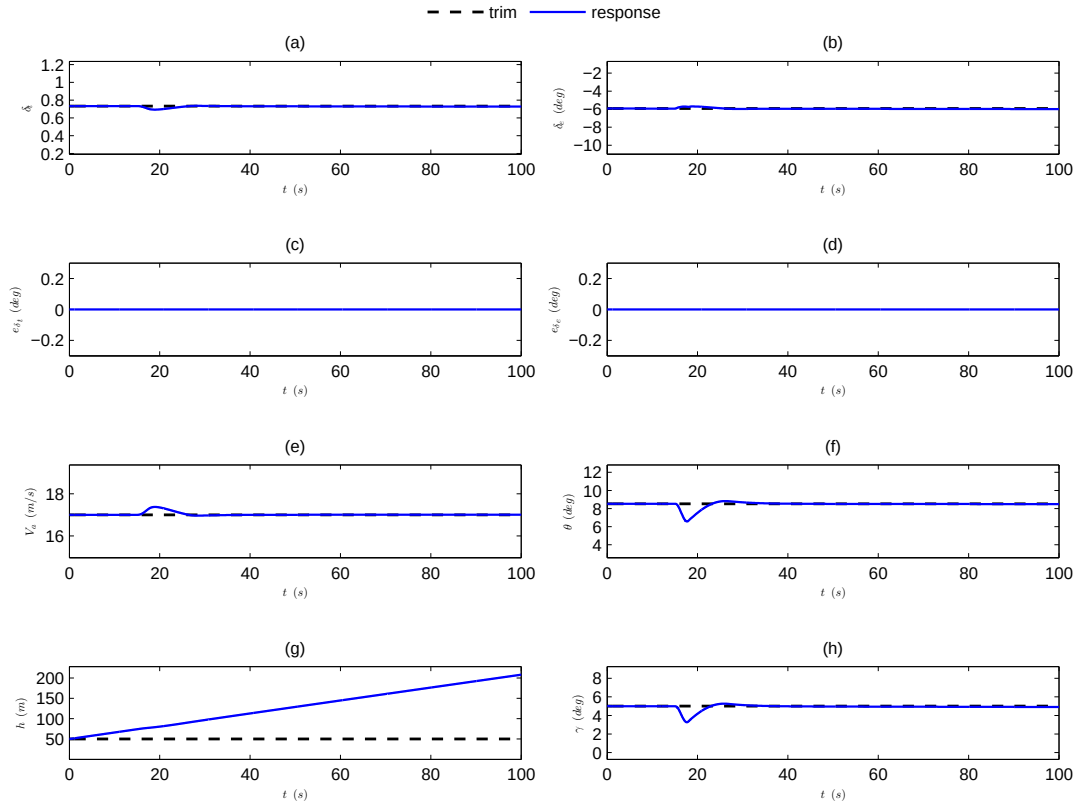

Figure 4.19 : Longitudinal response of level climb in PIL simulation.

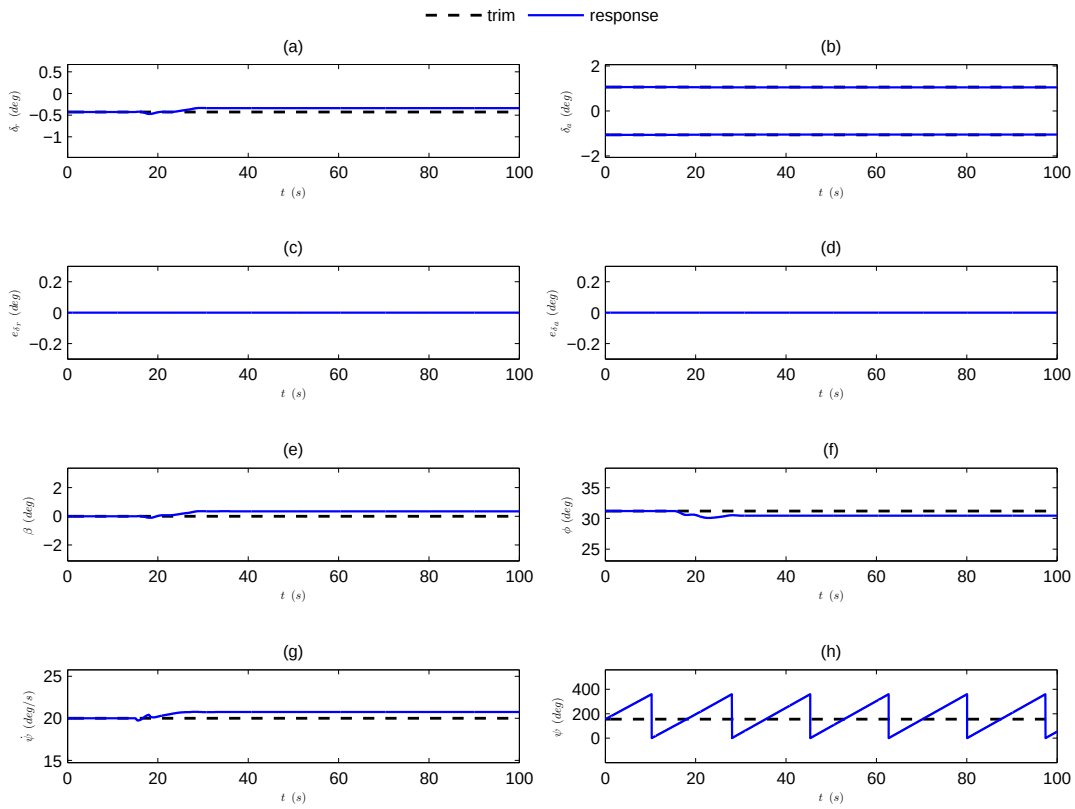

Figure 4.20 : Lateral response of level turn in PIL simulation.

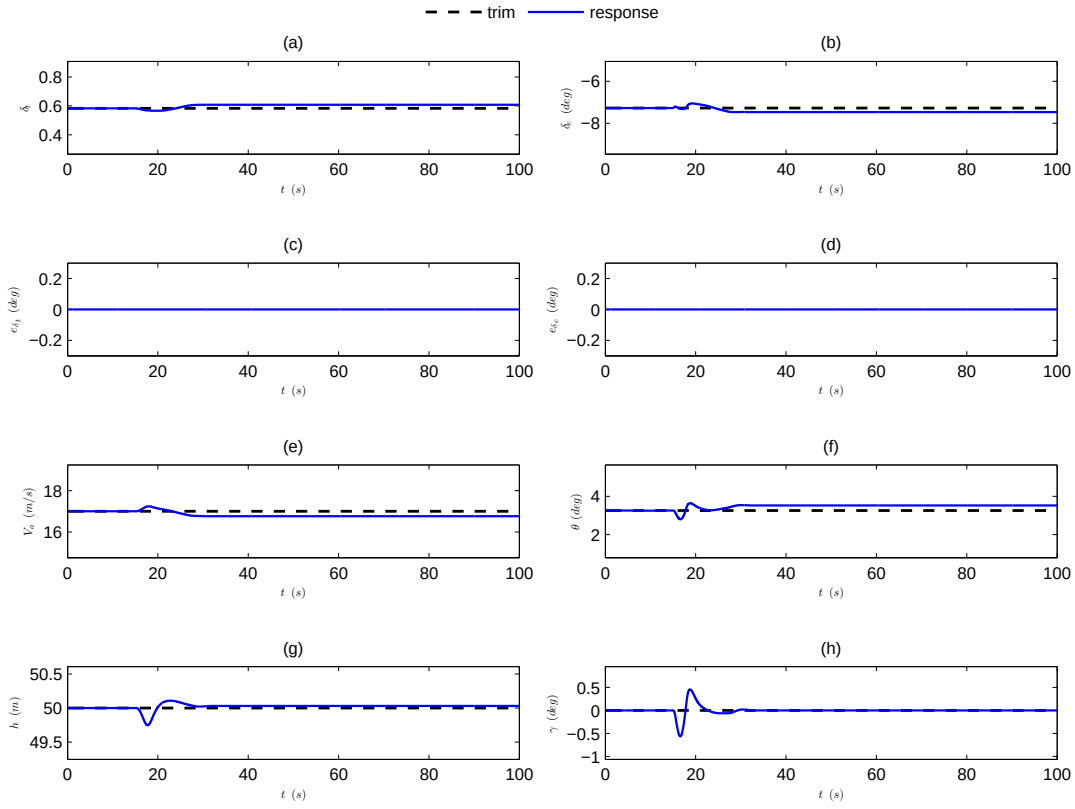

Figure 4.21 : Longitudinal response of level turn in PIL simulation.

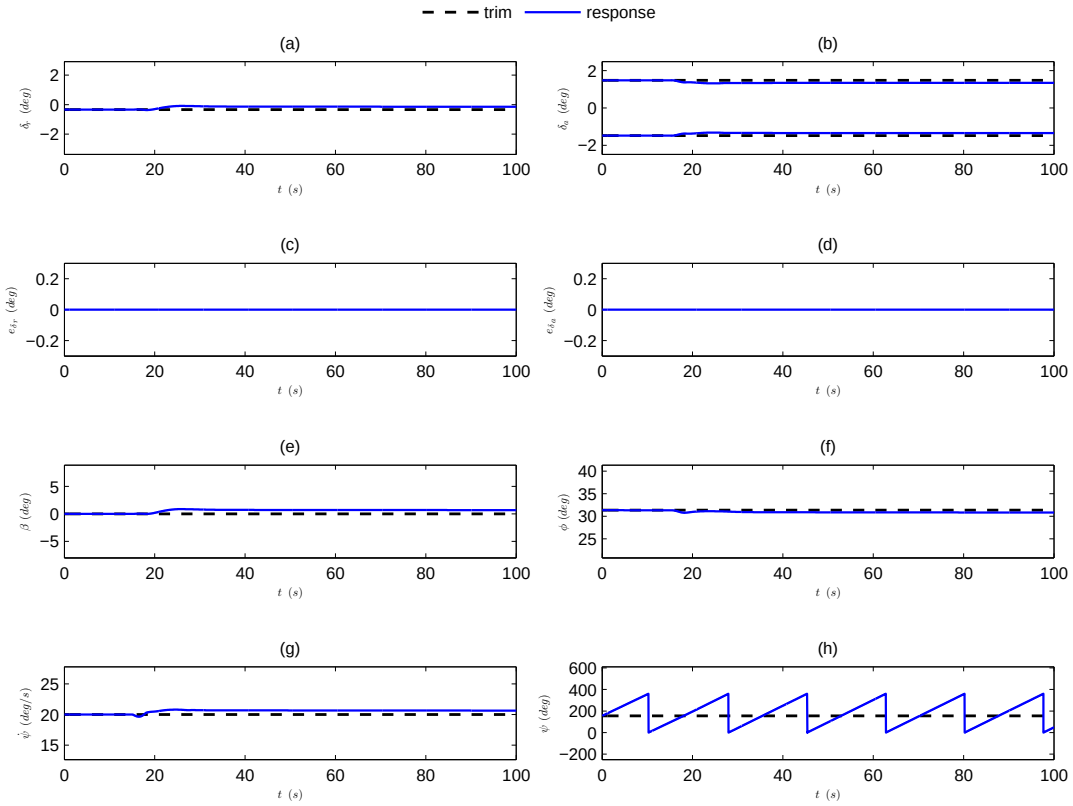

Figure 4.22 : Lateral response of climbing turn in PIL simulation.

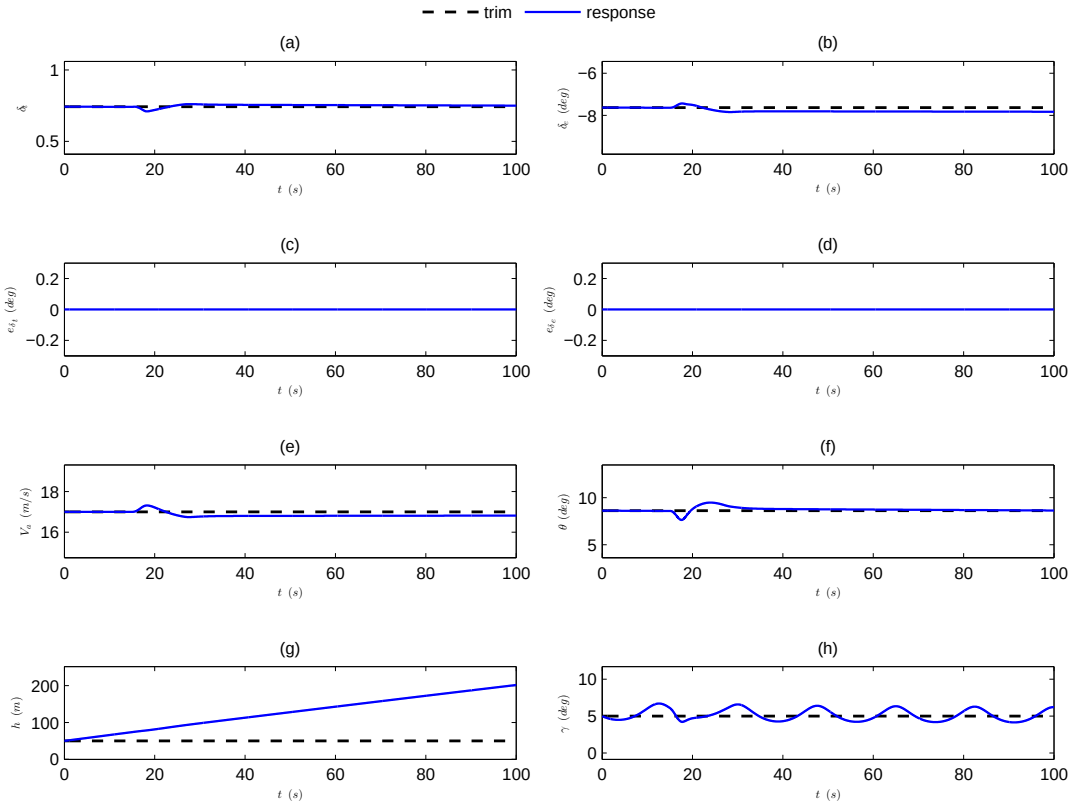

Figure 4.23 : Longitudinal response of climbing turn in PIL simulation.

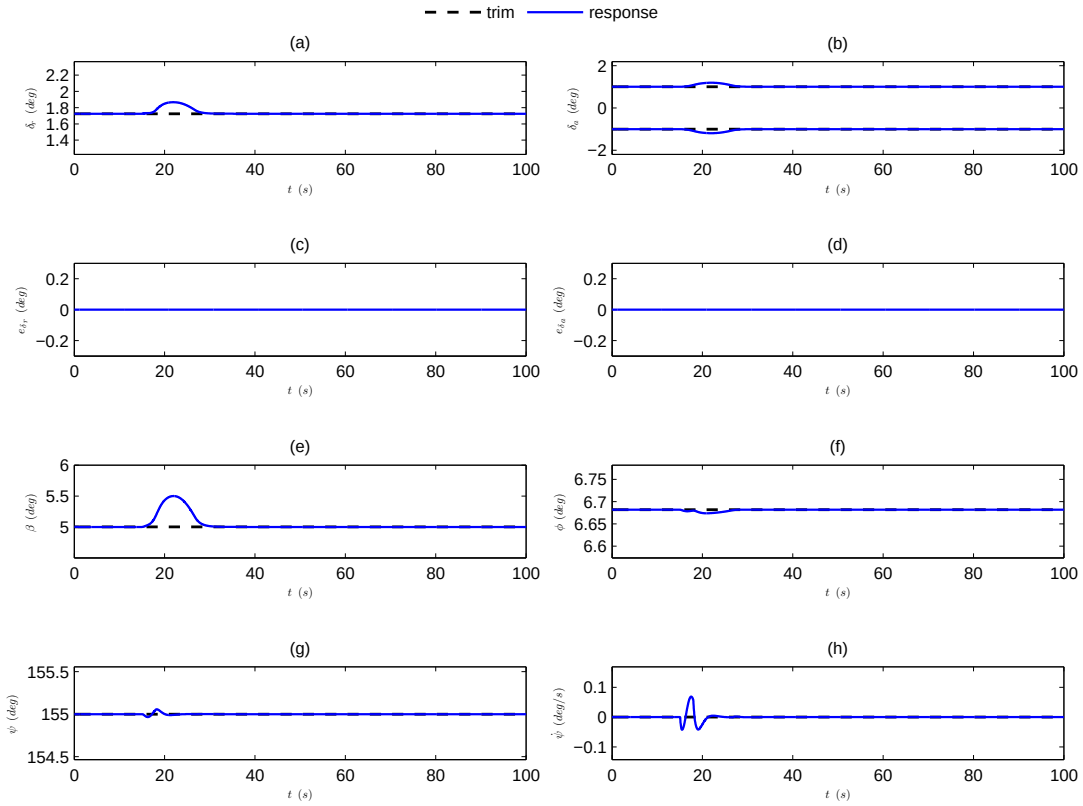

Figure 4.24 : Lateral response of level steady heading sideslip in PIL simulation.

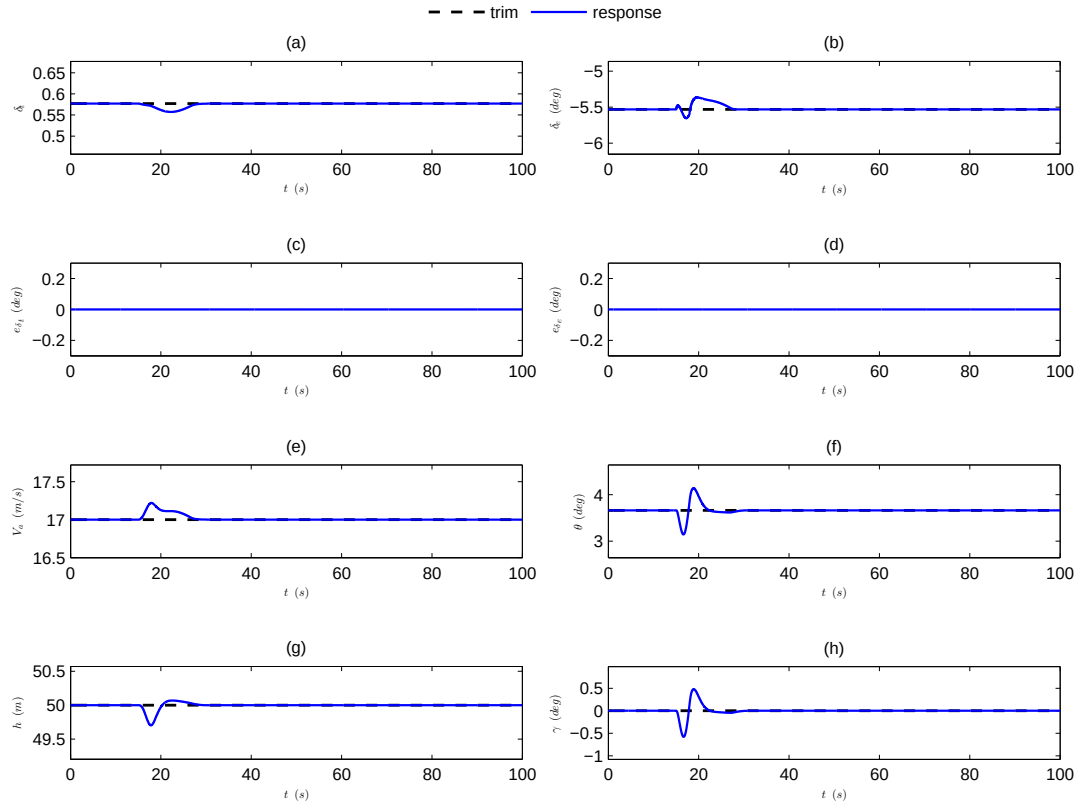

Figure 4.25 : Longitudinal response of level steady heading sideslip in PIL simulation.

where e_{δ_r}, e_{δ_a}, e_{δ_t} and e_{δ_e} are the errors of the control inputs rudder, aileron, throttle and elevator generated by the model and the object code as indicated in Figure 4.15. Computational error and communications delay are not obtained in the PIL simulations as can be seen in Figures from 4.16(c,d) to 4.25(c,d). Therefore, BeagleBone Black Rev C to be used in this thesis shows that the right choice is made for the target hardware.

The constrained lateral and longitudinal MIMO MPCs generate input signals all time and change their values different from the trim values of each dependent on the WG within the saturation limits in Table 4.1 as seen in all Figures from 4.16(a,b) to 4.25(a,b). Thus, they provide the all states to track the trim references under the windy conditions such as SW and especially WG occurring at $15^{th}s$.

Generally, no oscillations and no SSEs are obtained until a sudden WG occurs at $15^{th}s$ since the system is not perturbed or not excited with any references different from the trim values as can be clearly seen in all Figures of PIL simulations from 4.16 to 4.25.

In the simulations of straight and level in Figures 4.16 and 4.17, level climb in Figures 4.18 and 4.19 and level steady heading sideslip in Figures 4.24 and 4.25, the states generally track the trim references with small SSEs as shown in Table A.9. Besides that in the simulations of level turn in Figures 4.20 and 4.21 and climbing turn in Figures 4.22 and 4.23, bigger SSEs comparing with the other simulations are observed. The SSEs of sideslip angle β, roll angle ϕ, pitch angle θ and yaw rate $\dot{\psi}$ occurs when the WG occurs at $15^{th}s$. Since in a coordinated flight, a change in the wind strength or direction like a WG causes a change in the sideslip [52]. However it is seen that when the SSE of β is obtained as nearly zero, especially the SSE of ϕ along with θ and $\dot{\psi}$ increases. Thus, the SSEs of them is minimized during the MPCs tuning in order to provide the coordinated turn with small SSEs.

As shown in Table A.10, the biggest settling time is obtained in inertial-referenced flight path angle γ in climbing turn in exchange for getting small SSE and overshoot. The biggest MPO is obtained in β in climbing turn as shown in Table A.11. Even though it is not a big MPO value in general, it is expected to be obtained in β due to the effect of the WG on β particularly in climbing turn. On the other hand, γ oscillates

sinusoidally in Figure 4.23(h) since it is a function of θ and inertial speed V_g whose magnitude changes with SW [42].

5. CONCLUSIONS AND RECOMMENDATIONS

UAVs are important to have a place for the usage in the various civil and military applications like battlefield and police surveillance, reconnaissance, combat, targeting, decoying, crop dusting, observations, TV broadcasting, photography, logistics etc. Thus the control of them is extremely important from the standpoint of carrying out their duties in a desired and controlled manner.

As a 1^{st} study of this thesis, design of the constrained lateral and longitudinal MIMO MPCs for 5 flight scenarios such as straight and level, level climb, level turn, climbing turn and level steady heading sideslip are investigated with the simulations of the nonlinear closed loop models. The MPCs are used for the control objectives like roll, pitch and yaw attitude, altitude and speed hold along with turn coordination. The performance of the MPCs are tested under 3 different conditions and compared for each flight scenario. Firstly, the performance of them is tested under nominal conditions. Secondly, under 2 UOs as a_x and a_z. Finally, under 2 UOs as mentioned before and 1 UOD on V_a with a random step-like noise having a magnitude of 1. The results of the simulations show that the proposed MPCs can achieve satisfactory performance and flying qualities for the all flight scenarios considered in this study under the specified test conditions. Modelling errors due to the linearization of the NL model at trim operating points are compensated by the help of Kalman state observer as a result of assigning a_x and a_z among the NL model outputs as unmeasured and adding a unit step as UOD to the V_a. Thus, steady state and especially transient state response of the simulations are improved in most cases comparing with the nominal condition. Originally, the proposed MPCs enable to change more than one references of the states at any time. In this way, the controllers provide more flexibility in terms of tracking complex trajectories comparing with the classical controllers and the another MPC applications discussed in Chapter 1. Also, they are applicable for the all flight scenarios even in real time without switching like some classical controllers in the literature.

In 2^{nd} study of the thesis, the performance of the MPCs without any UOs, UODs and MNs applied to the nonlinear UAV model is tested in the PIL simulations under the windy conditions such as SW and WG while SW components are taken into account to the dynamics of the UAV model in trim calculations. Windy conditions are one of the most important parameters in testing performance of controllers. Thus, their effects must be taken into account in design of controllers and controllers must be robust to disturbances like winds. PIL simulation is crucial in the way of the test of the code generated from a controller model run on an actual target hardware before an HIL simulation or actual flight test. BeagleBone Black Rev C is used as a target hardware in the PIL simulations. The same fixed wing UAV is targeted to perform PIL simulations for the same flight scenarios under the specified windy conditions in a desired and controlled manner. The results of the PIL simulations show that the MPCs can achieve satisfactory performance and flying qualities for the all flight scenarios under the specified windy conditions and no computational error and no communications delay are obtained. Originally, BeableBone Black Rev C is found practicable beside the MPCs enable to change more than one references of the states at any time under the windy conditions, which provide more flexibility in terms of tracking complex trajectories.

In future, HIL simulations are considered to be performed when all required hardware are provided. Then actual flight tests could be investigated after HIL simulations are resulted in encouraging outputs.

REFERENCES

[1] **Paw, Y.** (2009). Synthesis and Validation of Flight Control for UAV, *Ph.D. thesis*, University of Minnesota. Major: Aerospace Engineering and Mechanics.

[2] **Murch, A., D.A. and Balas, G.**, (2014), University of Minnesota UAV Flight Control Research Group, *available at:* `http://www.uav.aem.umn.edu` *(accessed 2014 May 18)*.

[3] **Beard, R.W. and McLain, T.W.** (2012). *Small Unmanned Aircraft: Theory and Practice*, Princeton University Press, Princeton, NJ, USA.

[4] **The MathWorks, I.** (2012). *Aerospace Blockset User's Guide*, The MathWorks, Inc., Natick, MA, USA.

[5] **Seborg, D.**, **Mellichamp, D.**, **Edgar, T. and Doyle, F.** (2010). *Process Dynamics and Control*, John Wiley & Sons, `https://books.google.ca/books?id=\_PQ42kOvtfwC`.

[6] **Bemporad, A.**, (2012). Model Predictive Control Toolbox User's Guide, The Mathworks, Inc.

[7] **Raemaekers, A.** (2007). Design of a model predictive controller to control UAVs, **Technical Report**, `http://www.narcis.nl/publication/RecordID/oai:library.tue.nl:657983`.

[8] **Chao, H.**, **Cao, Y. and Chen, Y.** (2010). Autopilots for small unmanned aerial vehicles: A survey, *International Journal of Control, Automation and Systems*, *8*(1), 36–44.

[9] **Sartori, D.** (2014). Design, Implementation and Testing of Advanced Control Laws for Fixed-wing UAVs, *Ph.D. thesis*, Politecnico di Torino.

[10] **Kada, B. and Ghazzawi, Y.** Robust PID Controller Design for an UAV Flight Control System, *Proceedings of the World Congress on Engineering and Computer Science 2011 Vol II, WCECS '11, October 19 - 21, 2011, San Francisco, USA*.

[11] **Santoso, F.**, **Liu, M. and Egan, G.** (2008). H_2 and H_∞ robust autopilot synthesis for longitudinal flight of a special unmanned aerial vehicle: a comparative study, *Control Theory Applications, IET*, *2*(7), 583–594.

[12] **Andrievsky, B. and Fradkov, A.** (2003). Combined adaptive controller for UAV guidance, *European Control Conference (ECC), 2003*, pp.2662–2666.

[13] **Tu, H. and Du, X.** (2010). The Design of Small UAV Autopilot Hardware System Based on DSP, *Intelligent Computation Technology and Automation (ICICTA), 2010 International Conference on*, volume 3, pp.780–783.

[14] **Guanglin, H.**, **Rujun, G. and Shi, Y.** (2007). Application of FPGA in Small UAV Autopilot Based on Embedded Linux System, *Industrial Electronics Society, 2007. IECON 2007. 33rd Annual Conference of the IEEE*, pp.731–734.

[15] **Paw, Y.C. and Balas, G.J.** (2011). Development and application of an integrated framework for small UAV flight control development, *Mechatronics*, *21*(5), 789 – 802, `http://www.sciencedirect.com/science/article/pii/S0957415810001674`, special Issue on Development of Autonomous Unmanned Aerial Vehicles.

[16] **Lizarraga, M.**, **Elkaim, G.H.**, **Horn, G.**, **Curry, R.**, **Dobrokhodov, V. and Kaminer, I.** (2009). Low Cost Rapidly Reconfigurable UAV Autopilot for Research and Development of Guidance, Navigation and Control Algorithms, *ASME/IEEE MESA09*, International Conference on Mechatronic and Embedded Systems and Applications, International Conference on Mechatronic and Embedded Systems and Applications, San Diego, CA.

[17] **Jung, D.**, **Levy, E.**, **Zhou, D.**, **Fink, R.**, **Moshe, J.**, **Earl, A. and Tsiotras, P.** (2005). Design and Development of a Low-Cost Test-Bed for Undergraduate Education in UAVs, *Decision and Control, 2005 and 2005 European Control Conference. CDC-ECC '05. 44th IEEE Conference on*, pp.2739–2744.

[18] **Miller, J.A.**, **Minear, P.D.**, **Niessner, A.F.**, **DeLullo, A.M.**, **Geiger, B.R.**, **Long, L.N. and Horn, J.F.** (2007). Intelligent Unmanned Air Vehicle Flight Systems, *Journal of Aerospace Computing Information and Communication*, *4*, 816–835.

[19] **Johnson, E.N.**, **Turbe, M.A. and Neidhoefer, J.C.** (2006). Flight Test Results of Autonomous Fixed-Wing UAV Transitions to and from Stationary Hover, *In Proceedings of the AIAA Guidance, Navigation, and Control Conference Exhibit*.

[20] **Gu, Y.**, **Seanor, B.**, **Campa, G.**, **Napolitano, M.**, **Rowe, L.**, **Gururajan, S. and Wan, S.** (2006). Design and Flight Testing Evaluation of Formation Control Laws, *Control Systems Technology, IEEE Transactions on*, *14*(6), 1105–1112.

[21] **Puttige, V.** (2009). Neural Network Based Adaptive Control for Autonomous Flight of Fixed Wing Unmanned Aerial Vehicles, *Ph.D. thesis*, University of New South Wales, Australian Defence Force Academy, School of Engineering and Information Technology.

[22] **Babaei, A.**, **Mortazavi, M. and Moradi, M.** (2011). Classical and fuzzy-genetic autopilot design for unmanned aerial vehicles, *Applied Soft Computing*, *11*(1), 365 – 372.

[23] **Samal, M.** (2009). Neural Network Based Identification and Control of an Unmanned Helicopter, *Ph.D. thesis*, University of New South Wales, Australian Defence Force Academy, School of Engineering and Information Technology.

[24] **Castillo, C.**, **Moreno, W. and Valavanis, K.** (2007). Unmanned helicopter waypoint trajectory tracking using model predictive control, *Control Automation, 2007. MED '07. Mediterranean Conference on*, pp.1–8.

[25] **Wan, E.A. and Bogdanov, A.** (2001). Model predictive neural control with applications to a 6 DOF helicopter model, *American Control Conference, 2001. Proceedings of the 2001*, volume 1, pp.488–493 vol.1.

[26] **Klančar, G. and Škrjanc, I.** (2007). Tracking-error model-based predictive control for mobile robots in real time, *Robotics and Autonomous Systems*, *55*(6), 460 – 469, http://www.sciencedirect.com/science/article/pii/S0921889007000140.

[27] **Maciejowski, J.M.** (2002). *Predictive control with constraints*, Prentice Hall, Essex, England.

[28] **Wang, L.** (2009). *Model Predictive Control System Design and Implementation Using MATLAB*, Springer Publishing Company, Incorporated, 1st edition.

[29] **Joelianto, E.**, **Sumarjono, E.M.**, **Budiyono, A. and Penggalih, D.R.** (2011). Model predictive control for autonomous unmanned helicopters, *Aircraft Engineering and Aerospace Technology*, *83*(6), 375–387, http://dx.doi.org/10.1108/00022661111173252.

[30] **Kang, Y. and Hedrick, J.** (2009). Linear Tracking for a Fixed-Wing UAV Using Nonlinear Model Predictive Control, *Control Systems Technology, IEEE Transactions on*, *17*(5), 1202–1210.

[31] **Garcia, G.A. and Keshmiri, S.** (2011). Nonlinear Model Predictive Controller for Navigation, Guidance and Control of a Fixed-Wing UAV, *AIAA Guidance, Navigation, and Control Conference, 08 - 11 August 2011, Portland, Oregon*.

[32] **Gros, S.**, **Quirynen, R. and Diehl, M.** (2012). Aircraft control based on fast non-linear MPC amp; multiple-shooting, *51st IEEE Annual Conference on Decision and Control*, pp.1142–1147.

[33] **jun Yang, Z.**, **hui Qi, X. and lin Shan, G.** (2009). Simulation of flight control laws design using model predictive controllers, *2009 International Conference on Mechatronics and Automation*, pp.4213–4218.

[34] **Lumbar, S.**, **Dolanc, G.**, **Vrečko, D.**, **Strmčnik, S. and Matko, D.** (2010). Automatic guidance of an aircraft using predictive control in a visual servoing scheme, *IFAC Proceedings Volumes*, *43*(15), 1 – 6, http://www.sciencedirect.com/science/article/pii/S1474667015318073.

[35] **Oettershagen, P.**, **Melzer, A.**, **Leutenegger, S.**, **Alexis, K. and Siegwart, R.** (2014). Explicit model predictive control and L1-navigation strategies for fixed-wing UAV path tracking, *Control and Automation (MED), 2014 22nd Mediterranean Conference of*, pp.1159–1165.

[36] **Ulker, H.**, **Baykara, C. and Ozsoy, C.** Design of MPCs for a Fixed Wing UAV, *Aircraft Engineering and Aerospace Technology*, (in press).

[37] **Hervas, J.R.**, **Reyhanoglu, M.**, **Tang, H. and Kayacan, E.** (2016). Nonlinear control of fixed-wing {UAVs} in presence of stochastic winds, *Communications in Nonlinear Science and Numerical Simulation*, *33*, 57 – 69, `http://www.sciencedirect.com/science/article/pii/S1007570415003135`.

[38] **Liu, C.**, **McAree, O. and Chen, W.H.** (2013). Path-following control for small fixed-wing unmanned aerial vehicles under wind disturbances, *International Journal of Robust and Nonlinear Control*, *23*(15), 1682–1698, `http://dx.doi.org/10.1002/rnc.2938`.

[39] **Kottenstette, N.** (2010). Constructive Non-Linear Control Design With Applications to Quad-Rotor and Fixed-Wing Aircraft, **Technical Report**, Institute for Software Integrated Systems, Vanderbilt University, Nashville, TN.

[40] **Divakar, D. and Ashwini, K.G.** (2011). A Processor in Loop Test Method for Life Critical Systems, *Proc. of Int. Colloquiums on Computer Electronics Electrical Mechanical and Civil*, pp.124–128.

[41] **Currie, J.**, **Prince-Pike, A. and Wilson, D.I.** (2012). Auto-code generation for fast embedded Model Predictive Controllers, *Mechatronics and Machine Vision in Practice (M2VIP), 2012 19th International Conference*, pp.116–122.

[42] **Wahid, M.A.** (2015). Flight Guidance Along 3D+T Trajectories And Space Indexed Traffic Management, *Ph.D. thesis*, Universite de Toulouse.

[43] **Patankar, S.**, **Schinstock, D. and Caplinger, R.** (2006). Application of Pendulum Method to UAV Momental Ellipsoid Estimation, *6th AIAA Aviation Technology, Integration and Operations Conference (ATIO)*.

[44] **Jardin, M. and Mueller, E.** (2007). Optimized Measurements of UAV Mass Moment of Inertia with a Bifilar Pendulum, *AIAA Guidance, Navigation and Control Conference and Exhibit Guidance, Navigation, and Control and Co-located Conferences*.

[45] **Stevens, B.L. and Lewis, F.L.** (1992). *Aircraft control and simulation*, Wiley-Interscience, J. Wiley and sons, New York, Chichester, Brisbane, `http://opac.inria.fr/record=b1105347`.

[46] **Ferreira, H.C.**, **Baptista, R.S.**, **Ishihara, J.Y. and Borges, G.A.** (2011). Disturbance rejection in a fixed wing UAV using nonlinear H_∞ state feedback, *2011 9th IEEE International Conference on Control and Automation (ICCA)*, pp.386–391.

[47] **Klein, V. and Morelli, E.** (2006). *Aircraft System Identification: Theory and Practice*, AIAA education series, American Institute of Aeronautics and Astronautics, https://books.google.com.tr/books?id=SC90QgAACAAJ.

[48] **Dorobantu, A.**, **Murch, A.**, **Mettler, B. and Balas, G.** (2013). System identification for small, low-cost, fixed-wing unmanned aircraft, *Journal of Aircraft*, *50*(4), 1117–1130.

[49] **Cook, V.** (2013). *Flight Dynamics Principles: A Linear Systems Approach to Aircraft Stability and Control*, Aerospace Engineering, Butterworth-Heinemann.

[50] **Fitzgerald, P.** (2004). Flight Control System Design For Autonomous UAV Carrier Landing, *Ph.D. thesis*, Cranfield University.

[51] **Danapalasingam, K.A.**, **la Cour-Harbo, A. and Bisgaard, M.** (2009). Feedforward control of an autonomous helicopter using trim inputs, *AIAA Infotech@ Aerospace & AIAA Unmanned... Unlimited Conference and Exhibit*.

[52] **Sebbane, Y.** (2015). *Smart Autonomous Aircraft: Flight Control and Planning for UAV*, CRC Press, https://books.google.com.tr/books?id=Q2jmCgAAQBAJ.

[53] **Reitz, B.** (2014). Control System Development for Autonomous Aerobatic Maneuvering with a Fixed-Wing Aircraft, *Ph.D. thesis*, Auburn University.

[54] **Jixing, L.** (2012). Coordinated-turn control law design of aircraft based on optimal tracking, *IET Conference Proceedings*, 730–733(3).

[55] **Render, P.M.**, (2010). Maneuver of Fixed-Wing Combat Aircraft, John Wiley and Sons, Ltd.

[56] **BeagleBoard**, (2016), https://beagleboard.org/black.

[57] **The MathWorks, I.** (2010). *Real-Time Workshop Embedded Coder User's Guide*, The MathWorks, Inc., Natick, MA, USA.

APPENDICES

APPENDIX A : Numeric Values of the Model Parameters and Transient and Steady State Analysis of the UAV

APPENDIX A

Table A.1 : Aircraft geometry [1, 2].

Parameter	Description	Value and Units
A_w	wing reference area	$0.3m^2$
b	wing span	$1.2m$
c	wing chord	$0.3m$
m	gross take off weight	$1.9kg$

Table A.2 : Moment of inertia data [1, 2].

Moment of inertia	Value (kgm^2)
J_x	7.15×10^{-2}
J_y	8.63×10^{-2}
J_z	1.53×10^{-1}
J_{xz}	1.40×10^{-2}
J_p	1.30×10^{-4}

Table A.3 : Numerical values of aerodynamic coefficients [1, 2].

Lift Force	Drag Force	Side Force	Roll moment	Pitch moment	Yaw moment
1.1×10^{-1}	4.4×10^{-2}	-4.8×10^{-1}	-5.4×10^{-2}	-2.7×10^{-2}	7.2×10^{-2}
4.58	1.3×10^{-2}	1.9×10^{-1}	1.1×10^{-2}	-7.2×10^{-1}	-1.8×10^{-1}
1.97	3.0×10^{-2}	-3.7×10^{-2}	-4.4×10^{-1}	-8.4×10^{-1}	1.1×10^{-1}
6.16		1.5×10^{-1}	1.0×10^{-1}	-1.0×10	-1.8×10^{-1}
2.3×10^{-1}			-1.6×10^{-2}	-1.3×10	
9.8×10^{-2}					

Table A.4 : Trim points obtained for each flight scenario.

States	Straight and Level	Level Climb	Level Turn	Climbing Turn	Level Steady Heading Sideslip
$V_a(m/s)$	17	17	17	17	17
$h(m)$	50	50	50	50	50
$\alpha(^\circ)$	3.1	3.1	3.8	3.8	3.1
$\beta(^\circ)$	2.1×10^{-7}	3.7×10^{-7}	-1.2×10^{-6}	-1.0×10^{-5}	5
$\gamma(^\circ)$	-0.0004	5	2.8×10^{-5}	5	0.0008
$\phi(^\circ)$	-0.1	-0.1	31.2	31.3	6.7
$\theta(^\circ)$	3.1	8.1	3.3	8.2	3.7
$\psi(^\circ)$	155	155	155	155	155
$\dot{\psi}(^\circ)$	0	0	20	20	0
$p(^\circ/s)$	3.4×10^{-6}	3.1×10^{-6}	-1.1	-2.9	4.3×10^{-6}
$q(^\circ/s)$	-1.5×10^{-5}	-2.0×10^{-5}	10.3	10.3	3.2×10^{-5}
$r(^\circ/s)$	1.7×10^{-7}	-6.3×10^{-7}	17.1	16.9	-7.7×10^{-6}
$a_x(m/s^2)$	0.5	1.4	0.8	1.6	0.6
$a_z(m/s^2)$	-9.8	-9.7	-11.4	-11.3	-9.7
$\delta_t(nd)$	0.6	0.7	0.6	0.7	0.6
$\delta_e(^\circ)$	-5.5	-5.9	-7.3	-7.6	-5.5
$\delta_r(^\circ)$	0.2	0.2	-0.4	-0.3	1.7
$\delta_{a_l}(^\circ)$	-0.6	-0.8	-1.1	-1.5	-0.9
$\delta_{a_r}(^\circ)$	0.6	0.8	1.1	1.5	0.9
$u_{sw}(m/s)$	0	0	0	0	0
$v_{sw}(m/s)$	0	0	0	0	0

Table A.5 : Trim points obtained for each flight scenario in case of presence of SW.

States	Straight and Level	Level Climb	Level Turn	Climbing Turn	Level Steady Heading Sideslip
$V_a(m/s)$	17	17	17	17	17
$h(m)$	50	50	50	50	50
$\alpha(^\circ)$	3.1	3.1	3.8	3.8	3.1
$\beta(^\circ)$	1.8×10^{-7}	-1.6×10^{-5}	-1.1×10^{-6}	-1.9×10^{-5}	5
$\gamma(^\circ)$	-0.0001	5	2.5×10^{-5}	5	0.0001
$\phi(^\circ)$	-0.1	-0.1	31.2	31.3	6.7
$\theta(^\circ)$	3.1	8.5	3.3	8.6	3.7
$\psi(^\circ)$	155	155	155	155	155
$\dot{\psi}(^\circ)$	0	0	20	20	0
$p(^\circ/s)$	2.9×10^{-6}	2.2×10^{-6}	-1.1	-3.0	4.5×10^{-6}
$q(^\circ/s)$	-1.3×10^{-5}	-1.7×10^{-5}	10.3	10.3	3.5×10^{-5}
$r(^\circ/s)$	1.5×10^{-7}	1.1×10^{-6}	17.1	16.7	-8.1×10^{-6}
$a_x(m/s^2)$	0.5	1.5	0.8	1.7	0.6
$a_z(m/s^2)$	-9.8	-9.7	-11.4	-11.3	-9.7
$\delta_t(nd)$	0.6	0.7	0.6	0.7	0.6
$\delta_e(^\circ)$	-5.5	-5.9	-7.3	-7.6	-5.5
$\delta_r(^\circ)$	0.2	0.3	-0.4	-0.3	1.7
$\delta_{a_l}(^\circ)$	-0.6	-0.8	-1.1	-1.5	-0.9
$\delta_{a_r}(^\circ)$	0.6	0.8	1.1	1.5	0.9
$u_{sw}(m/s)$	2.4	2.4	2.4	2.4	2.4
$v_{sw}(m/s)$	2.4	2.4	2.4	2.4	2.4

Full linear state space model obtained in straight and level flight:

$$A_f = \begin{pmatrix}
0 & 0 & 0 & 1 & 0 & 0.05 & 0 & 0 & 0 & 0 & 0 & 0 & 0 \\
0 & 0 & 0 & 0 & 1 & 0 & 0 & 0 & 0 & 0 & 0 & 0 & 0 \\
0 & 0 & 0 & 0 & 0 & 1 & 0 & 0 & 0 & 0 & 0 & 0 & 0 \\
0 & 0 & 0 & -16.14 & -0.14 & 3.38 & 0.06 & -2.83 & 0 & 0 & 0 & 0 & -0.01 \\
0 & 0 & 0 & 0 & -15.85 & 1.24 & 1.04 & 0 & -7.43 & 0 & 0 & 0 & -0.01 \\
0 & 0 & 0 & 0.52 & -0.71 & -2.78 & 0.01 & 1.71 & 0 & 0 & 0 & 0 & 0 \\
0 & -9.79 & 0 & 0 & -0.87 & 0 & -0.6 & 0 & 0.8 & 0 & 0 & 0 & 0.01 \\
9.79 & 0 & 0 & 0.88 & 0 & -16.82 & 0 & -0.87 & 0 & 0 & 0 & 0 & 0 \\
0.02 & -0.53 & 0 & 0 & 15.72 & 0 & -0.75 & 0 & -7.58 & 0 & 0 & 0 & 0 \\
0.91 & 0 & -17 & 0 & 0 & 0 & 0 & -1 & 0 & 0 & 0 & 0 & 0 \\
0 & 0 & 0 & 0 & 0 & 0 & 1 & 0 & 0.05 & 0 & 0 & 0 & 0 \\
0 & -17 & 0 & 0 & 0 & 0 & -0.05 & 0 & 1 & 0 & 0 & 0 & 0 \\
0 & 0 & 0 & 0 & 0 & 0 & 135.84 & 0 & 7.31 & 0 & 0 & -0.08 & -5.92
\end{pmatrix}$$

$$B_f = \begin{pmatrix}
0 & 0 & 0 & 0 & 0 & 0 & 0 & 0 \\
0 & 0 & 0 & 0 & 0 & 0 & 0 & 0 \\
0 & 0 & 0 & 0 & 0 & 0 & 0 & 0 \\
9.27 & 0 & -5.02 & 78.45 & -78.45 & 33.11 & -33.11 & -156.91 \\
0 & -134.07 & 0 & 4.36 & 3 & 2.63 & 2.63 & -1.35 \\
0.84 & 0 & -82.27 & -5.77 & 5.77 & -1.8 & 1.8 & 11.54 \\
0 & 0.47 & -0.84 & 0.19 & -0.19 & 0.35 & 0.35 & -0.39 \\
0 & 0 & 5.32 & 0 & 0 & 0 & 0 & 0 \\
0 & -2.71 & -0.05 & 6.62 & -6.62 & -10.28 & -10.28 & -13.24 \\
0 & 0 & 0 & 0 & 0 & 0 & 0 & 0 \\
0 & 0 & 0 & 0 & 0 & 0 & 0 & 0 \\
0 & 0 & 0 & 0 & 0 & 0 & 0 & 0 \\
2506.06 & 0 & 0 & 0 & 0 & 0 & 0 & 0
\end{pmatrix}$$

$$C_f = \begin{pmatrix}
0 & 0 & 0 & 0 & 0 & 0 & 1 & 0 & 0.05 & 0 & 0 & 0 & 0 \\
0 & 0 & 0 & 0 & 0 & 0 & 0 & 0.06 & 0 & 0 & 0 & 0 & 0 \\
0 & 0 & 0 & 0 & 0 & 0 & 0 & 0 & 0.06 & 0 & 0 & 0 & 0 \\
0 & 0 & 0 & 0 & 0 & 0 & 0 & 0 & 0 & 0 & 0 & -1 & 0 \\
1 & 0 & 0 & 0 & 0 & 0 & 0 & 0 & 0 & 0 & 0 & 0 & 0 \\
0 & 1 & 0 & 0 & 0 & 0 & 0 & 0 & 0 & 0 & 0 & 0 & 0 \\
0 & 0 & 1 & 0 & 0 & 0 & 0 & 0 & 0 & 0 & 0 & 0 & 0 \\
0 & 0 & 0 & 1 & 0 & 0 & 0 & 0 & 0 & 0 & 0 & 0 & 0 \\
0 & 0 & 0 & 0 & 1 & 0 & 0 & 0 & 0 & 0 & 0 & 0 & 0 \\
0 & 0 & 0 & 0 & 0 & 1 & 0 & 0 & 0 & 0 & 0 & 0 & 0 \\
0 & 1 & 0 & 0 & 0 & 0 & 0 & 0 & -0.06 & 0 & 0 & 0 & 0 \\
0 & 0 & 0 & 0 & 0.04 & 0 & -0.6 & 0 & 0.8 & 0 & 0 & 0 & 0.01 \\
0 & 0 & 0 & -0.04 & 0 & 0.16 & 0 & -0.87 & 0 & 0 & 0 & 0 & 0 \\
0 & 0 & 0 & 0 & -1.26 & 0 & -0.75 & 0 & -7.58 & 0 & 0 & 0 & 0
\end{pmatrix}$$

$$D_f = \begin{pmatrix}
0 & 0 & 0 & 0 & 0 & 0 & 0 & 0 \\
0 & 0 & 0 & 0 & 0 & 0 & 0 & 0 \\
0 & 0 & 0 & 0 & 0 & 0 & 0 & 0 \\
0 & 0 & 0 & 0 & 0 & 0 & 0 & 0 \\
0 & 0 & 0 & 0 & 0 & 0 & 0 & 0 \\
0 & 0 & 0 & 0 & 0 & 0 & 0 & 0 \\
0 & 0 & 0 & 0 & 0 & 0 & 0 & 0 \\
0 & 0 & 0 & 0 & 0 & 0 & 0 & 0 \\
0 & 0 & 0 & 0 & 0 & 0 & 0 & 0 \\
0 & 0 & 0 & 0 & 0 & 0 & 0 & 0 \\
0 & 0 & 0 & 0 & 0 & 0 & 0 & 0 \\
0 & 0 & 0 & 0 & 0 & 0 & 0 & 0 \\
0 & 0 & 0 & 0 & 0 & 0 & 0 & 0 \\
0 & 0.47 & -0.84 & 0.19 & -0.19 & 0.35 & 0.35 & -0.39 \\
0 & 0 & 5.32 & 0 & 0 & 0 & 0 & 0 \\
0 & -2.71 & -0.05 & 6.62 & -6.62 & -10.28 & -10.28 & -13.24
\end{pmatrix}$$

Lateral linear state space model obtained in straight and level flight:

$$A_{lat} = \begin{pmatrix} -0.87 & 0.88 & -16.82 & 9.79 & 0 \\ -2.83 & -16.14 & 3.38 & 0 & 0 \\ 1.71 & 0.52 & -2.78 & 0 & 0 \\ 0 & 1 & 0.05 & 0 & 0 \\ 0 & 0 & 1 & 0 & 0 \end{pmatrix}$$

$$B_{lat} = \begin{pmatrix} 0 & 5.32 \\ -156.91 & -5.02 \\ 11.54 & -82.27 \\ 0 & 0 \\ 0 & 0 \end{pmatrix}$$

$$C_{lat} = \begin{pmatrix} 0.06 & 0 & 0 & 0 & 0 \\ 0 & 1 & 0 & 0 & 0 \\ 0 & 0 & 1 & 0 & 0 \\ 0 & 0 & 0 & 1 & 0 \\ 0 & 0 & 0 & 0 & 1 \end{pmatrix}$$

$$D_{lat} = \begin{pmatrix} 0 & 0 \\ 0 & 0 \\ 0 & 0 \\ 0 & 0 \\ 0 & 0 \end{pmatrix}$$

Longitudinal linear state space model obtained in straight and level flight:

$$A_{lon} = \begin{pmatrix} -0.6 & 0.8 & -0.87 & -9.79 & 0 & 0.01 \\ -0.75 & -7.58 & 15.72 & -0.53 & 0 & 0 \\ 1.04 & -7.43 & -15.85 & 0 & 0 & -0.01 \\ 0 & 0 & 1 & 0 & 0 & 0 \\ -0.05 & 1 & 0 & -17 & 0 & 0 \\ 135.84 & 7.31 & 0 & 0 & -0.08 & -5.92 \end{pmatrix}$$

$$B_{lon} = \begin{pmatrix} 0.47 & 0 \\ -2.71 & 0 \\ -134.07 & 0 \\ 0 & 0 \\ 0 & 0 \\ 0 & 2506.06 \end{pmatrix}$$

$$C_{lon} = \begin{pmatrix} 1 & 0.05 & 0 & 0 & 0 & 0 \\ 0 & 0.06 & 0 & 0 & 0 & 0 \\ 0 & 0 & 1 & 0 & 0 & 0 \\ 0 & 0 & 0 & 1 & 0 & 0 \\ 0 & 0 & 0 & 0 & -1 & 0 \\ -0.6 & 0.8 & 0.04 & 0 & 0 & 0.01 \\ -0.75 & -7.58 & -1.26 & 0 & 0 & 0 \end{pmatrix}$$

$$D_{lon} = \begin{pmatrix} 0 & 0 \\ 0 & 0 \\ 0 & 0 \\ 0 & 0 \\ 0 & 0 \\ 0.47 & 0 \\ -2.71 & 0 \end{pmatrix}$$

Full linear state space model obtained in level climb flight:

$$A_f = \begin{pmatrix}
0 & 0 & 0 & 1 & 0 & 0.14 & 0 & 0 & 0 & 0 & 0 & 0 & 0 \\
0 & 0 & 0 & 0 & 1 & 0 & 0 & 0 & 0 & 0 & 0 & 0 & 0 \\
0 & 0 & 0 & 0 & 0 & 1.01 & 0 & 0 & 0 & 0 & 0 & 0 & 0 \\
0 & 0 & 0 & -16.14 & -0.15 & 3.38 & -0.01 & -2.83 & 0 & 0 & 0 & 0 & -0.01 \\
0 & 0 & 0 & 0 & -15.85 & 1.34 & 1.18 & 0 & -7.42 & 0 & 0 & 0 & -0.01 \\
0 & 0 & 0 & 0.52 & -0.77 & -2.78 & 0 & 1.71 & 0 & 0 & 0 & 0 & 0 \\
0 & -9.71 & 0 & 0 & -0.86 & 0 & -0.63 & 0 & 0.79 & 0 & 0 & 0 & 0.01 \\
9.71 & 0 & 0 & 0.86 & 0 & -16.82 & 0 & -0.88 & 0 & 0 & 0 & 0 & 0 \\
0.02 & -1.37 & 0 & 0 & 15.72 & 0 & -0.74 & 0 & -7.58 & 0 & 0 & 0 & 0 \\
0.9 & 0 & -16.94 & 0 & 0 & 0 & 0 & -1 & 0 & 0 & 0 & 0 & 0 \\
0 & -1.48 & 0 & 0 & 0 & 0 & 0.99 & 0 & 0.14 & 0 & 0 & 0 & 0 \\
0 & -16.94 & 0 & 0 & 0 & 0 & -0.14 & 0 & 0.99 & 0 & 0 & 0 & 0 \\
0 & 0 & 0 & 0 & 0 & 0 & 135.02 & 0 & 7.15 & 0 & 0 & -0.11 & -6.57
\end{pmatrix}$$

$$B_f = \begin{pmatrix}
0 & 0 & 0 & 0 & 0 & 0 & 0 & 0 \\
0 & 0 & 0 & 0 & 0 & 0 & 0 & 0 \\
0 & 0 & 0 & 0 & 0 & 0 & 0 & 0 \\
10.29 & 0 & -5.02 & 78.45 & -78.45 & 33.11 & -33.11 & -156.91 \\
0 & -134.07 & 0 & 4.36 & 3 & 2.63 & 2.63 & -1.35 \\
0.94 & 0 & -82.27 & -5.77 & 5.77 & -1.8 & 1.8 & 11.54 \\
0 & 0.47 & -0.84 & 0.2 & -0.2 & 0.35 & 0.35 & -0.39 \\
0 & 0 & 5.32 & 0 & 0 & 0 & 0 & 0 \\
0 & -2.71 & -0.04 & 6.62 & -6.62 & -10.28 & -10.28 & -13.24 \\
0 & 0 & 0 & 0 & 0 & 0 & 0 & 0 \\
0 & 0 & 0 & 0 & 0 & 0 & 0 & 0 \\
0 & 0 & 0 & 0 & 0 & 0 & 0 & 0 \\
2780.84 & 0 & 0 & 0 & 0 & 0 & 0 & 0
\end{pmatrix}$$

$$C_f = \begin{pmatrix}
0 & 0 & 0 & 0 & 0 & 0 & 1 & 0 & 0.05 & 0 & 0 & 0 & 0 \\
0 & 0 & 0 & 0 & 0 & 0 & 0 & 0.06 & 0 & 0 & 0 & 0 & 0 \\
0 & 0 & 0 & 0 & 0 & 0 & 0 & 0 & 0.06 & 0 & 0 & 0 & 0 \\
0 & 0 & 0 & 0 & 0 & 0 & 0 & 0 & 0 & 0 & 0 & -1 & 0 \\
1 & 0 & 0 & 0 & 0 & 0 & 0 & 0 & 0 & 0 & 0 & 0 & 0 \\
0 & 1 & 0 & 0 & 0 & 0 & 0 & 0 & 0 & 0 & 0 & 0 & 0 \\
0 & 0 & 1 & 0 & 0 & 0 & 0 & 0 & 0 & 0 & 0 & 0 & 0 \\
0 & 0 & 0 & 1 & 0 & 0 & 0 & 0 & 0 & 0 & 0 & 0 & 0 \\
0 & 0 & 0 & 0 & 1 & 0 & 0 & 0 & 0 & 0 & 0 & 0 & 0 \\
0 & 0 & 0 & 0 & 0 & 1 & 0 & 0 & 0 & 0 & 0 & 0 & 0 \\
0 & 1 & 0 & 0 & 0 & 0 & 0 & 0 & -0.06 & 0 & 0 & 0 & 0 \\
0 & 0 & 0 & 0 & 0.04 & 0 & -0.63 & 0 & 0.79 & 0 & 0 & 0 & 0.01 \\
0 & 0 & 0 & -0.04 & 0 & 0.16 & 0 & -0.88 & 0 & 0 & 0 & 0 & 0 \\
0 & 0 & 0 & 0 & -1.26 & 0 & -0.74 & 0 & -7.58 & 0 & 0 & 0 & 0
\end{pmatrix}$$

$$D_f = \begin{pmatrix}
0 & 0 & 0 & 0 & 0 & 0 & 0 & 0 \\
0 & 0 & 0 & 0 & 0 & 0 & 0 & 0 \\
0 & 0 & 0 & 0 & 0 & 0 & 0 & 0 \\
0 & 0 & 0 & 0 & 0 & 0 & 0 & 0 \\
0 & 0 & 0 & 0 & 0 & 0 & 0 & 0 \\
0 & 0 & 0 & 0 & 0 & 0 & 0 & 0 \\
0 & 0 & 0 & 0 & 0 & 0 & 0 & 0 \\
0 & 0 & 0 & 0 & 0 & 0 & 0 & 0 \\
0 & 0 & 0 & 0 & 0 & 0 & 0 & 0 \\
0 & 0 & 0 & 0 & 0 & 0 & 0 & 0 \\
0 & 0 & 0 & 0 & 0 & 0 & 0 & 0 \\
0 & 0 & 0 & 0 & 0 & 0 & 0 & 0 \\
0 & 0 & 0 & 0 & 0 & 0 & 0 & 0 \\
0 & 0.47 & -0.84 & 0.2 & -0.2 & 0.35 & 0.35 & -0.39 \\
0 & 0 & 5.32 & 0 & 0 & 0 & 0 & 0 \\
0 & -2.71 & -0.04 & 6.62 & -6.62 & -10.28 & -10.28 & -13.24
\end{pmatrix}$$

Lateral linear state space model obtained in level climb flight:

$$A_{lat} = \begin{pmatrix} -0.88 & 0.86 & -16.82 & 9.71 & 0 \\ -2.83 & -16.14 & 3.38 & 0 & 0 \\ 1.71 & 0.52 & -2.78 & 0 & 0 \\ 0 & 1 & 0.14 & 0 & 0 \\ 0 & 0 & 1.01 & 0 & 0 \end{pmatrix}$$

$$B_{lat} = \begin{pmatrix} 0 & 5.32 \\ -156.91 & -5.02 \\ 11.54 & -82.27 \\ 0 & 0 \\ 0 & 0 \end{pmatrix}$$

$$C_{lat} = \begin{pmatrix} 0.06 & 0 & 0 & 0 & 0 \\ 0 & 1 & 0 & 0 & 0 \\ 0 & 0 & 1 & 0 & 0 \\ 0 & 0 & 0 & 1 & 0 \\ 0 & 0 & 0 & 0 & 1 \end{pmatrix}$$

$$D_{lat} = \begin{pmatrix} 0 & 0 \\ 0 & 0 \\ 0 & 0 \\ 0 & 0 \\ 0 & 0 \end{pmatrix}$$

Longitudinal linear state space model obtained in level climb flight:

$$A_{lon} = \begin{pmatrix} -0.63 & 0.79 & -0.86 & -9.71 & 0 & 0.01 \\ -0.74 & -7.58 & 15.72 & -1.37 & 0 & 0 \\ 1.18 & -7.42 & -15.85 & 0 & 0 & -0.01 \\ 0 & 0 & 1 & 0 & 0 & 0 \\ -0.14 & 0.99 & 0 & -16.94 & 0 & 0 \\ 135.02 & 7.15 & 0 & 0 & -0.11 & -6.57 \end{pmatrix}$$

$$B_{lon} = \begin{pmatrix} 0.47 & 0 \\ -2.71 & 0 \\ -134.07 & 0 \\ 0 & 0 \\ 0 & 0 \\ 0 & 2780.84 \end{pmatrix}$$

$$C_{lon} = \begin{pmatrix} 1 & 0.05 & 0 & 0 & 0 & 0 \\ 0 & 0.06 & 0 & 0 & 0 & 0 \\ 0 & 0 & 1 & 0 & 0 & 0 \\ 0 & 0 & 0 & 1 & 0 & 0 \\ 0 & 0 & 0 & 0 & -1 & 0 \\ -0.63 & 0.79 & 0.04 & 0 & 0 & 0.01 \\ -0.74 & -7.58 & -1.26 & 0 & 0 & 0 \end{pmatrix}$$

$$D_{lon} = \begin{pmatrix} 0 & 0 \\ 0 & 0 \\ 0 & 0 \\ 0 & 0 \\ 0 & 0 \\ 0.47 & 0 \\ -2.71 & 0 \end{pmatrix}$$

Full linear state space model obtained in level turn flight:

$$A_f = \begin{pmatrix}
0 & 0.35 & 0 & 1 & 0.03 & 0.05 & 0 & 0 & 0 & 0 & 0 & 0 & 0 \\
-0.35 & 0 & 0 & 0 & 0.86 & -0.52 & 0 & 0 & 0 & 0 & 0 & 0 & 0 \\
0 & 0.02 & 0 & 0 & 0.52 & 0.86 & 0 & 0 & 0 & 0 & 0 & 0 & 0 \\
0 & 0 & 0 & -16.11 & -0.43 & 3.2 & -0.01 & -2.84 & 0 & 0 & 0 & 0 & -0.01 \\
0 & 0 & 0 & 0.29 & -15.85 & 1.33 & 1.26 & 0 & -7.41 & 0 & 0 & 0 & -0.01 \\
0 & 0 & 0 & 0.5 & -0.77 & -2.82 & 0.07 & 1.71 & 0 & 0 & 0 & 0 & 0 \\
0 & -9.79 & 0 & 0 & -1.05 & 0 & -0.6 & 0.3 & 0.72 & 0 & 0 & 0 & 0.01 \\
8.37 & -0.28 & 0 & 1.06 & 0 & -16.81 & -0.3 & -0.88 & -0.02 & 0 & 0 & 0 & 0 \\
-5.07 & -0.46 & 0 & 0 & 15.71 & 0 & -0.66 & 0.02 & -7.59 & 0 & 0 & 0 & 0 \\
0.94 & 0 & -16.99 & 0 & 0 & 0 & 0 & -0.86 & 0.52 & 0 & 0 & 0 & 0 \\
-0.03 & 0 & 0.57 & 0 & 0 & 0 & 1 & 0.03 & 0.05 & 0 & 0 & 0 & 0 \\
-0.57 & -16.99 & 0 & 0 & 0 & 0 & -0.06 & 0.52 & 0.85 & 0 & 0 & 0 & 0 \\
0 & 0 & 0 & 0 & 0 & 0 & 135.8 & 0 & 8.79 & 0 & 0 & -0.09 & -5.97
\end{pmatrix}$$

$$B_f = \begin{pmatrix}
0 & 0 & 0 & 0 & 0 & 0 & 0 & 0 \\
0 & 0 & 0 & 0 & 0 & 0 & 0 & 0 \\
0 & 0 & 0 & 0 & 0 & 0 & 0 & 0 \\
9.36 & 0 & -5.03 & 78.45 & -78.45 & 33.11 & -33.11 & -156.91 \\
0 & -134.07 & 0.01 & 4.36 & 3 & 2.63 & 2.63 & -1.35 \\
0.85 & 0 & -82.27 & -5.77 & 5.77 & -1.8 & 1.8 & 11.54 \\
0 & 0.47 & 0.84 & 0.18 & -0.18 & 0.36 & 0.36 & -0.37 \\
0 & 0 & 5.32 & 0 & 0 & 0 & 0 & 0 \\
0 & -2.71 & 0.05 & 6.63 & -6.63 & -10.28 & -10.28 & -13.26 \\
0 & 0 & 0 & 0 & 0 & 0 & 0 & 0 \\
0 & 0 & 0 & 0 & 0 & 0 & 0 & 0 \\
0 & 0 & 0 & 0 & 0 & 0 & 0 & 0 \\
2528.85 & 0 & 0 & 0 & 0 & 0 & 0 & 0
\end{pmatrix}$$

$$C_f = \begin{pmatrix} 0 & 0 & 0 & 0 & 0 & 0 & 1 & 0 & 0.06 & 0 & 0 & 0 & 0 \\ 0 & 0 & 0 & 0 & 0 & 0 & 0 & 0.06 & 0 & 0 & 0 & 0 & 0 \\ 0 & 0 & 0 & 0 & 0 & 0 & 0 & 0 & 0.06 & 0 & 0 & 0 & 0 \\ 0 & 0 & 0 & 0 & 0 & 0 & 0 & 0 & 0 & 0 & 0 & -1 & 0 \\ 1 & 0 & 0 & 0 & 0 & 0 & 0 & 0 & 0 & 0 & 0 & 0 & 0 \\ 0 & 1 & 0 & 0 & 0 & 0 & 0 & 0 & 0 & 0 & 0 & 0 & 0 \\ 0 & 0 & 1 & 0 & 0 & 0 & 0 & 0 & 0 & 0 & 0 & 0 & 0 \\ 0 & 0 & 0 & 1 & 0 & 0 & 0 & 0 & 0 & 0 & 0 & 0 & 0 \\ 0 & 0 & 0 & 0 & 1 & 0 & 0 & 0 & 0 & 0 & 0 & 0 & 0 \\ 0 & 0 & 0 & 0 & 0 & 1 & 0 & 0 & 0 & 0 & 0 & 0 & 0 \\ 0.03 & 1 & 0 & 0 & 0 & 0 & 0 & -0.03 & -0.05 & 0 & 0 & 0 & 0 \\ 0 & 0 & 0 & 0 & 0.04 & 0 & -0.6 & 0 & 0.9 & 0 & 0 & 0 & 0.01 \\ 0 & 0 & 0 & -0.04 & 0 & 0.16 & 0 & -0.88 & 0 & 0 & 0 & 0 & 0 \\ 0 & 0 & 0 & 0 & -1.26 & 0 & -0.84 & 0 & -7.59 & 0 & 0 & 0 & 0 \end{pmatrix}$$

$$D_f = \begin{pmatrix} 0 & 0 & 0 & 0 & 0 & 0 & 0 & 0 \\ 0 & 0 & 0 & 0 & 0 & 0 & 0 & 0 \\ 0 & 0 & 0 & 0 & 0 & 0 & 0 & 0 \\ 0 & 0 & 0 & 0 & 0 & 0 & 0 & 0 \\ 0 & 0 & 0 & 0 & 0 & 0 & 0 & 0 \\ 0 & 0 & 0 & 0 & 0 & 0 & 0 & 0 \\ 0 & 0 & 0 & 0 & 0 & 0 & 0 & 0 \\ 0 & 0 & 0 & 0 & 0 & 0 & 0 & 0 \\ 0 & 0 & 0 & 0 & 0 & 0 & 0 & 0 \\ 0 & 0 & 0 & 0 & 0 & 0 & 0 & 0 \\ 0 & 0 & 0 & 0 & 0 & 0 & 0 & 0 \\ 0 & 0 & 0 & 0 & 0 & 0 & 0 & 0 \\ 0 & 0.47 & 0.84 & 0.18 & -0.18 & 0.36 & 0.36 & -0.37 \\ 0 & 0 & 5.32 & 0 & 0 & 0 & 0 & 0 \\ 0 & -2.71 & 0.05 & 6.63 & -6.63 & -10.28 & -10.28 & -13.26 \end{pmatrix}$$

Lateral linear state space model obtained in level turn flight:

$$A_{lat} = \begin{pmatrix} -0.88 & 1.06 & -16.81 & 8.37 & 0 \\ -2.84 & -16.11 & 3.2 & 0 & 0 \\ 1.71 & 0.5 & -2.82 & 0 & 0 \\ 0 & 1 & 0.05 & 0 & 0 \\ 0 & 0 & 0.86 & 0 & 0 \end{pmatrix}$$

$$B_{lat} = \begin{pmatrix} 0 & 5.32 \\ -156.91 & -5.03 \\ 11.54 & -82.27 \\ 0 & 0 \\ 0 & 0 \end{pmatrix}$$

$$C_{lat} = \begin{pmatrix} 0.06 & 0 & 0 & 0 & 0 \\ 0 & 1 & 0 & 0 & 0 \\ 0 & 0 & 1 & 0 & 0 \\ 0 & 0 & 0 & 1 & 0 \\ 0 & 0 & 0 & 0 & 1 \end{pmatrix}$$

$$D_{lat} = \begin{pmatrix} 0 & 0 \\ 0 & 0 \\ 0 & 0 \\ 0 & 0 \\ 0 & 0 \end{pmatrix}$$

Longitudinal linear state space model obtained in level turn flight:

$$A_{lon} = \begin{pmatrix} -0.6 & 0.72 & -1.05 & -9.79 & 0 & 0.01 \\ -0.66 & -7.59 & 15.71 & -0.46 & 0 & 0 \\ 1.26 & -7.41 & -15.85 & 0 & 0 & -0.01 \\ 0 & 0 & 0.86 & 0 & 0 & 0 \\ -0.06 & 0.85 & 0 & -16.99 & 0 & 0 \\ 135.8 & 8.79 & 0 & 0 & -0.09 & -5.97 \end{pmatrix}$$

$$B_{lon} = \begin{pmatrix} 0.47 & 0 \\ -2.71 & 0 \\ -134.07 & 0 \\ 0 & 0 \\ 0 & 0 \\ 0 & 2528.85 \end{pmatrix}$$

$$C_{lon} = \begin{pmatrix} 1 & 0.06 & 0 & 0 & 0 & 0 \\ 0 & 0.06 & 0 & 0 & 0 & 0 \\ 0 & 0 & 1 & 0 & 0 & 0 \\ 0 & 0 & 0 & 1 & 0 & 0 \\ 0 & 0 & 0 & 0 & -1 & 0 \\ -0.6 & 0.9 & 0.04 & 0 & 0 & 0.01 \\ -0.84 & -7.59 & -1.26 & 0 & 0 & 0 \end{pmatrix}$$

$$D_{lon} = \begin{pmatrix} 0 & 0 \\ 0 & 0 \\ 0 & 0 \\ 0 & 0 \\ 0 & 0 \\ 0.47 & 0 \\ -2.71 & 0 \end{pmatrix}$$

Full linear state space model obtained in climbing turn flight:

$$A_f = \begin{pmatrix} 0 & 0.35 & 0 & 1 & 0.07 & 0.12 & 0 & 0 & 0 & 0 & 0 & 0 & 0 \\ -0.35 & 0 & 0 & 0 & 0.85 & -0.52 & 0 & 0 & 0 & 0 & 0 & 0 & 0 \\ 0 & 0.05 & 0 & 0 & 0.53 & 0.86 & 0 & 0 & 0 & 0 & 0 & 0 & 0 \\ 0 & 0 & 0 & -16.11 & -0.45 & 3.2 & -0.11 & -2.84 & -0.01 & 0 & 0 & 0 & -0.01 \\ 0 & 0 & 0 & 0.3 & -15.85 & 1.39 & 1.38 & 0 & -7.4 & 0 & 0 & 0 & -0.01 \\ 0 & 0 & 0 & 0.5 & -0.82 & -2.82 & 0.07 & 1.71 & 0 & 0 & 0 & 0 & 0 \\ 0 & -9.71 & 0 & 0 & -1.03 & 0 & -0.63 & 0.29 & 0.71 & 0 & 0 & 0 & 0.01 \\ 8.29 & -0.72 & 0 & 1.04 & 0 & -16.81 & -0.3 & -0.88 & -0.05 & 0 & 0 & 0 & 0 \\ -5.05 & -1.18 & 0 & 0 & 15.71 & 0 & -0.66 & 0.05 & -7.59 & 0 & 0 & 0 & 0 \\ 0.92 & 0 & -16.93 & 0 & 0 & 0 & 0 & -0.85 & 0.52 & 0 & 0 & 0 & 0 \\ -0.08 & -1.48 & 0.56 & 0 & 0 & 0 & 0.99 & 0.07 & 0.12 & 0 & 0 & 0 & 0 \\ -0.55 & -16.93 & 0 & 0 & 0 & 0 & -0.14 & 0.51 & 0.85 & 0 & 0 & 0 & 0 \\ 0 & 0 & 0 & 0 & 0 & 0 & 134.78 & 0 & 8.54 & 0 & 0 & -0.12 & -6.61 \end{pmatrix}$$

$$B_f = \begin{pmatrix} 0 & 0 & 0 & 0 & 0 & 0 & 0 & 0 \\ 0 & 0 & 0 & 0 & 0 & 0 & 0 & 0 \\ 0 & 0 & 0 & 0 & 0 & 0 & 0 & 0 \\ 10.35 & 0 & -5.03 & 78.45 & -78.45 & 33.11 & -33.11 & -156.91 \\ 0 & -134.07 & 0.01 & 4.36 & 3 & 2.63 & 2.63 & -1.35 \\ 0.94 & 0 & -82.27 & -5.77 & 5.77 & -1.8 & 1.8 & 11.54 \\ 0 & 0.47 & 0.84 & 0.19 & -0.19 & 0.36 & 0.36 & -0.38 \\ 0 & 0 & 5.32 & 0 & 0 & 0 & 0 & 0 \\ 0 & -2.71 & 0.05 & 6.63 & -6.63 & -10.28 & -10.28 & -13.26 \\ 0 & 0 & 0 & 0 & 0 & 0 & 0 & 0 \\ 0 & 0 & 0 & 0 & 0 & 0 & 0 & 0 \\ 0 & 0 & 0 & 0 & 0 & 0 & 0 & 0 \\ 2798.02 & 0 & 0 & 0 & 0 & 0 & 0 & 0 \end{pmatrix}$$

$$C_f = \begin{pmatrix}
0 & 0 & 0 & 0 & 0 & 0 & 1 & 0 & 0.06 & 0 & 0 & 0 & 0 \\
0 & 0 & 0 & 0 & 0 & 0 & 0 & 0.06 & 0 & 0 & 0 & 0 & 0 \\
0 & 0 & 0 & 0 & 0 & 0 & 0 & 0 & 0.06 & 0 & 0 & 0 & 0 \\
0 & 0 & 0 & 0 & 0 & 0 & 0 & 0 & 0 & 0 & 0 & -1 & 0 \\
1 & 0 & 0 & 0 & 0 & 0 & 0 & 0 & 0 & 0 & 0 & 0 & 0 \\
0 & 1 & 0 & 0 & 0 & 0 & 0 & 0 & 0 & 0 & 0 & 0 & 0 \\
0 & 0 & 1 & 0 & 0 & 0 & 0 & 0 & 0 & 0 & 0 & 0 & 0 \\
0 & 0 & 0 & 1 & 0 & 0 & 0 & 0 & 0 & 0 & 0 & 0 & 0 \\
0 & 0 & 0 & 0 & 1 & 0 & 0 & 0 & 0 & 0 & 0 & 0 & 0 \\
0 & 0 & 0 & 0 & 0 & 1 & 0 & 0 & 0 & 0 & 0 & 0 & 0 \\
0.03 & 1 & 0 & 0 & 0 & 0 & 0 & -0.03 & -0.05 & 0 & 0 & 0 & 0 \\
0 & 0 & 0 & 0 & 0.04 & 0 & -0.63 & 0 & 0.89 & 0 & 0 & 0 & 0.01 \\
0 & 0 & 0 & -0.04 & 0 & 0.16 & 0 & -0.88 & 0 & 0 & 0 & 0 & 0 \\
0 & 0 & 0 & 0 & -1.26 & 0 & -0.84 & 0 & -7.59 & 0 & 0 & 0 & 0
\end{pmatrix}$$

$$D_f = \begin{pmatrix}
0 & 0 & 0 & 0 & 0 & 0 & 0 & 0 \\
0 & 0 & 0 & 0 & 0 & 0 & 0 & 0 \\
0 & 0 & 0 & 0 & 0 & 0 & 0 & 0 \\
0 & 0 & 0 & 0 & 0 & 0 & 0 & 0 \\
0 & 0 & 0 & 0 & 0 & 0 & 0 & 0 \\
0 & 0 & 0 & 0 & 0 & 0 & 0 & 0 \\
0 & 0 & 0 & 0 & 0 & 0 & 0 & 0 \\
0 & 0 & 0 & 0 & 0 & 0 & 0 & 0 \\
0 & 0 & 0 & 0 & 0 & 0 & 0 & 0 \\
0 & 0 & 0 & 0 & 0 & 0 & 0 & 0 \\
0 & 0 & 0 & 0 & 0 & 0 & 0 & 0 \\
0 & 0 & 0 & 0 & 0 & 0 & 0 & 0 \\
0 & 0.47 & 0.84 & 0.19 & -0.19 & 0.36 & 0.36 & -0.38 \\
0 & 0 & 5.32 & 0 & 0 & 0 & 0 & 0 \\
0 & -2.71 & 0.05 & 6.63 & -6.63 & -10.28 & -10.28 & -13.26
\end{pmatrix}$$

Lateral linear state space model obtained in climbing turn flight:

$$A_{lat} = \begin{pmatrix} -0.88 & 1.04 & -16.81 & 8.29 & 0 \\ -2.84 & -16.11 & 3.2 & 0 & 0 \\ 1.71 & 0.5 & -2.82 & 0 & 0 \\ 0 & 1 & 0.12 & 0 & 0 \\ 0 & 0 & 0.86 & 0 & 0 \end{pmatrix}$$

$$B_{lat} = \begin{pmatrix} 0 & 5.32 \\ -156.91 & -5.03 \\ 11.54 & -82.27 \\ 0 & 0 \\ 0 & 0 \end{pmatrix}$$

$$C_{lat} = \begin{pmatrix} 0.06 & 0 & 0 & 0 & 0 \\ 0 & 1 & 0 & 0 & 0 \\ 0 & 0 & 1 & 0 & 0 \\ 0 & 0 & 0 & 1 & 0 \\ 0 & 0 & 0 & 0 & 1 \end{pmatrix}$$

$$D_{lat} = \begin{pmatrix} 0 & 0 \\ 0 & 0 \\ 0 & 0 \\ 0 & 0 \\ 0 & 0 \end{pmatrix}$$

Longitudinal linear state space model obtained in climbing turn flight:

$$A_{lon} = \begin{pmatrix} -0.63 & 0.71 & -1.03 & -9.71 & 0 & 0.01 \\ -0.66 & -7.59 & 15.71 & -1.18 & 0 & 0 \\ 1.38 & -7.4 & -15.85 & 0 & 0 & -0.01 \\ 0 & 0 & 0.85 & 0 & 0 & 0 \\ -0.14 & 0.85 & 0 & -16.93 & 0 & 0 \\ 134.78 & 8.54 & 0 & 0 & -0.12 & -6.61 \end{pmatrix}$$

$$B_{lon} = \begin{pmatrix} 0.47 & 0 \\ -2.71 & 0 \\ -134.07 & 0 \\ 0 & 0 \\ 0 & 0 \\ 0 & 2798.02 \end{pmatrix}$$

$$C_{lon} = \begin{pmatrix} 1 & 0.06 & 0 & 0 & 0 & 0 \\ 0 & 0.06 & 0 & 0 & 0 & 0 \\ 0 & 0 & 1 & 0 & 0 & 0 \\ 0 & 0 & 0 & 1 & 0 & 0 \\ 0 & 0 & 0 & 0 & -1 & 0 \\ -0.63 & 0.89 & 0.04 & 0 & 0 & 0.01 \\ -0.84 & -7.59 & -1.26 & 0 & 0 & 0 \end{pmatrix}$$

$$D_{lon} = \begin{pmatrix} 0 & 0 \\ 0 & 0 \\ 0 & 0 \\ 0 & 0 \\ 0 & 0 \\ 0.47 & 0 \\ -2.71 & 0 \end{pmatrix}$$

Full linear state space model obtained in level steady heading sideslip flight:

$$A_f = \begin{pmatrix}
0 & 0 & 0 & 1 & 0.01 & 0.07 & 0 & 0 & 0 & 0 & 0 & 0 & 0 \\
0 & 0 & 0 & 0 & 0.99 & -0.12 & 0 & 0 & 0 & 0 & 0 & 0 & 0 \\
0 & 0 & 0 & 0 & 0.12 & 1 & 0 & 0 & 0 & 0 & 0 & 0 & 0 \\
0 & 0 & 0 & -16.14 & -0.15 & 3.38 & 0.31 & -2.81 & -0.06 & 0 & 0 & 0 & -0.01 \\
0 & 0 & 0 & 0 & -15.85 & 1.25 & 1.06 & 0.06 & -7.45 & 0 & 0 & 0 & -0.01 \\
0 & 0 & 0 & 0.52 & -0.72 & -2.78 & -0.14 & 1.7 & -0.01 & 0 & 0 & 0 & 0 \\
0 & -9.78 & 0 & 0 & -0.9 & 1.47 & -0.6 & 0.09 & 0.82 & 0 & 0 & 0 & 0.01 \\
9.72 & -0.07 & 0 & 0.91 & 0 & -16.75 & -0.06 & -0.88 & -0.02 & 0 & 0 & 0 & 0 \\
-1.14 & -0.64 & 0 & -1.48 & 15.65 & 0 & -0.71 & -0.09 & -7.6 & 0 & 0 & 0 & 0 \\
1.12 & 0 & -16.95 & 0 & 0 & 0 & 0 & -0.99 & 0.12 & 0 & 0 & 0 & 0 \\
0.09 & 0 & -1.36 & 0 & 0 & 0 & 1 & 0.01 & 0.07 & 0 & 0 & 0 & 0 \\
1.36 & -16.95 & 0 & 0 & 0 & 0 & -0.07 & 0.12 & 0.99 & 0 & 0 & 0 & 0 \\
0 & 0 & 0 & 0 & 0 & 0 & 135.34 & 11.86 & 7.6 & 0 & 0 & -0.08 & -5.95
\end{pmatrix}$$

$$B_f = \begin{pmatrix}
0 & 0 & 0 & 0 & 0 & 0 & 0 & 0 \\
0 & 0 & 0 & 0 & 0 & 0 & 0 & 0 \\
0 & 0 & 0 & 0 & 0 & 0 & 0 & 0 \\
9.32 & -0.03 & -5.02 & 78.53 & -78.53 & 32.99 & -33.22 & -157.05 \\
0 & -134.06 & 0 & 4.35 & 3.01 & 2.64 & 2.64 & -1.34 \\
0.85 & 0 & -82.27 & -5.76 & 5.76 & -1.81 & 1.79 & 11.52 \\
0 & 0.47 & -1.3 & -0.66 & 0.66 & 0.38 & 0.38 & 1.32 \\
0 & 0.03 & 5.22 & -0.03 & 0.03 & -0.02 & -0.02 & 0.05 \\
0 & -2.71 & -0.07 & 6.58 & -6.58 & -10.28 & -10.28 & -13.15 \\
0 & 0 & 0 & 0 & 0 & 0 & 0 & 0 \\
0 & 0 & 0 & 0 & 0 & 0 & 0 & 0 \\
0 & 0 & 0 & 0 & 0 & 0 & 0 & 0 \\
2518.32 & 0 & 0 & 0 & 0 & 0 & 0 & 0
\end{pmatrix}$$

$$C_f = \begin{pmatrix}
0 & 0 & 0 & 0 & 0 & 0 & 0.99 & 0.09 & 0.06 & 0 & 0 & 0 & 0 \\
0 & 0 & 0 & 0 & 0 & 0 & -0.01 & 0.06 & 0 & 0 & 0 & 0 & 0 \\
0 & 0 & 0 & 0 & 0 & 0 & 0 & 0 & 0.06 & 0 & 0 & 0 & 0 \\
0 & 0 & 0 & 0 & 0 & 0 & 0 & 0 & 0 & 0 & 0 & -1 & 0 \\
1 & 0 & 0 & 0 & 0 & 0 & 0 & 0 & 0 & 0 & 0 & 0 & 0 \\
0 & 1 & 0 & 0 & 0 & 0 & 0 & 0 & 0 & 0 & 0 & 0 & 0 \\
0 & 0 & 1 & 0 & 0 & 0 & 0 & 0 & 0 & 0 & 0 & 0 & 0 \\
0 & 0 & 0 & 1 & 0 & 0 & 0 & 0 & 0 & 0 & 0 & 0 & 0 \\
0 & 0 & 0 & 0 & 1 & 0 & 0 & 0 & 0 & 0 & 0 & 0 & 0 \\
0 & 0 & 0 & 0 & 0 & 1 & 0 & 0 & 0 & 0 & 0 & 0 & 0 \\
-0.08 & 1 & 0 & 0 & 0 & 0 & 0 & -0.01 & -0.06 & 0 & 0 & 0 & 0 \\
0 & 0 & 0 & 0 & 0.05 & -0.01 & -0.6 & 0.09 & 0.82 & 0 & 0 & 0 & 0.01 \\
0 & 0 & 0 & -0.04 & 0 & 0.16 & -0.06 & -0.88 & -0.02 & 0 & 0 & 0 & 0 \\
0 & 0 & 0 & 0 & -1.26 & 0 & -0.71 & -0.09 & -7.6 & 0 & 0 & 0 & 0
\end{pmatrix}$$

$$D_f = \begin{pmatrix}
0 & 0 & 0 & 0 & 0 & 0 & 0 & 0 \\
0 & 0 & 0 & 0 & 0 & 0 & 0 & 0 \\
0 & 0 & 0 & 0 & 0 & 0 & 0 & 0 \\
0 & 0 & 0 & 0 & 0 & 0 & 0 & 0 \\
0 & 0 & 0 & 0 & 0 & 0 & 0 & 0 \\
0 & 0 & 0 & 0 & 0 & 0 & 0 & 0 \\
0 & 0 & 0 & 0 & 0 & 0 & 0 & 0 \\
0 & 0 & 0 & 0 & 0 & 0 & 0 & 0 \\
0 & 0 & 0 & 0 & 0 & 0 & 0 & 0 \\
0 & 0 & 0 & 0 & 0 & 0 & 0 & 0 \\
0 & 0 & 0 & 0 & 0 & 0 & 0 & 0 \\
0 & 0 & 0 & 0 & 0 & 0 & 0 & 0 \\
0 & 0.47 & -1.3 & -0.66 & 0.66 & 0.38 & 0.38 & 1.32 \\
0 & 0.03 & 5.22 & -0.03 & 0.03 & -0.02 & -0.02 & 0.05 \\
0 & -2.71 & -0.07 & 6.58 & -6.58 & -10.28 & -10.28 & -13.15
\end{pmatrix}$$

Lateral linear state space model obtained in level steady heading sideslip flight:

$$A_{lat} = \begin{pmatrix} -0.88 & 0.91 & -16.75 & 9.72 & 0 \\ -2.81 & -16.14 & 3.38 & 0 & 0 \\ 1.7 & 0.52 & -2.78 & 0 & 0 \\ 0 & 1 & 0.07 & 0 & 0 \\ 0 & 0 & 1 & 0 & 0 \end{pmatrix}$$

$$B_{lat} = \begin{pmatrix} 0.05 & 5.22 \\ -157.05 & -5.02 \\ 11.52 & -82.27 \\ 0 & 0 \\ 0 & 0 \end{pmatrix}$$

$$C_{lat} = \begin{pmatrix} 0.06 & 0 & 0 & 0 & 0 \\ 0 & 1 & 0 & 0 & 0 \\ 0 & 0 & 1 & 0 & 0 \\ 0 & 0 & 0 & 1 & 0 \\ 0 & 0 & 0 & 0 & 1 \end{pmatrix}$$

$$D_{lat} = \begin{pmatrix} 0 & 0 \\ 0 & 0 \\ 0 & 0 \\ 0 & 0 \\ 0 & 0 \end{pmatrix}$$

Longitudinal linear state space model obtained in level steady heading sideslip flight:

$$A_{lon} = \begin{pmatrix} -0.6 & 0.82 & -0.9 & -9.78 & 0 & 0.01 \\ -0.71 & -7.6 & 15.65 & -0.64 & 0 & 0 \\ 1.06 & -7.45 & -15.85 & 0 & 0 & -0.01 \\ 0 & 0 & 0.99 & 0 & 0 & 0 \\ -0.07 & 0.99 & 0 & -16.95 & 0 & 0 \\ 135.34 & 7.6 & 0 & 0 & -0.08 & -5.95 \end{pmatrix}$$

$$B_{lon} = \begin{pmatrix} 0.47 & 0 \\ -2.71 & 0 \\ -134.06 & 0 \\ 0 & 0 \\ 0 & 0 \\ 0 & 2518.32 \end{pmatrix}$$

$$C_{lon} = \begin{pmatrix} 0.99 & 0.06 & 0 & 0 & 0 & 0 \\ 0 & 0.06 & 0 & 0 & 0 & 0 \\ 0 & 0 & 1 & 0 & 0 & 0 \\ 0 & 0 & 0 & 1 & 0 & 0 \\ 0 & 0 & 0 & 0 & -1 & 0 \\ -0.6 & 0.82 & 0.05 & 0 & 0 & 0.01 \\ -0.71 & -7.6 & -1.26 & 0 & 0 & 0 \end{pmatrix}$$

$$D_{lon} = \begin{pmatrix} 0 & 0 \\ 0 & 0 \\ 0 & 0 \\ 0 & 0 \\ 0 & 0 \\ 0.47 & 0 \\ -2.71 & 0 \end{pmatrix}$$

Full linear state space model obtained in straight and level flight in case of presence of steady wind:

$$A_f = \begin{pmatrix}
0 & 0 & 0 & 1 & 0 & 0.05 & 0 & 0 & 0 & 0 & 0 & 0 & 0 \\
0 & 0 & 0 & 0 & 1 & 0 & 0 & 0 & 0 & 0 & 0 & 0 & 0 \\
0 & 0 & 0 & 0 & 0 & 1 & 0 & 0 & 0 & 0 & 0 & 0 & 0 \\
0 & 0 & 0 & -16.17 & -0.14 & 3.38 & 0.06 & -2.84 & 0 & 0 & 0 & 0 & -0.01 \\
0 & 0 & 0 & 0 & -15.88 & 1.24 & 1.05 & 0 & -7.44 & 0 & 0 & 0 & -0.01 \\
0 & 0 & 0 & 0.52 & -0.71 & -2.79 & 0.01 & 1.71 & 0 & 0 & 0 & 0 & 0 \\
0 & -9.79 & 0 & 0 & -0.88 & 0 & -0.6 & 0 & 0.81 & 0 & 0 & 0 & 0.01 \\
9.79 & 0 & 0 & 0.89 & 0 & -16.82 & 0 & -0.88 & 0 & 0 & 0 & 0 & 0 \\
0.02 & -0.54 & 0 & 0 & 15.71 & 0 & -0.74 & 0 & -7.6 & 0 & 0 & 0 & 0 \\
0.39 & 0 & -7.18 & 0 & 0 & 0 & -0.9 & -0.42 & -0.05 & 0 & 0 & 0 & 0 \\
0.84 & 0 & -15.41 & 0 & 0 & 0 & 0.42 & -0.91 & 0.02 & 0 & 0 & 0 & 0 \\
0 & -17 & 0 & 0 & 0 & 0 & -0.05 & 0 & 1 & 0 & 0 & 0 & 0 \\
0 & 0 & 0 & 0 & 0 & 0 & 136.11 & 0 & 7.45 & 0 & 0 & -0.08 & -5.93
\end{pmatrix}$$

$$B_f = \begin{pmatrix}
0 & 0 & 0 & 0 & 0 & 0 & 0 \\
0 & 0 & 0 & 0 & 0 & 0 & 0 \\
0 & 0 & 0 & 0 & 0 & 0 & 0 \\
9.28 & 0 & -5.03 & 78.61 & -78.61 & 33.17 & -33.17 \\
0 & -134.33 & 0 & 3.02 & 3.01 & 2.64 & 2.64 \\
0.85 & 0 & -82.44 & -5.78 & 5.78 & -1.8 & 1.8 \\
0 & 0.47 & -0.84 & 0.65 & -0.19 & 0.36 & 0.36 \\
0 & 0 & 5.33 & 0 & 0 & 0 & 0 \\
0 & -2.72 & -0.05 & -6.59 & -6.64 & -10.3 & -10.3 \\
0 & 0 & 0 & 0 & 0 & 0 & 0 \\
0 & 0 & 0 & 0 & 0 & 0 & 0 \\
0 & 0 & 0 & 0 & 0 & 0 & 0 \\
2508.25 & 0 & 0 & 0 & 0 & 0 & 0
\end{pmatrix}$$

$$C_f = \begin{pmatrix} 1 & 0 & 0 & 0 & 0 & 0 & 0 & 0 & 0 & 0 & 0 & 0 & 0 \\ 0 & 1 & 0 & 0 & 0 & 0 & 0 & 0 & 0 & 0 & 0 & 0 & 0 \\ 0 & 0 & 1 & 0 & 0 & 0 & 0 & 0 & 0 & 0 & 0 & 0 & 0 \\ 0 & 0 & 0 & 1 & 0 & 0 & 0 & 0 & 0 & 0 & 0 & 0 & 0 \\ 0 & 0 & 0 & 0 & 1 & 0 & 0 & 0 & 0 & 0 & 0 & 0 & 0 \\ 0 & 0 & 0 & 0 & 0 & 1 & 0 & 0 & 0 & 0 & 0 & 0 & 0 \\ 0 & 0 & 0 & 0 & 0.04 & 0 & -0.6 & 0 & 0.81 & 0 & 0 & 0 & 0.01 \\ 0 & 0 & 0 & -0.04 & 0 & 0.16 & 0 & -0.88 & 0 & 0 & 0 & 0 & 0 \\ 0 & 0 & 0 & 0 & -1.26 & 0 & -0.74 & 0 & -7.6 & 0 & 0 & 0 & 0 \\ 0 & 0 & 0 & 0 & 0 & 0 & 1 & 0 & 0.05 & 0 & 0 & 0 & 0 \\ 0 & 0 & 0 & 0 & 0 & 0 & 0 & 0.06 & 0 & 0 & 0 & 0 & 0 \\ 0 & 0 & 0 & 0 & 0 & 0 & 0 & 0 & 0.06 & 0 & 0 & 0 & 0 \\ 0 & 0 & 0 & 0 & 0 & 0 & 0 & 0 & 0 & 0 & 0 & -1 & 0 \\ 0 & 0.92 & 0 & 0 & 0 & 0 & 0 & 0 & -0.05 & 0 & 0 & 0 & 0 \end{pmatrix}$$

$$D_f = \begin{pmatrix} 0 & 0 & 0 & 0 & 0 & 0 & 0 \\ 0 & 0 & 0 & 0 & 0 & 0 & 0 \\ 0 & 0 & 0 & 0 & 0 & 0 & 0 \\ 0 & 0 & 0 & 0 & 0 & 0 & 0 \\ 0 & 0 & 0 & 0 & 0 & 0 & 0 \\ 0 & 0 & 0 & 0 & 0 & 0 & 0 \\ 0 & 0.47 & -0.84 & 0.65 & -0.19 & 0.36 & 0.36 \\ 0 & 0 & 5.33 & 0 & 0 & 0 & 0 \\ 0 & -2.72 & -0.05 & -6.59 & -6.64 & -10.3 & -10.3 \\ 0 & 0 & 0 & 0 & 0 & 0 & 0 \\ 0 & 0 & 0 & 0 & 0 & 0 & 0 \\ 0 & 0 & 0 & 0 & 0 & 0 & 0 \\ 0 & 0 & 0 & 0 & 0 & 0 & 0 \\ 0 & 0 & 0 & 0 & 0 & 0 & 0 \end{pmatrix}$$

Lateral linear state space model obtained in straight and level flight in case of presence of steady wind:

$$A_{lat} = \begin{pmatrix} -0.88 & 0.89 & -16.82 & 9.79 & 0 \\ -2.84 & -16.17 & 3.38 & 0 & 0 \\ 1.71 & 0.52 & -2.79 & 0 & 0 \\ 0 & 1 & 0.05 & 0 & 0 \\ 0 & 0 & 1 & 0 & 0 \end{pmatrix}$$

$$B_{lat} = \begin{pmatrix} 0 & 0 & 5.33 \\ 78.61 & -78.61 & -5.03 \\ -5.78 & 5.78 & -82.44 \\ 0 & 0 & 0 \\ 0 & 0 & 0 \end{pmatrix}$$

$$C_{lat} = \begin{pmatrix} 0.06 & 0 & 0 & 0 & 0 \\ 0 & 1 & 0 & 0 & 0 \\ 0 & 0 & 1 & 0 & 0 \\ 0 & 0 & 0 & 1 & 0 \\ 0 & 0 & 0 & 0 & 1 \end{pmatrix}$$

$$D_{lat} = \begin{pmatrix} 0 & 0 & 0 \\ 0 & 0 & 0 \\ 0 & 0 & 0 \\ 0 & 0 & 0 \\ 0 & 0 & 0 \end{pmatrix}$$

Longitudinal linear state space model obtained in straight and level flight in case of presence of steady wind:

$$A_{lon} = \begin{pmatrix} -0.6 & 0.81 & -0.88 & -9.79 & 0 & 0.01 \\ -0.74 & -7.6 & 15.71 & -0.54 & 0 & 0 \\ 1.05 & -7.44 & -15.88 & 0 & 0 & -0.01 \\ 0 & 0 & 1 & 0 & 0 & 0 \\ -0.05 & 1 & 0 & -17 & 0 & 0 \\ 136.11 & 7.45 & 0 & 0 & -0.08 & -5.93 \end{pmatrix}$$

$$B_{lon} = \begin{pmatrix} 0.47 & 0 \\ -2.72 & 0 \\ -134.33 & 0 \\ 0 & 0 \\ 0 & 0 \\ 0 & 2508.25 \end{pmatrix}$$

$$C_{lon} = \begin{pmatrix} 1 & 0.05 & 0 & 0 & 0 & 0 \\ 0 & 0.06 & 0 & 0 & 0 & 0 \\ 0 & 0 & 1 & 0 & 0 & 0 \\ 0 & 0 & 0 & 1 & 0 & 0 \\ 0 & 0 & 0 & 0 & -1 & 0 \\ -0.6 & 0.81 & 0.04 & 0 & 0 & 0.01 \\ -0.74 & -7.6 & -1.26 & 0 & 0 & 0 \end{pmatrix}$$

$$D_{lon} = \begin{pmatrix} 0 & 0 \\ 0 & 0 \\ 0 & 0 \\ 0 & 0 \\ 0 & 0 \\ 0.47 & 0 \\ -2.72 & 0 \end{pmatrix}$$

Full linear state space model obtained in level climb flight in case of presence of steady wind:

$$A_f = \begin{pmatrix}
0 & 0 & 0 & 1 & 0 & 0.15 & 0 & 0 & 0 & 0 & 0 & 0 & 0 \\
0 & 0 & 0 & 0 & 1 & 0 & 0 & 0 & 0 & 0 & 0 & 0 & 0 \\
0 & 0 & 0 & 0 & 0 & 1.01 & 0 & 0 & 0 & 0 & 0 & 0 & 0 \\
0 & 0 & 0 & -16.17 & -0.15 & 3.38 & -0.01 & -2.84 & 0 & 0 & 0 & 0 & -0.01 \\
0 & 0 & 0 & 0 & -15.88 & 1.35 & 1.2 & 0 & -7.43 & 0 & 0 & 0 & -0.02 \\
0 & 0 & 0 & 0.52 & -0.77 & -2.79 & 0 & 1.71 & 0 & 0 & 0 & 0 & 0 \\
0 & -9.7 & 0 & 0 & -0.87 & 0 & -0.64 & 0 & 0.8 & 0 & 0 & 0 & 0.01 \\
9.7 & 0 & 0 & 0.88 & 0 & -16.82 & 0 & -0.88 & 0 & 0 & 0 & 0 & 0 \\
0.02 & -1.45 & 0 & 0 & 15.71 & 0 & -0.73 & 0 & -7.6 & 0 & 0 & 0 & 0 \\
0.39 & 1.46 & -7.15 & 0 & 0 & 0 & -0.9 & -0.42 & -0.14 & 0 & 0 & 0 & 0 \\
0.83 & -0.68 & -15.34 & 0 & 0 & 0 & 0.42 & -0.91 & 0.06 & 0 & 0 & 0 & 0 \\
0 & -16.92 & 0 & 0 & 0 & 0 & -0.15 & 0 & 0.99 & 0 & 0 & 0 & 0 \\
0 & 0 & 0 & 0 & 0 & 0 & 135.11 & 0 & 7.32 & 0 & 0 & -0.12 & -6.63
\end{pmatrix}$$

$$B_f = \begin{pmatrix}
0 & 0 & 0 & 0 & 0 & 0 & 0 \\
0 & 0 & 0 & 0 & 0 & 0 & 0 \\
0 & 0 & 0 & 0 & 0 & 0 & 0 \\
10.37 & 0 & -5.03 & 78.61 & -78.61 & 33.17 & -33.17 \\
0 & -134.33 & 0 & 3.02 & 3.01 & 2.64 & 2.64 \\
0.94 & 0 & -82.44 & -5.78 & 5.78 & -1.8 & 1.8 \\
0 & 0.47 & -0.84 & 0.65 & -0.19 & 0.36 & 0.36 \\
0 & 0 & 5.33 & 0 & 0 & 0 & 0 \\
0 & -2.72 & -0.05 & -6.59 & -6.64 & -10.3 & -10.3 \\
0 & 0 & 0 & 0 & 0 & 0 & 0 \\
0 & 0 & 0 & 0 & 0 & 0 & 0 \\
0 & 0 & 0 & 0 & 0 & 0 & 0 \\
2803.04 & 0 & 0 & 0 & 0 & 0 & 0
\end{pmatrix}$$

$$C_f = \begin{pmatrix} 1 & 0 & 0 & 0 & 0 & 0 & 0 & 0 & 0 & 0 & 0 & 0 & 0 \\ 0 & 1 & 0 & 0 & 0 & 0 & 0 & 0 & 0 & 0 & 0 & 0 & 0 \\ 0 & 0 & 1 & 0 & 0 & 0 & 0 & 0 & 0 & 0 & 0 & 0 & 0 \\ 0 & 0 & 0 & 1 & 0 & 0 & 0 & 0 & 0 & 0 & 0 & 0 & 0 \\ 0 & 0 & 0 & 0 & 1 & 0 & 0 & 0 & 0 & 0 & 0 & 0 & 0 \\ 0 & 0 & 0 & 0 & 0 & 1 & 0 & 0 & 0 & 0 & 0 & 0 & 0 \\ 0 & 0 & 0 & 0 & 0.04 & 0 & -0.64 & 0 & 0.8 & 0 & 0 & 0 & 0.01 \\ 0 & 0 & 0 & -0.04 & 0 & 0.16 & 0 & -0.88 & 0 & 0 & 0 & 0 & 0 \\ 0 & 0 & 0 & 0 & -1.26 & 0 & -0.73 & 0 & -7.6 & 0 & 0 & 0 & 0 \\ 0 & 0 & 0 & 0 & 0 & 0 & 1 & 0 & 0.05 & 0 & 0 & 0 & 0 \\ 0 & 0 & 0 & 0 & 0 & 0 & 0 & 0.06 & 0 & 0 & 0 & 0 & 0 \\ 0 & 0 & 0 & 0 & 0 & 0 & 0 & 0 & 0.06 & 0 & 0 & 0 & 0 \\ 0 & 0 & 0 & 0 & 0 & 0 & 0 & 0 & 0 & 0 & 0 & -1 & 0 \\ 0 & 0.92 & -0.01 & 0 & 0 & 0 & 0 & 0 & -0.05 & 0 & 0 & 0 & 0 \end{pmatrix}$$

$$D_f = \begin{pmatrix} 0 & 0 & 0 & 0 & 0 & 0 & 0 \\ 0 & 0 & 0 & 0 & 0 & 0 & 0 \\ 0 & 0 & 0 & 0 & 0 & 0 & 0 \\ 0 & 0 & 0 & 0 & 0 & 0 & 0 \\ 0 & 0 & 0 & 0 & 0 & 0 & 0 \\ 0 & 0 & 0 & 0 & 0 & 0 & 0 \\ 0 & 0.47 & -0.84 & 0.65 & -0.19 & 0.36 & 0.36 \\ 0 & 0 & 5.33 & 0 & 0 & 0 & 0 \\ 0 & -2.72 & -0.05 & -6.59 & -6.64 & -10.3 & -10.3 \\ 0 & 0 & 0 & 0 & 0 & 0 & 0 \\ 0 & 0 & 0 & 0 & 0 & 0 & 0 \\ 0 & 0 & 0 & 0 & 0 & 0 & 0 \\ 0 & 0 & 0 & 0 & 0 & 0 & 0 \\ 0 & 0 & 0 & 0 & 0 & 0 & 0 \end{pmatrix}$$

Lateral linear state space model obtained in level climb flight in case of presence of steady wind:

$$A_{lat} = \begin{pmatrix} -0.88 & 0.88 & -16.82 & 9.7 & 0 \\ -2.84 & -16.17 & 3.38 & 0 & 0 \\ 1.71 & 0.52 & -2.79 & 0 & 0 \\ 0 & 1 & 0.15 & 0 & 0 \\ 0 & 0 & 1.01 & 0 & 0 \end{pmatrix}$$

$$B_{lat} = \begin{pmatrix} 0 & 0 & 5.33 \\ 78.61 & -78.61 & -5.03 \\ -5.78 & 5.78 & -82.44 \\ 0 & 0 & 0 \\ 0 & 0 & 0 \end{pmatrix}$$

$$C_{lat} = \begin{pmatrix} 0.06 & 0 & 0 & 0 & 0 \\ 0 & 1 & 0 & 0 & 0 \\ 0 & 0 & 1 & 0 & 0 \\ 0 & 0 & 0 & 1 & 0 \\ 0 & 0 & 0 & 0 & 1 \end{pmatrix}$$

$$D_{lat} = \begin{pmatrix} 0 & 0 & 0 \\ 0 & 0 & 0 \\ 0 & 0 & 0 \\ 0 & 0 & 0 \\ 0 & 0 & 0 \end{pmatrix}$$

Longitudinal linear state space model obtained in level climb flight in case of presence of steady wind:

$$A_{lon} = \begin{pmatrix} -0.64 & 0.8 & -0.87 & -9.7 & 0 & 0.01 \\ -0.73 & -7.6 & 15.71 & -1.45 & 0 & 0 \\ 1.2 & -7.43 & -15.88 & 0 & 0 & -0.02 \\ 0 & 0 & 1 & 0 & 0 & 0 \\ -0.15 & 0.99 & 0 & -16.92 & 0 & 0 \\ 135.11 & 7.32 & 0 & 0 & -0.12 & -6.63 \end{pmatrix}$$

$$B_{lon} = \begin{pmatrix} 0.47 & 0 \\ -2.72 & 0 \\ -134.33 & 0 \\ 0 & 0 \\ 0 & 0 \\ 0 & 2803.04 \end{pmatrix}$$

$$C_{lon} = \begin{pmatrix} 1 & 0.05 & 0 & 0 & 0 & 0 \\ 0 & 0.06 & 0 & 0 & 0 & 0 \\ 0 & 0 & 1 & 0 & 0 & 0 \\ 0 & 0 & 0 & 1 & 0 & 0 \\ 0 & 0 & 0 & 0 & -1 & 0 \\ -0.64 & 0.8 & 0.04 & 0 & 0 & 0.01 \\ -0.73 & -7.6 & -1.26 & 0 & 0 & 0 \end{pmatrix}$$

$$D_{lon} = \begin{pmatrix} 0 & 0 \\ 0 & 0 \\ 0 & 0 \\ 0 & 0 \\ 0 & 0 \\ 0.47 & 0 \\ -2.72 & 0 \end{pmatrix}$$

Full linear state space model obtained in level turn flight in case of presence of steady wind:

$$A_f = \begin{pmatrix} 0 & 0.35 & 0 & 1 & 0.03 & 0.05 & 0 & 0 & 0 & 0 & 0 & 0 & 0 \\ -0.35 & 0 & 0 & 0 & 0.86 & -0.52 & 0 & 0 & 0 & 0 & 0 & 0 & 0 \\ 0 & 0.02 & 0 & 0 & 0.52 & 0.86 & 0 & 0 & 0 & 0 & 0 & 0 & 0 \\ 0 & 0 & 0 & -16.14 & -0.43 & 3.21 & -0.01 & -2.85 & 0 & 0 & 0 & 0 & -0.01 \\ 0 & 0 & 0 & 0.29 & -15.88 & 1.33 & 1.27 & 0 & -7.42 & 0 & 0 & 0 & -0.01 \\ 0 & 0 & 0 & 0.5 & -0.77 & -2.82 & 0.07 & 1.71 & 0 & 0 & 0 & 0 & 0 \\ 0 & -9.79 & 0 & 0 & -1.08 & 0 & -0.6 & 0.3 & 0.73 & 0 & 0 & 0 & 0.01 \\ 8.37 & -0.29 & 0 & 1.09 & 0 & -16.81 & -0.3 & -0.88 & -0.02 & 0 & 0 & 0 & 0 \\ -5.07 & -0.48 & 0 & 0 & 15.7 & 0 & -0.65 & 0.02 & -7.61 & 0 & 0 & 0 & 0 \\ 0.44 & 0 & -7.71 & 0 & 0 & 0 & -0.9 & -0.39 & 0.17 & 0 & 0 & 0 & 0 \\ 0.86 & 0 & -15.15 & 0 & 0 & 0 & 0.42 & -0.76 & 0.49 & 0 & 0 & 0 & 0 \\ -0.58 & -16.99 & 0 & 0 & 0 & 0 & -0.06 & 0.52 & 0.85 & 0 & 0 & 0 & 0 \\ 0 & 0 & 0 & 0 & 0 & 0 & 136.06 & 0 & 9.04 & 0 & 0 & -0.09 & -5.98 \end{pmatrix}$$

$$B_f = \begin{pmatrix} 0 & 0 & 0 & 0 & 0 & 0 & 0 \\ 0 & 0 & 0 & 0 & 0 & 0 & 0 \\ 0 & 0 & 0 & 0 & 0 & 0 & 0 \\ 9.36 & 0 & -5.04 & 78.61 & -78.61 & 33.17 & -33.17 \\ 0 & -134.33 & 0.01 & 3.02 & 3.01 & 2.64 & 2.64 \\ 0.85 & 0 & -82.44 & -5.78 & 5.78 & -1.8 & 1.8 \\ 0 & 0.48 & 0.84 & 0.67 & -0.17 & 0.38 & 0.38 \\ 0 & 0 & 5.33 & 0 & 0 & 0 & 0 \\ 0 & -2.71 & 0.06 & -6.59 & -6.64 & -10.3 & -10.3 \\ 0 & 0 & 0 & 0 & 0 & 0 & 0 \\ 0 & 0 & 0 & 0 & 0 & 0 & 0 \\ 0 & 0 & 0 & 0 & 0 & 0 & 0 \\ 2531.12 & 0 & 0 & 0 & 0 & 0 & 0 \end{pmatrix}$$

$$C_f = \begin{pmatrix} 1 & 0 & 0 & 0 & 0 & 0 & 0 & 0 & 0 & 0 & 0 & 0 & 0 \\ 0 & 1 & 0 & 0 & 0 & 0 & 0 & 0 & 0 & 0 & 0 & 0 & 0 \\ 0 & 0 & 1 & 0 & 0 & 0 & 0 & 0 & 0 & 0 & 0 & 0 & 0 \\ 0 & 0 & 0 & 1 & 0 & 0 & 0 & 0 & 0 & 0 & 0 & 0 & 0 \\ 0 & 0 & 0 & 0 & 1 & 0 & 0 & 0 & 0 & 0 & 0 & 0 & 0 \\ 0 & 0 & 0 & 0 & 0 & 1 & 0 & 0 & 0 & 0 & 0 & 0 & 0 \\ 0 & 0 & 0 & 0 & 0.05 & 0 & -0.6 & 0 & 0.92 & 0 & 0 & 0 & 0.01 \\ 0 & 0 & 0 & -0.04 & 0 & 0.16 & 0 & -0.88 & 0 & 0 & 0 & 0 & 0 \\ 0 & 0 & 0 & 0 & -1.26 & 0 & -0.83 & 0 & -7.61 & 0 & 0 & 0 & 0 \\ 0 & 0 & 0 & 0 & 0 & 0 & 1 & 0 & 0.07 & 0 & 0 & 0 & 0 \\ 0 & 0 & 0 & 0 & 0 & 0 & 0 & 0.06 & 0 & 0 & 0 & 0 & 0 \\ 0 & 0 & 0 & 0 & 0 & 0 & 0 & 0 & 0.06 & 0 & 0 & 0 & 0 \\ 0 & 0 & 0 & 0 & 0 & 0 & 0 & 0 & 0 & 0 & 0 & -1 & 0 \\ 0.03 & 0.93 & 0 & 0 & 0 & 0 & 0 & -0.03 & -0.05 & 0 & 0 & 0 & 0 \end{pmatrix}$$

$$D_f = \begin{pmatrix} 0 & 0 & 0 & 0 & 0 & 0 & 0 \\ 0 & 0 & 0 & 0 & 0 & 0 & 0 \\ 0 & 0 & 0 & 0 & 0 & 0 & 0 \\ 0 & 0 & 0 & 0 & 0 & 0 & 0 \\ 0 & 0 & 0 & 0 & 0 & 0 & 0 \\ 0 & 0 & 0 & 0 & 0 & 0 & 0 \\ 0 & 0.48 & 0.84 & 0.67 & -0.17 & 0.38 & 0.38 \\ 0 & 0 & 5.33 & 0 & 0 & 0 & 0 \\ 0 & -2.71 & 0.06 & -6.59 & -6.64 & -10.3 & -10.3 \\ 0 & 0 & 0 & 0 & 0 & 0 & 0 \\ 0 & 0 & 0 & 0 & 0 & 0 & 0 \\ 0 & 0 & 0 & 0 & 0 & 0 & 0 \\ 0 & 0 & 0 & 0 & 0 & 0 & 0 \\ 0 & 0 & 0 & 0 & 0 & 0 & 0 \end{pmatrix}$$

Lateral linear state space model obtained in level turn flight in case of presence of steady wind:

$$A_{lat} = \begin{pmatrix} -0.88 & 1.09 & -16.81 & 8.37 & 0 \\ -2.85 & -16.14 & 3.21 & 0 & 0 \\ 1.71 & 0.5 & -2.82 & 0 & 0 \\ 0 & 1 & 0.05 & 0 & 0 \\ 0 & 0 & 0.86 & 0 & 0 \end{pmatrix}$$

$$B_{lat} = \begin{pmatrix} 0 & 0 & 5.33 \\ 78.61 & -78.61 & -5.04 \\ -5.78 & 5.78 & -82.44 \\ 0 & 0 & 0 \\ 0 & 0 & 0 \end{pmatrix}$$

$$C_{lat} = \begin{pmatrix} 0.06 & 0 & 0 & 0 & 0 \\ 0 & 1 & 0 & 0 & 0 \\ 0 & 0 & 1 & 0 & 0 \\ 0 & 0 & 0 & 1 & 0 \\ 0 & 0 & 0 & 0 & 1 \end{pmatrix}$$

$$D_{lat} = \begin{pmatrix} 0 & 0 & 0 \\ 0 & 0 & 0 \\ 0 & 0 & 0 \\ 0 & 0 & 0 \\ 0 & 0 & 0 \end{pmatrix}$$

Longitudinal linear state space model obtained in level turn flight in case of presence of steady wind:

$$A_{lon} = \begin{pmatrix} -0.6 & 0.73 & -1.08 & -9.79 & 0 & 0.01 \\ -0.65 & -7.61 & 15.7 & -0.48 & 0 & 0 \\ 1.27 & -7.42 & -15.88 & 0 & 0 & -0.01 \\ 0 & 0 & 0.86 & 0 & 0 & 0 \\ -0.06 & 0.85 & 0 & -16.99 & 0 & 0 \\ 136.06 & 9.04 & 0 & 0 & -0.09 & -5.98 \end{pmatrix}$$

$$B_{lon} = \begin{pmatrix} 0.48 & 0 \\ -2.71 & 0 \\ -134.33 & 0 \\ 0 & 0 \\ 0 & 0 \\ 0 & 2531.12 \end{pmatrix}$$

$$C_{lon} = \begin{pmatrix} 1 & 0.07 & 0 & 0 & 0 & 0 \\ 0 & 0.06 & 0 & 0 & 0 & 0 \\ 0 & 0 & 1 & 0 & 0 & 0 \\ 0 & 0 & 0 & 1 & 0 & 0 \\ 0 & 0 & 0 & 0 & -1 & 0 \\ -0.6 & 0.92 & 0.05 & 0 & 0 & 0.01 \\ -0.83 & -7.61 & -1.26 & 0 & 0 & 0 \end{pmatrix}$$

$$D_{lon} = \begin{pmatrix} 0 & 0 \\ 0 & 0 \\ 0 & 0 \\ 0 & 0 \\ 0 & 0 \\ 0.48 & 0 \\ -2.71 & 0 \end{pmatrix}$$

Full linear state space model obtained in climbing turn flight in case of presence of steady wind:

$$A_f = \begin{pmatrix}
0 & 0.35 & 0 & 1 & 0.08 & 0.13 & 0 & 0 & 0 & 0 & 0 & 0 & 0 \\
-0.35 & 0 & 0 & 0 & 0.85 & -0.52 & 0 & 0 & 0 & 0 & 0 & 0 & 0 \\
0 & 0.05 & 0 & 0 & 0.53 & 0.86 & 0 & 0 & 0 & 0 & 0 & 0 & 0 \\
0 & 0 & 0 & -16.14 & -0.45 & 3.21 & -0.12 & -2.85 & -0.01 & 0 & 0 & 0 & -0.01 \\
0 & 0 & 0 & 0.3 & -15.88 & 1.4 & 1.42 & 0 & -7.41 & 0 & 0 & 0 & -0.01 \\
0 & 0 & 0 & 0.5 & -0.82 & -2.82 & 0.07 & 1.71 & 0 & 0 & 0 & 0 & 0 \\
0 & -9.7 & 0 & 0 & -1.07 & 0 & -0.64 & 0.29 & 0.73 & 0 & 0 & 0 & 0.01 \\
8.28 & -0.76 & 0 & 1.08 & 0 & -16.81 & -0.3 & -0.88 & -0.05 & 0 & 0 & 0 & 0 \\
-5.04 & -1.25 & 0 & 0 & 15.7 & 0 & -0.64 & 0.05 & -7.61 & 0 & 0 & 0 & 0 \\
0.48 & 1.45 & -7.67 & 0 & 0 & 0 & -0.9 & -0.43 & 0.1 & 0 & 0 & 0 & 0 \\
0.83 & -0.68 & -15.08 & 0 & 0 & 0 & 0.42 & -0.74 & 0.53 & 0 & 0 & 0 & 0 \\
-0.57 & -16.91 & 0 & 0 & 0 & 0 & -0.15 & 0.51 & 0.84 & 0 & 0 & 0 & 0 \\
0 & 0 & 0 & 0 & 0 & 0 & 134.86 & 0 & 8.87 & 0 & 0 & -0.12 & -6.67
\end{pmatrix}$$

$$B_f = \begin{pmatrix}
0 & 0 & 0 & 0 & 0 & 0 & 0 \\
0 & 0 & 0 & 0 & 0 & 0 & 0 \\
0 & 0 & 0 & 0 & 0 & 0 & 0 \\
10.43 & 0 & -5.04 & 78.61 & -78.61 & 33.17 & -33.17 \\
0 & -134.33 & 0.01 & 3.02 & 3.01 & 2.64 & 2.64 \\
0.95 & 0 & -82.44 & -5.78 & 5.78 & -1.8 & 1.8 \\
0 & 0.48 & 0.84 & 0.67 & -0.17 & 0.38 & 0.38 \\
0 & 0 & 5.33 & 0 & 0 & 0 & 0 \\
0 & -2.71 & 0.06 & -6.59 & -6.64 & -10.3 & -10.3 \\
0 & 0 & 0 & 0 & 0 & 0 & 0 \\
0 & 0 & 0 & 0 & 0 & 0 & 0 \\
0 & 0 & 0 & 0 & 0 & 0 & 0 \\
2818.59 & 0 & 0 & 0 & 0 & 0 & 0
\end{pmatrix}$$

$$C_f = \begin{pmatrix} 1 & 0 & 0 & 0 & 0 & 0 & 0 & 0 & 0 & 0 & 0 & 0 & 0 \\ 0 & 1 & 0 & 0 & 0 & 0 & 0 & 0 & 0 & 0 & 0 & 0 & 0 \\ 0 & 0 & 1 & 0 & 0 & 0 & 0 & 0 & 0 & 0 & 0 & 0 & 0 \\ 0 & 0 & 0 & 1 & 0 & 0 & 0 & 0 & 0 & 0 & 0 & 0 & 0 \\ 0 & 0 & 0 & 0 & 1 & 0 & 0 & 0 & 0 & 0 & 0 & 0 & 0 \\ 0 & 0 & 0 & 0 & 0 & 1 & 0 & 0 & 0 & 0 & 0 & 0 & 0 \\ 0 & 0 & 0 & 0 & 0.05 & 0 & -0.64 & 0 & 0.91 & 0 & 0 & 0 & 0.01 \\ 0 & 0 & 0 & -0.04 & 0 & 0.16 & 0 & -0.88 & 0 & 0 & 0 & 0 & 0 \\ 0 & 0 & 0 & 0 & -1.26 & 0 & -0.82 & 0 & -7.61 & 0 & 0 & 0 & 0 \\ 0 & 0 & 0 & 0 & 0 & 0 & 1 & 0 & 0.07 & 0 & 0 & 0 & 0 \\ 0 & 0 & 0 & 0 & 0 & 0 & 0 & 0.06 & 0 & 0 & 0 & 0 & 0 \\ 0 & 0 & 0 & 0 & 0 & 0 & 0 & 0 & 0.06 & 0 & 0 & 0 & 0 \\ 0 & 0 & 0 & 0 & 0 & 0 & 0 & 0 & 0 & 0 & 0 & -1 & 0 \\ 0.03 & 0.93 & -0.01 & 0 & 0 & 0 & 0 & -0.03 & -0.05 & 0 & 0 & 0 & 0 \end{pmatrix}$$

$$D_f = \begin{pmatrix} 0 & 0 & 0 & 0 & 0 & 0 & 0 \\ 0 & 0 & 0 & 0 & 0 & 0 & 0 \\ 0 & 0 & 0 & 0 & 0 & 0 & 0 \\ 0 & 0 & 0 & 0 & 0 & 0 & 0 \\ 0 & 0 & 0 & 0 & 0 & 0 & 0 \\ 0 & 0 & 0 & 0 & 0 & 0 & 0 \\ 0 & 0.48 & 0.84 & 0.67 & -0.17 & 0.38 & 0.38 \\ 0 & 0 & 5.33 & 0 & 0 & 0 & 0 \\ 0 & -2.71 & 0.06 & -6.59 & -6.64 & -10.3 & -10.3 \\ 0 & 0 & 0 & 0 & 0 & 0 & 0 \\ 0 & 0 & 0 & 0 & 0 & 0 & 0 \\ 0 & 0 & 0 & 0 & 0 & 0 & 0 \\ 0 & 0 & 0 & 0 & 0 & 0 & 0 \\ 0 & 0 & 0 & 0 & 0 & 0 & 0 \end{pmatrix}$$

Lateral linear state space model obtained in climbing turn flight in case of presence of steady wind:

$$A_{lat} = \begin{pmatrix} -0.88 & 1.08 & -16.81 & 8.28 & 0 \\ -2.85 & -16.14 & 3.21 & 0 & 0 \\ 1.71 & 0.5 & -2.82 & 0 & 0 \\ 0 & 1 & 0.13 & 0 & 0 \\ 0 & 0 & 0.86 & 0 & 0 \end{pmatrix}$$

$$B_{lat} = \begin{pmatrix} 0 & 0 & 5.33 \\ 78.61 & -78.61 & -5.04 \\ -5.78 & 5.78 & -82.44 \\ 0 & 0 & 0 \\ 0 & 0 & 0 \end{pmatrix}$$

$$C_{lat} = \begin{pmatrix} 0.06 & 0 & 0 & 0 & 0 \\ 0 & 1 & 0 & 0 & 0 \\ 0 & 0 & 1 & 0 & 0 \\ 0 & 0 & 0 & 1 & 0 \\ 0 & 0 & 0 & 0 & 1 \end{pmatrix}$$

$$D_{lat} = \begin{pmatrix} 0 & 0 & 0 \\ 0 & 0 & 0 \\ 0 & 0 & 0 \\ 0 & 0 & 0 \\ 0 & 0 & 0 \end{pmatrix}$$

Longitudinal linear state space model obtained in climbing turn flight in case of presence of steady wind:

$$A_{lon} = \begin{pmatrix} -0.64 & 0.73 & -1.07 & -9.7 & 0 & 0.01 \\ -0.64 & -7.61 & 15.7 & -1.25 & 0 & 0 \\ 1.42 & -7.41 & -15.88 & 0 & 0 & -0.01 \\ 0 & 0 & 0.85 & 0 & 0 & 0 \\ -0.15 & 0.84 & 0 & -16.91 & 0 & 0 \\ 134.86 & 8.87 & 0 & 0 & -0.12 & -6.67 \end{pmatrix}$$

$$B_{lon} = \begin{pmatrix} 0.48 & 0 \\ -2.71 & 0 \\ -134.33 & 0 \\ 0 & 0 \\ 0 & 0 \\ 0 & 2818.59 \end{pmatrix}$$

$$C_{lon} = \begin{pmatrix} 1 & 0.07 & 0 & 0 & 0 & 0 \\ 0 & 0.06 & 0 & 0 & 0 & 0 \\ 0 & 0 & 1 & 0 & 0 & 0 \\ 0 & 0 & 0 & 1 & 0 & 0 \\ 0 & 0 & 0 & 0 & -1 & 0 \\ -0.64 & 0.91 & 0.05 & 0 & 0 & 0.01 \\ -0.82 & -7.61 & -1.26 & 0 & 0 & 0 \end{pmatrix}$$

$$D_{lon} = \begin{pmatrix} 0 & 0 \\ 0 & 0 \\ 0 & 0 \\ 0 & 0 \\ 0 & 0 \\ 0.48 & 0 \\ -2.71 & 0 \end{pmatrix}$$

Full linear state space model obtained in level steady heading sideslip flight in case of presence of steady wind:

$$A_f = \begin{pmatrix}
0 & 0 & 0 & 1 & 0.01 & 0.06 & 0 & 0 & 0 & 0 & 0 & 0 & 0 \\
0 & 0 & 0 & 0 & 0.99 & -0.12 & 0 & 0 & 0 & 0 & 0 & 0 & 0 \\
0 & 0 & 0 & 0 & 0.12 & 1 & 0 & 0 & 0 & 0 & 0 & 0 & 0 \\
0 & 0 & 0 & -16.17 & -0.15 & 3.38 & 0.31 & -2.82 & -0.06 & 0 & 0 & 0 & -0.01 \\
0 & 0 & 0 & 0 & -15.88 & 1.25 & 1.05 & 0.06 & -7.47 & 0 & 0 & 0 & -0.01 \\
0 & 0 & 0 & 0.52 & -0.71 & -2.79 & -0.14 & 1.7 & -0.01 & 0 & 0 & 0 & 0 \\
0 & -9.79 & 0 & 0 & -0.87 & 1.47 & -0.6 & 0.09 & 0.81 & 0 & 0 & 0 & 0.01 \\
9.72 & -0.07 & 0 & 0.88 & 0 & -16.76 & -0.06 & -0.88 & -0.02 & 0 & 0 & 0 & 0 \\
-1.14 & -0.62 & 0 & -1.48 & 15.65 & 0 & -0.73 & -0.09 & -7.62 & 0 & 0 & 0 & 0 \\
0.38 & 0 & -5.92 & 0 & 0 & 0 & -0.9 & -0.43 & -0.01 & 0 & 0 & 0 & 0 \\
1.02 & 0 & -15.93 & 0 & 0 & 0 & 0.42 & -0.9 & 0.13 & 0 & 0 & 0 & 0 \\
1.36 & -16.95 & 0 & 0 & 0 & 0 & -0.06 & 0.12 & 0.99 & 0 & 0 & 0 & 0 \\
0 & 0 & 0 & 0 & 0 & 0 & 135.62 & 11.88 & 7.35 & 0 & 0 & -0.08 & -5.96
\end{pmatrix}$$

$$B_f = \begin{pmatrix}
0 & 0 & 0 & 0 & 0 & 0 & 0 \\
0 & 0 & 0 & 0 & 0 & 0 & 0 \\
0 & 0 & 0 & 0 & 0 & 0 & 0 \\
9.32 & -0.03 & -5.03 & 78.54 & -78.68 & 33.06 & -33.28 \\
0 & -134.33 & 0 & 3.01 & 3.02 & 2.64 & 2.64 \\
0.85 & 0 & -82.43 & -5.78 & 5.77 & -1.81 & 1.79 \\
0 & 0.47 & -1.3 & -0.19 & 0.65 & 0.36 & 0.36 \\
0 & 0.03 & 5.23 & -0.05 & 0.03 & -0.02 & -0.02 \\
0 & -2.72 & -0.07 & -6.64 & -6.59 & -10.3 & -10.3 \\
0 & 0 & 0 & 0 & 0 & 0 & 0 \\
0 & 0 & 0 & 0 & 0 & 0 & 0 \\
0 & 0 & 0 & 0 & 0 & 0 & 0 \\
2520.23 & 0 & 0 & 0 & 0 & 0 & 0
\end{pmatrix}$$

$$C_f = \begin{pmatrix} 1 & 0 & 0 & 0 & 0 & 0 & 0 & 0 & 0 & 0 & 0 & 0 & 0 \\ 0 & 1 & 0 & 0 & 0 & 0 & 0 & 0 & 0 & 0 & 0 & 0 & 0 \\ 0 & 0 & 1 & 0 & 0 & 0 & 0 & 0 & 0 & 0 & 0 & 0 & 0 \\ 0 & 0 & 0 & 1 & 0 & 0 & 0 & 0 & 0 & 0 & 0 & 0 & 0 \\ 0 & 0 & 0 & 0 & 1 & 0 & 0 & 0 & 0 & 0 & 0 & 0 & 0 \\ 0 & 0 & 0 & 0 & 0 & 1 & 0 & 0 & 0 & 0 & 0 & 0 & 0 \\ 0 & 0 & 0 & 0 & 0.04 & -0.01 & -0.6 & 0.09 & 0.81 & 0 & 0 & 0 & 0.01 \\ 0 & 0 & 0 & -0.04 & 0 & 0.16 & -0.06 & -0.88 & -0.02 & 0 & 0 & 0 & 0 \\ 0 & 0 & 0 & 0 & -1.26 & 0 & -0.73 & -0.09 & -7.62 & 0 & 0 & 0 & 0 \\ 0 & 0 & 0 & 0 & 0 & 0 & 0.99 & 0.09 & 0.05 & 0 & 0 & 0 & 0 \\ 0 & 0 & 0 & 0 & 0 & 0 & -0.01 & 0.06 & 0 & 0 & 0 & 0 & 0 \\ 0 & 0 & 0 & 0 & 0 & 0 & 0 & 0 & 0.06 & 0 & 0 & 0 & 0 \\ 0 & 0 & 0 & 0 & 0 & 0 & 0 & 0 & 0 & 0 & 0 & -1 & 0 \\ -0.07 & 0.91 & 0 & 0 & 0 & 0 & 0 & -0.01 & -0.05 & 0 & 0 & 0 & 0 \end{pmatrix}$$

$$D_f = \begin{pmatrix} 0 & 0 & 0 & 0 & 0 & 0 & 0 \\ 0 & 0 & 0 & 0 & 0 & 0 & 0 \\ 0 & 0 & 0 & 0 & 0 & 0 & 0 \\ 0 & 0 & 0 & 0 & 0 & 0 & 0 \\ 0 & 0 & 0 & 0 & 0 & 0 & 0 \\ 0 & 0 & 0 & 0 & 0 & 0 & 0 \\ 0 & 0.47 & -1.3 & -0.19 & 0.65 & 0.36 & 0.36 \\ 0 & 0.03 & 5.23 & -0.05 & 0.03 & -0.02 & -0.02 \\ 0 & -2.72 & -0.07 & -6.64 & -6.59 & -10.3 & -10.3 \\ 0 & 0 & 0 & 0 & 0 & 0 & 0 \\ 0 & 0 & 0 & 0 & 0 & 0 & 0 \\ 0 & 0 & 0 & 0 & 0 & 0 & 0 \\ 0 & 0 & 0 & 0 & 0 & 0 & 0 \\ 0 & 0 & 0 & 0 & 0 & 0 & 0 \end{pmatrix}$$

Lateral linear state space model obtained in level steady heading sideslip flight in case of presence of steady wind:

$$A_{lat} = \begin{pmatrix} -0.88 & 0.88 & -16.76 & 9.72 & 0 \\ -2.82 & -16.17 & 3.38 & 0 & 0 \\ 1.7 & 0.52 & -2.79 & 0 & 0 \\ 0 & 1 & 0.06 & 0 & 0 \\ 0 & 0 & 1 & 0 & 0 \end{pmatrix}$$

$$B_{lat} = \begin{pmatrix} -0.05 & 0.03 & 5.23 \\ 78.54 & -78.68 & -5.03 \\ -5.78 & 5.77 & -82.43 \\ 0 & 0 & 0 \\ 0 & 0 & 0 \end{pmatrix}$$

$$C_{lat} = \begin{pmatrix} 0.06 & 0 & 0 & 0 & 0 \\ 0 & 1 & 0 & 0 & 0 \\ 0 & 0 & 1 & 0 & 0 \\ 0 & 0 & 0 & 1 & 0 \\ 0 & 0 & 0 & 0 & 1 \end{pmatrix}$$

$$D_{lat} = \begin{pmatrix} 0 & 0 & 0 \\ 0 & 0 & 0 \\ 0 & 0 & 0 \\ 0 & 0 & 0 \\ 0 & 0 & 0 \end{pmatrix}$$

Longitudinal linear state space model obtained in level steady heading sideslip flight in case of presence of steady wind:

$$A_{lon} = \begin{pmatrix} -0.6 & 0.81 & -0.87 & -9.79 & 0 & 0.01 \\ -0.73 & -7.62 & 15.65 & -0.62 & 0 & 0 \\ 1.05 & -7.47 & -15.88 & 0 & 0 & -0.01 \\ 0 & 0 & 0.99 & 0 & 0 & 0 \\ -0.06 & 0.99 & 0 & -16.95 & 0 & 0 \\ 135.62 & 7.35 & 0 & 0 & -0.08 & -5.96 \end{pmatrix}$$

$$B_{lon} = \begin{pmatrix} 0.47 & 0 \\ -2.72 & 0 \\ -134.33 & 0 \\ 0 & 0 \\ 0 & 0 \\ 0 & 2520.23 \end{pmatrix}$$

$$C_{lon} = \begin{pmatrix} 0.99 & 0.05 & 0 & 0 & 0 & 0 \\ 0 & 0.06 & 0 & 0 & 0 & 0 \\ 0 & 0 & 1 & 0 & 0 & 0 \\ 0 & 0 & 0 & 1 & 0 & 0 \\ 0 & 0 & 0 & 0 & -1 & 0 \\ -0.6 & 0.81 & 0.04 & 0 & 0 & 0.01 \\ -0.73 & -7.62 & -1.26 & 0 & 0 & 0 \end{pmatrix}$$

$$D_{lon} = \begin{pmatrix} 0 & 0 \\ 0 & 0 \\ 0 & 0 \\ 0 & 0 \\ 0 & 0 \\ 0.47 & 0 \\ -2.72 & 0 \end{pmatrix}$$

Table A.6 : Steady state errors in the nonlinear simulations.

States		Straight and Level	Level Climb	Level Turn	Climbing Turn	Level Steady Heading Sideslip
$V_a(m/s)$	nom	0.01	0.06	0.03	0.01	0.01
	UO	0	0.02	0.02	0.08	0
	UO & UOD	0	0.03	0.01	0.01	0
$h(m)$	nom	0.01	...	0.12	...	0.02
	UO	0.04	...	0.04	...	0.01
	UO & UOD	0.04	...	0.03	...	0.01
$\beta(^\circ)$	nom	0.01	0.02	1.46	1.06	0.44
	UO	0.01	0.02	1.47	0.9	0.44
	UO & UOD	0.01	0.02	1.49	1.17	0.44
$\gamma(^\circ)$	nom	0	0.01	0	0.36	0
	UO	0	0.19	0	0.27	0
	UO & UOD	0	0.11	0	0.41	0
$\phi(^\circ)$	nom	0	0.05	0.02	0.03	0.13
	UO	0	0.04	0.03	0.19	0.13
	UO & UOD	0	0.04	0.03	0.06	0.13
$\theta(^\circ)$	nom	0.48	0.42	0.35	0.14	0.53
	UO	0.48	0.26	0.36	0.11	0.53
	UO & UOD	0.48	0.33	0.39	0.14	0.53
$\psi(^\circ)$	nom	0	0	...	...	0.21
	UO	0	0	...	...	0.21
	UO & UOD	0	0	...	...	0.21
$\dot{\psi}(^\circ/s)$	nom	0	0	0.45	0.97	0
	UO	0	0	0.46	1.34	0
	UO & UOD	0	0	0.48	0.76	0

Table A.7 : Settling times in the nonlinear simulations.

States (s)		Straight and Level	Level Climb	Level Turn	Climbing Turn	Level Steady Heading Sideslip
V_a	nom	5.7	13.49	9.53	43.24	9.27
	UO	5.68	6.04	6.38	43.06	5.6
	UO & UOD	6.77	6.31	6.47	6.44	5.88
h	nom	11.15	...	13.62	...	11.62
	UO	11.09	...	9.64	...	9.48
	UO & UOD	11.82	...	8.5	...	6.14
β	nom	9.57	9.71	11.05	50.94	9.87
	UO	9.56	9.57	10.84	72.84	9.76
	UO & UOD	9.59	9.48	10.87	11.06	9.77
γ	nom	16.56	19.21	13.09	96.36	10.94
	UO	17.08	10.07	9.73	94.89	8.15
	UO & UOD	16.26	12.19	8.64	71.88	6.23
ϕ	nom	13.73	7.82	8.17	13.24	11.75
	UO	13.55	8.18	7.92	42.82	12.17
	UO & UOD	14.1	8.32	7.89	7.78	12.15
θ	nom	16.51	20.73	11.49	93.26	8.78
	UO	17.65	10.49	10.34	92.69	9.52
	UO & UOD	16.17	7.72	10.4	18.61	9.7
ψ	nom	5.14	6	...	...	7.85
	UO	5.14	6.03	...	...	7.92
	UO & UOD	5.14	6.03	...	...	7.9
$\dot{\psi}$	nom	5.18	5.54	8.32	6.4	5.22
	UO	5.18	5.54	9.3	49.94	5.22
	UO & UOD	5.18	5.54	8.25	6.82	5.22

Table A.8 : Maximum overshoots in the nonlinear simulations.

States (%)		Straight and Level	Level Climb	Level Turn	Climbing Turn	Level Steady Heading Sideslip
V_a	nom	0.1	0.38	0.31	0.5	0.39
	UO	0.02	0.13	0.15	0.18	0.05
	UO & UOD	0.13	0.29	0.36	0.21	0.17
h	nom	0.08	...	0.17	...	0.03
	UO	0.07	...	0.06	...	0
	UO & UOD	0.07	...	0.05	...	0
β	nom	...	...	...	...	9.73
	UO	...	...	...	...	9.7
	UO & UOD	...	...	...	...	9.68
γ	nom	...	0	...	7.8	...
	UO	...	0.13	...	5.82	...
	UO & UOD	...	0.16	...	8.94	...
ϕ	nom	93.51	7.72	0.51	0.13	0
	UO	83.21	1.15	0.5	0.33	0
	UO & UOD	93.39	0.85	0.52	0.06	0
θ	nom	104.42	5.54	0.87	1.77	16.51
	UO	104.38	3.38	5.3	3.32	16.44
	UO & UOD	91.22	4.32	12.71	1.71	16.42
ψ	nom	0.06	0.06	...	...	0.24
	UO	0.06	0.06	...	...	0.22
	UO & UOD	0.06	0.06	...	...	0.23
$\dot{\psi}$	nom	...	...	18.68	12.62	...
	UO	...	...	20.62	1.62	...
	UO & UOD	...	...	22.45	6.81	...

Table A.9 : Steady state errors in the PIL simulations.

States	Straight and Level	Level Climb	Level Turn	Climbing Turn	Level Steady Heading Sideslip
$V_a(m/s)$	0	0.01	0.24	0.18	0
$h(m)$	0	...	0.03	...	0
$\beta(^\circ)$	0	0	0.35	0.68	0
$\gamma(^\circ)$	0	0.09	0	0.18	0
$\phi(^\circ)$	0	0	0.75	0.52	0
$\theta(^\circ)$	0	0.03	0.27	0.02	0
$\psi(^\circ)$	0	0	...	...	0
$\dot{\psi}(^\circ/s)$	0	0	0.74	0.63	0

Table A.10 : Settling times in the PIL simulations.

States (s)	Straight and Level	Level Climb	Level Turn	Climbing Turn	Level Steady Heading Sideslip
V_a	29.75	40.52	29.32	63.75	28.25
h	28.31	...	30.22	...	28.47
β	31.36	31.86	29.75	77.34	30.4
γ	29.06	65.58	31.48	99.32	29.15
ϕ	31.84	31.68	29.54	89.83	27.55
θ	29.32	41.36	30.65	91.92	29.08
ψ	31.87	32.38	...	...	30.17
$\dot{\psi}$	33.46	33.71	28.82	66.64	27.81

Table A.11 : Maximum overshoots in the PIL simulations.

States (%)	Straight and Level	Level Climb	Level Turn	Climbing Turn	Level Steady Heading Sideslip
V_a	1.28	2.17	2.87	2.97	1.3
h	0.15	...	0.16	...	0.14
β	...	...	...	...	10
γ	...	7.3	...	7.81	...
ϕ	0	0	2.47	1.69	0
θ	14.2	3.92	3.26	9.71	13.08
ψ	0.14	0.14	...	...	0.04
$\dot{\psi}$	...	...	0.13	0.76	...

CURRICULUM VITAE

Name Surname: Hakan ÜLKER

Place and Date of Birth: İzmir, 28.08.1984

E-Mail: ulkerhakan@gmail.com

EDUCATION:

- **B.Sc.:** 2007, University of Gaziantep, Faculty of Engineering, Department of Mechanical Engineering
- **M.Sc.:** 2010, İzmir Institute of Technology, Faculty of Engineering, Department of Mechanical Engineering

PROFESSIONAL EXPERIENCE AND REWARDS:

- 10.2007-11.2007 Design Engineer in Ekol Asansörleri San. ve Tic. Ltd. Şti., İzmir.
- 11.2007-09.2010 Assistant Factory Manager in Fet-Gaz Doğalgaz Malzemeleri. San. ve Tic. Ltd. Şti., İzmir.
- 09.2010-03.2011 Research Assistant at Department of Mechanical Engineering in Siirt University, Siirt.
- 03.2011-05.2014 Research Assistant at Department of Mechanical Engineering in İstanbul Technical University, İstanbul.
- 05.2014-Present Research Assistant at Department of Mechanical Engineering in Siirt University, Siirt.

PUBLICATIONS, PRESENTATIONS AND PATENTS ON THE THESIS:

- **Ulker, H.**, Baykara, C., Ozsoy, C., In press. Design of MPCs for a Fixed Wing UAV. *Aircraft Engineering and Aerospace Technology*, DOI: 10.1108/AEAT-08-2015-0198.R1.

OTHER PUBLICATIONS, PRESENTATIONS AND PATENTS:

- Balbay, A., Sahin, O., **Ulker, H.**, 2011. Experimental Investigation of Shelled Pistachio Grown in Siirt Province, Turkey. *6th International Advanced Technologies Symposium, (IATS'11)*, Elazig, Turkey.

- Balbay, A., **Ulker, H.**, Sahin, O., 2012. Drying Behaviours of Bittim (Pistacia terebinthus) in a Fixed Bed Drying System. *Sixth International Conference on Thermal Engineering: Theory and Applications (ICTEA 2012)*, Istanbul, Turkey.

- Balbay, A., Sahin, O., **Ulker, H.**, 2013. Modeling of Convective Drying Kinetics of Pistachio Kernels in a Fixed Bed Drying System. *Thermal Science*, 17(3), 839-846.

- Balbay, A., **Ulker, H.**, Sahin, O., 2013. An experimental study on drying of pistacia terebinthus in a fixed bed dryer. *Fluid Dynamics and Materials Processing*, 9(1), 1-10.

- Sahin, O., Pala, M., Balbay, A., Hansu, F., **Ulker, H.**, 2014. Energy Profile of Siirt. *International Conference on Energy and Management (ICEM 2014)*, Istanbul, Turkey.

- Balbay, A., **Ulker, H.**, Demirtas, S., Sahin, O., 2014. An Experimental Study on a Fully Automatic Controlled Irrigating System by Using Solar Energy in Siirt, Turkey. *SOLARTR 2014 Conference & Exhibition*, Izmir, Turkey.